Analysis of Engineered Polymer Structures for Blunt Impact Protection

Tony Kayhart, Mechanical Engineer
Infantry Combat Equipment Team
Natick Soldier RD&E Center

Steven Shpiner
Managing Director, R&D
Prescient Edge Corporation

Project ID:	(P-1377_11)-Natick-1017-01
Document No.:	1377-01 Natick-1017-01 LS-DYNA Analysis of Engineered Polymer Structures for Blunt Impact Protection Rev-0B.docx
Date Issued:	10/10/2018

Predictive Engineering, Inc.
Portland Oregon 97202
PH: 503.206.5571   FX: 866.215.1220
www.predictiveengineering.com

REV	DESCRIPTION OF CHANGE	DATE ISSUED	BY	
0	Formal Release	October 3, 2018	KG	GL
0A	Added additional documentation on model correlation	October 4, 2018	KG	GL
0B	Added additional documentation on material modeling from Paul Du Bois and editorial corrections.	October 10, 2018	KG	GL

Analysis by:
Kenneth Gollins, PhD
Staff Mechanical Engineer
Predictive Engineering, Inc.

Analysis by:
George Laird, PhD, PE
Principal Mechanical Engineer
Predictive Engineering, Inc.

Table of Contents

List of Figures

EXECUTIVE SUMMARY

OBJECTIVE

Engineered 3D open cell lattice structures are of great interest for their high energy absorption capabilities and excellent strength to stiffness ratio. Although lattice structures are built from simple repetitive cells, the global compressive response of the structure is not obvious. Further, characterization of these geometries grows increasingly more difficult when the lattice is manufactured through an additive process. Additive processes are inherently subjected to localized flaws due to the nature of how each subsequent layer is built on top of one another. Thus, material properties may be inconsistent between each production.

This work poses the significant challenge of generating a strain-rate dependent material law for complex thin lattice structures from raw bulk material of uniform shape. The difficulty arises because if a structure is sufficiently large, the overall macromechanical behavior may be unaffected by local flaws. However, the struts may be too thin to correlate well with bulk testing. If one is trying to capture the behavior of the lattice structure non-standardized tests should be performed to build a non-standard material law, especially for strain-rate dependency.

Furthermore, each parameter of the lattice (strut thickness, unit cell topology, etc..) can have a great effect on the behavior of the structure. As such, the objective of this work is to develop a structural/geometric optimization tool for blunt impact of an elastomer with the following optimization parameters:

a. The elastomer cannot plastically deform during the impact (it should return to its original state after some time)
b. Model should be material neutral (or at least elastomer neutral)
c. Should be capable of handling complex lattice/truss structures
d. Model should be capable of handling large deformations
e. Goal – reduce transmitted force
f. Goal – reduce mass

.

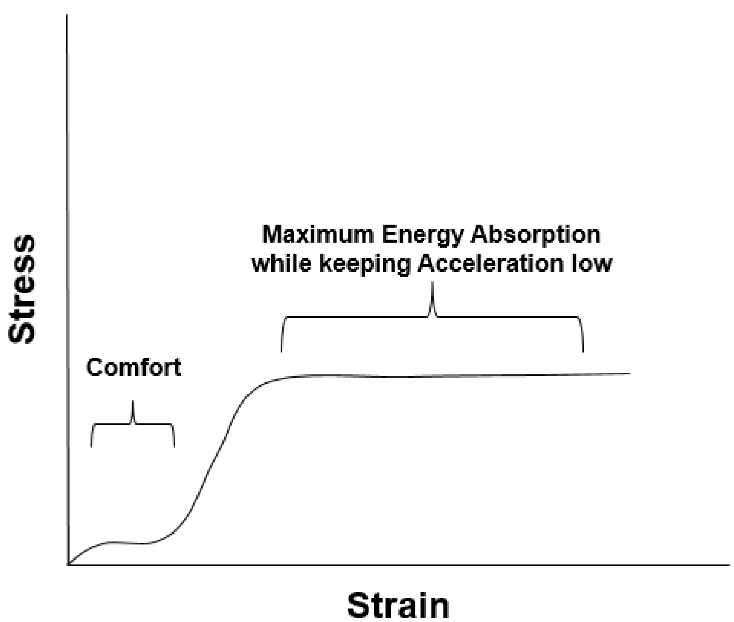

Why This Work is Important to the US Army

Additive manufacturing is the break-through technology of the 21st century. Although one can quickly manufacture or print 3D structures of complex shapes, the material characterization and numerical modeling of these structures lags far behind this capability and limits their practical application. The investment and facilities required to characterize these materials lies far outside the realm of industrial research and development and if we are to move additive manufacturing out of the laboratory and into the field, a dedicated and serious R&D program is required. Tomorrow's advanced soldier protection systems will not be made from monolithic structures but from combination of materials and shapes that will be impossible to manufacture using 20th century manufacturing techniques; in short, tomorrow is owned by additive manufacturing and currently, we have no good way to create digital prototypes to drive the design process.

The US Army Natick Soldier Systems Center is uniquely qualified to lead this effort and has taken the first initial steps. What has been learned and will be discussed in this report, is that additive manufactured structures are extremely difficult to experimentally characterize and likewise, extremely difficult to numerically simulate. These challenges confirm the importance of this work to the US Army's effort of equipping tomorrow's soldier with the best protective equipment possible.

General Findings

Two materials were characterized and applied to a set of three FEA models. Each FEA model was impacted at 10, 14 and 17 f/s. Table 1 shows the three geometries that were explored in this work.

Table 1: Three geometries as meshed for finite element analysis (FEA)

CVC E1	CBS E1	CF A1
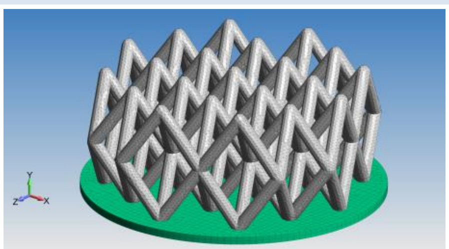	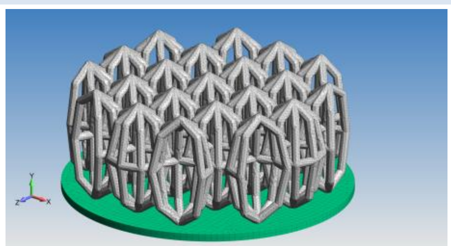	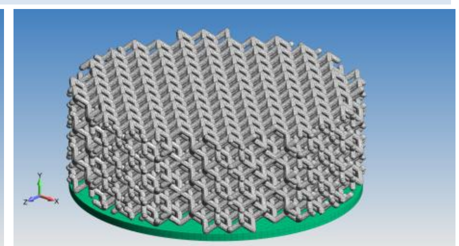

Table 2 presents a summary of the results as tabulated per impact velocity versus maximum impact force. As seen, the simulation over predicted the maximum impact force. This over prediction is due to difficulty of generating a material law for thin structures from a bulky specimen.

Table 2: Summary of Results

Material 1: Form2Flex / FLFLGRO2 – Photopolymer Resin						
Velocity	CVC E1		CBS E1		CF A1	
	Exp, kN	FEA, kN	Exp, kN	FEA, kN	Exp, kN	FEA, kN
10 f/s	2.1	10	4.6	13	5.5	8.4
14 f/s	8.1	25				
17 f/s	14.3	45				
Material 2: Carbon EP40						
Velocity	CVC E1		CBS E1		CF A1	
	Exp, kN	FEA, kN	Exp, kN	FEA, kN	Exp, kN	FEA, kN
10 f/s		21		21		13
14 f/s						
17 f/s						

Why Correlation Between Test and FEA Was Not Possible

Figure 1 sums up the comparison between the CVC E1 FEA and test by showing the impact force versus time. The difference is too large to explain by modeling assumptions. For example, by varying the friction value from 0.3 to 1.0, we could drop the maximum force from 10 to 8.3 kN, however, this is a long way from the experimental value of 2.1 kN. There is just something fundamentally different between the FEA model and the test.

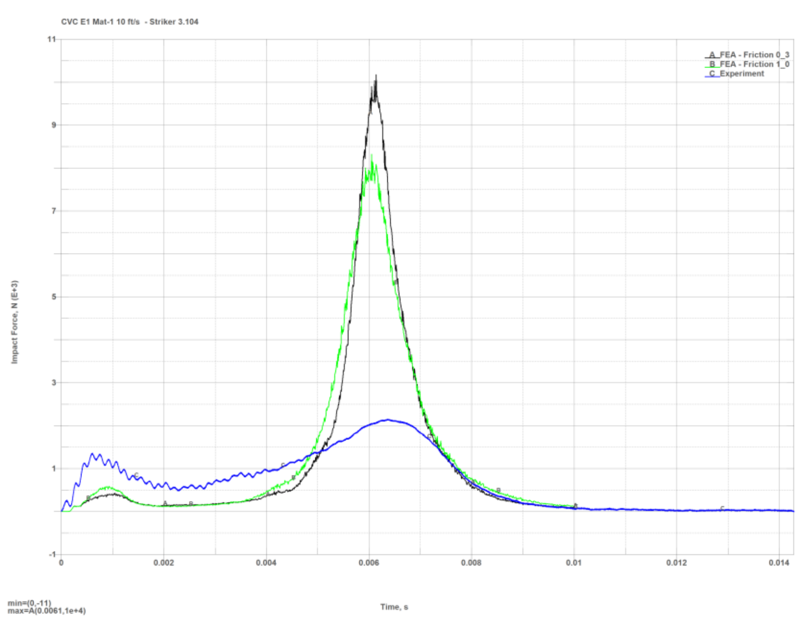

Figure 1: Comparison of FEA to test results using the CVC E1 geometry

In summary of our investigation why the FEA model fails to correlate with the test results, Table 3 provides a graphical summary of the challenges that were faced with model to test correlation. In brief, two dominant challenges were noted: (i) test data was taken on large, monolithic blocks (19 mm thick x 50 mm diameter) while the test articles were lattices having member diameters of 1 mm and (ii) material property data (Material 1) was gathered at a limited strain range from -0.6 to +0.6 whereas the analysis work showed that the lattice structures would exhibit much higher strain ranges from -0.9 (or higher) to likewise +0.9 (or higher).

Table 3: Graphical summary on why the FEA model did not correlate to test – Lessons Learned

Material Data from 50 mm Diameter Blocks

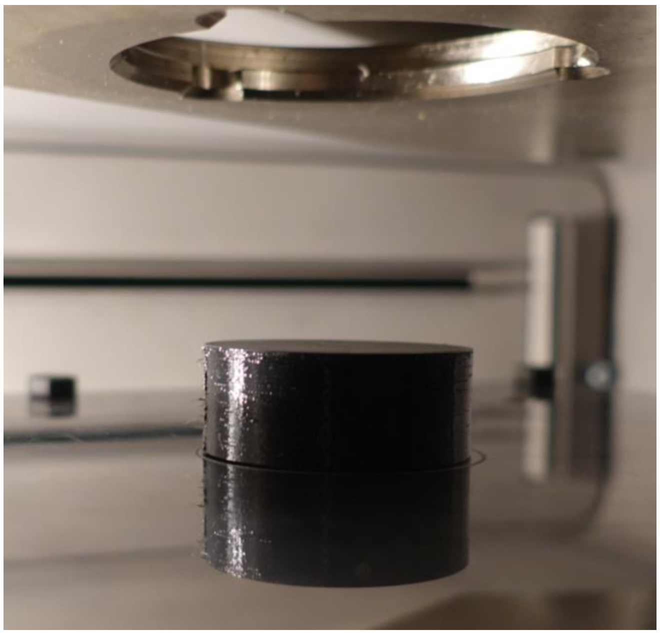

Impact Test Articles are Lattices of 1 mm

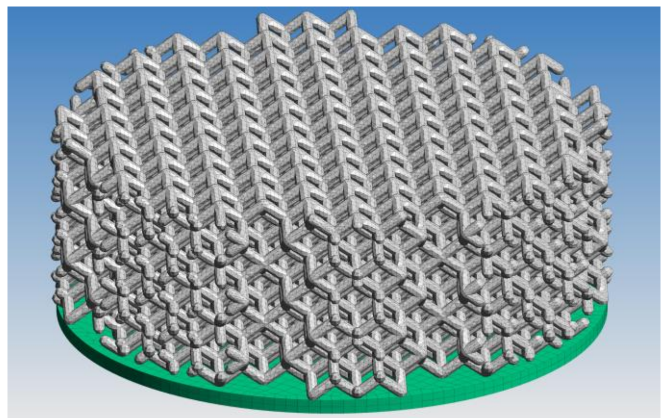

Material 1 test data is between -0.6 and +0.6 Strain

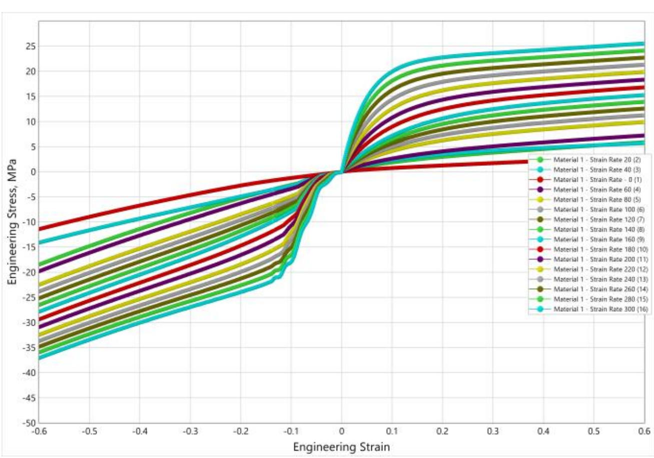

At 10 ft/s, the FEA Strain Far Exceeds the Test Data

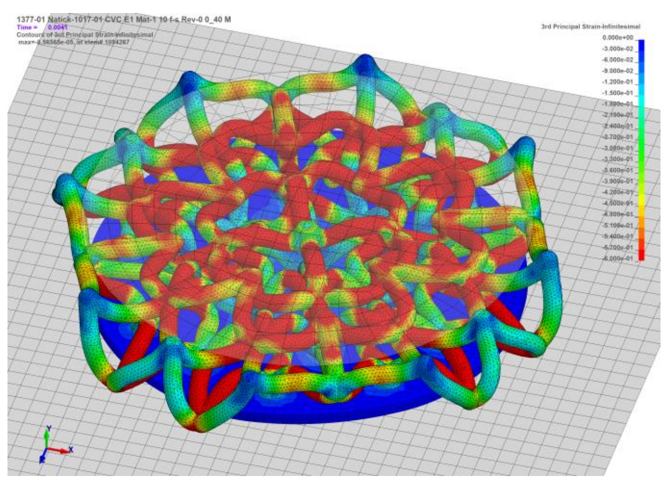

Recommendations for Follow-On Work

Basic Follow-On

Why we should perform this work

Rate dependent material properties for Material 1 were found through impact testing of a puck. The measured data from this test is not representative of the lattice structure as the block's size was shown to be too large (48mm OD x 19.05mm H) for comparison with the strut diameter (1.48 mm) of the lattice. Materials manufactured by additive processes are inherently subjected to localized flaws due to the nature of how each subsequent layer is built on top of one another. Thus, material properties may be inconsistent between each production. However, if the structure is sufficiently large, the overall macromechanical behavior may be unaffected by these flaws. If one is trying to capture the behavior of the lattice, non-standard tests should be performed to build the non-standard material laws.

In short, we should redo the testing strategy of the materials used in this investigation, rebuild the material models and re-work the impact results.

Why it is important

The foundation was laid for the characterization and simulation of additive materials but it is only partially built. This Basic Follow-On work would complete the foundation and provide a complete solution.

Optimization of Additive Materials toward Energy Absorbing Structures

Why we should perform this work

We now build on the prior foundation to explore more efficient methods to characterize and simulate lattice structures. One hypothesis is to look more closely at unit cell blocks. By exploring and optimizing groups of unit cells rather than large, computationally expensive blocks, it is understood that we could move faster and explore more options. By leveraging "lessons learned", new lattice structures will be developed and the most promising will then be combined into blocks for final testing. This effort links modern material modeling techniques into a production strategy that can be used for future developments.

Why it is important

The brute force approach of building large multi-unit cells has its attractions but limits the rate at new structures can be explore. If we are committed to truly accelerating this work, this optimization work must be done prior to the full-on production work of moving additive lattice structures into commercial use.

Applying Energy Absorbing Lattice Structures to Helmet Padding

Why we should perform this work

The final test of this work is its applicability toward the next generation of helmet padding. Candidate structures will be selected from the prior work and tailored to fit within the design envelope of a prototype helmet. Prior to experimental testing, various digital prototypes will be explored. The very best candidate will then be moved forward for testing. Experimental and numerical results will be compared and documented.

Why it is important

There is nothing like the application of research toward the development objective. By digitally prototyping the best candidates and then performing a full-on helmet test, the US Army can be assured that the job was done correctly and that the full benefits of this work can be leverage going forward. Data from this work could then be directly transferred to potential external helmet manufactures with little delay. This is truly where the laboratory drop kicks the results thru the manufacturing goal posts.

1. INTRODUCTION

This work was sponsored by the US Army Natick Soldier Systems Center and details a research investigation into the characterization of additive materials for the simulation of energy absorbing 3D lattice-like structures. The body of this report provides information on the materials studied, how they were characterized through experimental testing, the development of nonlinear, hyperelastic material models and the final correlation between experiment and finite element analysis (FEA) models.

The report first covers testing of the materials to develop FEA material laws, some background on the FEA models and finally, the simulation results for the 3D lattice structures.

2. STATIC TESTING OF ELASTOMERIC MATERIALS

Static testing provides useful baseline data for downstream impact simulations. It also obviously provides the baseline force versus compression response of the material at zero strain rate. Figure 2 shows the test setup with the elastomeric puck placed between the platens.

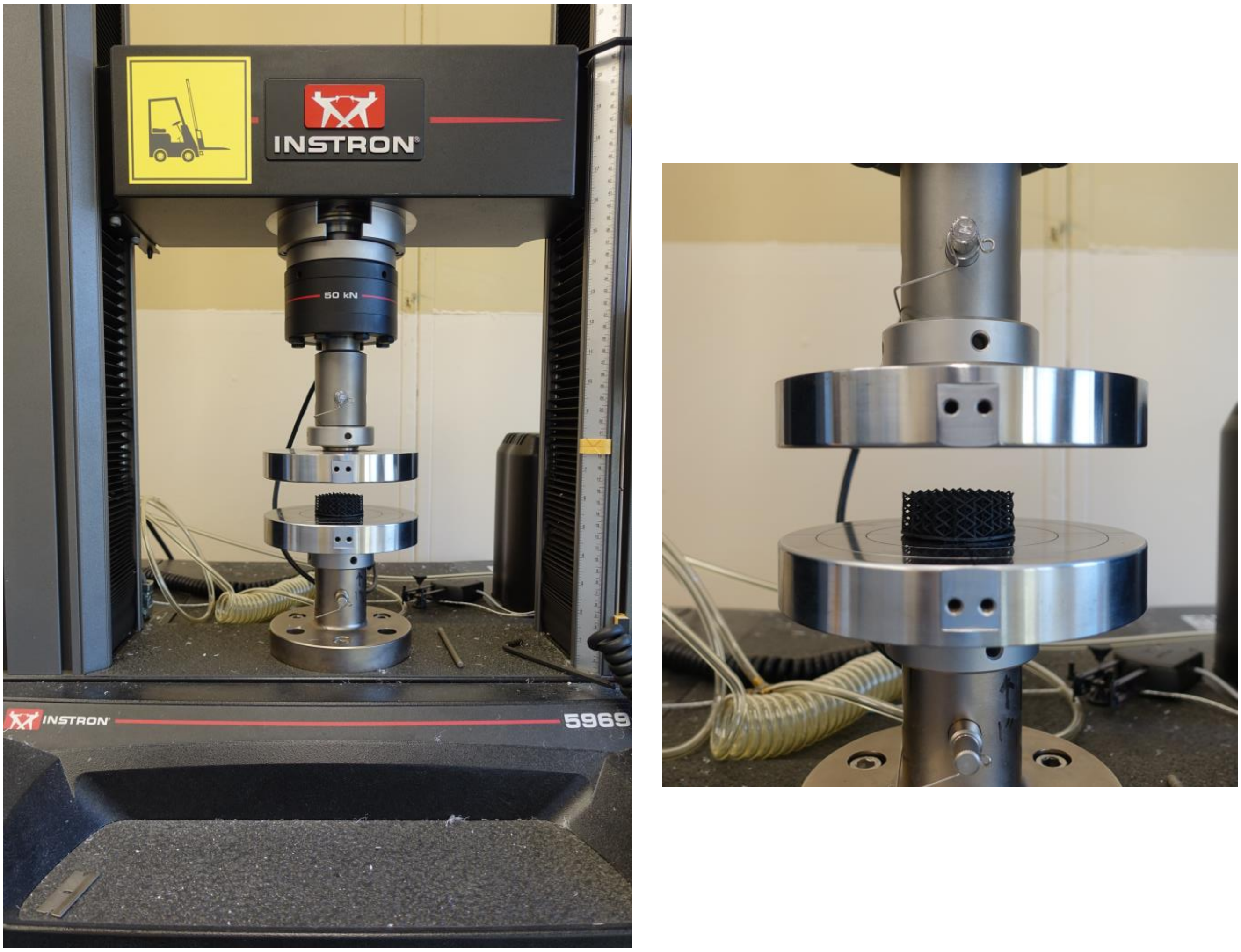

Figure 2: Static test setup

2.1 Static Compression Test Data

Static test data using a puck having a 48 mm diameter and 19.15 mm thick is shown in Figure 3. The raw experimental data was then processed by Natick into a clean curve. The last step is to convert the data into engineering stress versus strain data based on the puck's area (1,810 mm^2) and its height (19.15 mm). At maximum load, the stress in the puck is 21.9 MPa at an engineering strain of 52%.

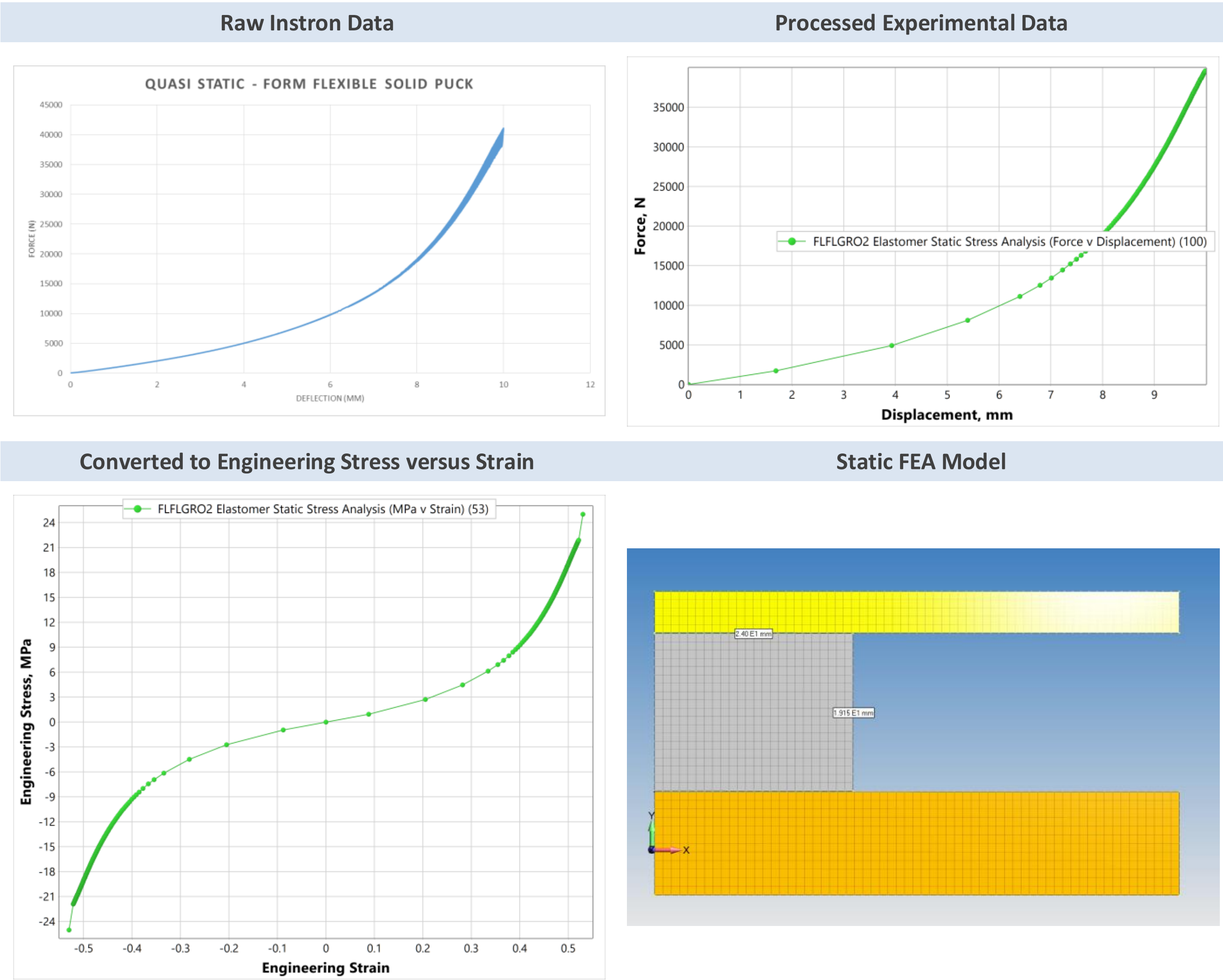

Figure 3: Static experimental test data

2.2 Static FEA Test Results

To verify the FEA static material model, the experimental test was simulated. Results from this simulation are shown in Figure 4. The top image shows the stress in the hockey puck under a 10 mm displacement. It is assumed that the platens do not restrain the elastomeric material. The bottom image shows the experimental and FEA results. The experiment and FEA results align closely. This verifies the FEA material model.

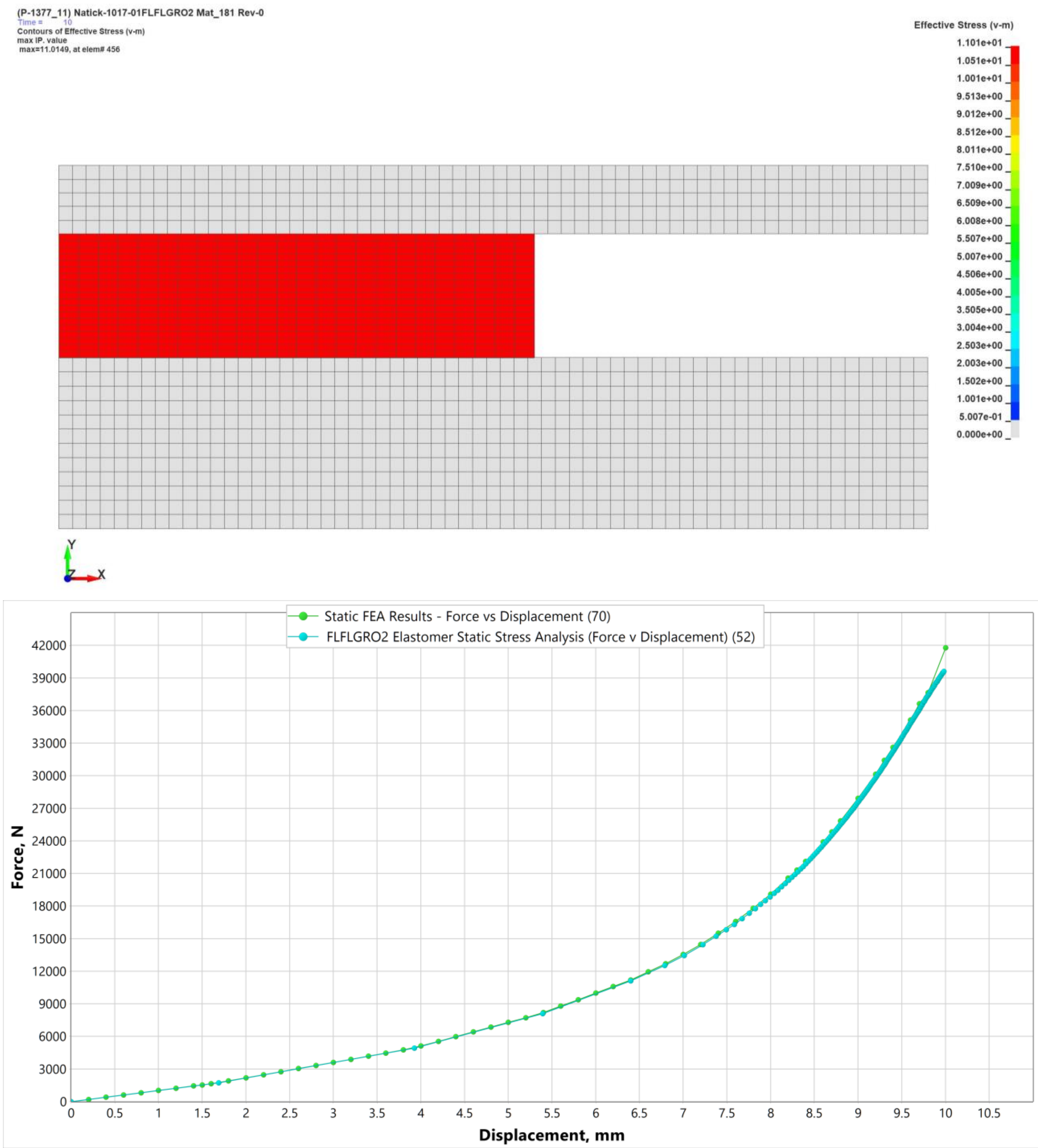

Figure 4: Static FEA and experimental results

3. IMPACT TESTING OF ELASTOMERIC MATERIALS

Figure 5 shows the experimental setup used to generate impact data of the various elastomers investigated in this report. Some test specifications: (i) total striker mass = 3.104 kg; (ii) Anvil = 1.00 inch thick stainless steel plate; (iii) Striker diameter = 50mm and (iv) Sample "puck" dimensions = 48 mm OD x 19.05 mm H. The impact rate is by striker head velocity: 10 feet per second (FPS) (3,048 mm/s), 14.1 FPS (4,300 mm/s) and 17.3 FPS (5,270 mm/s). During impact, data was sampled at 1,000 kHz or one data point at every μs. Testing conditions were performed under ambient (~21 °C) temperature.

Figure 5: Experimental setup to generate impact data on elastomeric materials

3.1 Example of Impact Data

An example of the type of experimental data generated during the impact test is shown in Figure 6.

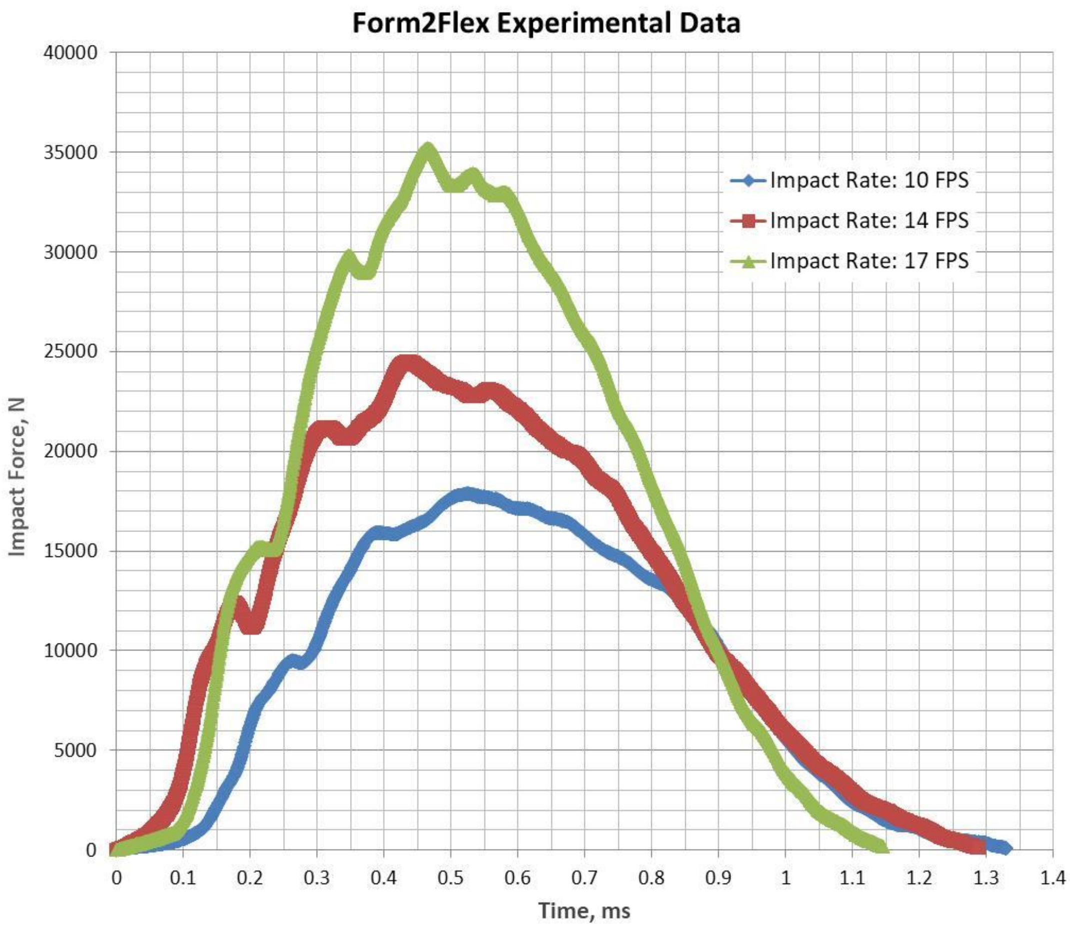

Figure 6: Elastomeric experimental impact data

4. FEA IMPACT MODEL

4.1 Idealization of Geometry into Axisymmetric FEA Model

Figure 7 shows the starting geometry provided by Natick, the idealization process and then the final axisymmetric FEA model. The FEA model shows the puck having a radius of 24 mm and a thickness of 19 mm and ties with the puck information provided by Natick (see Section 2).

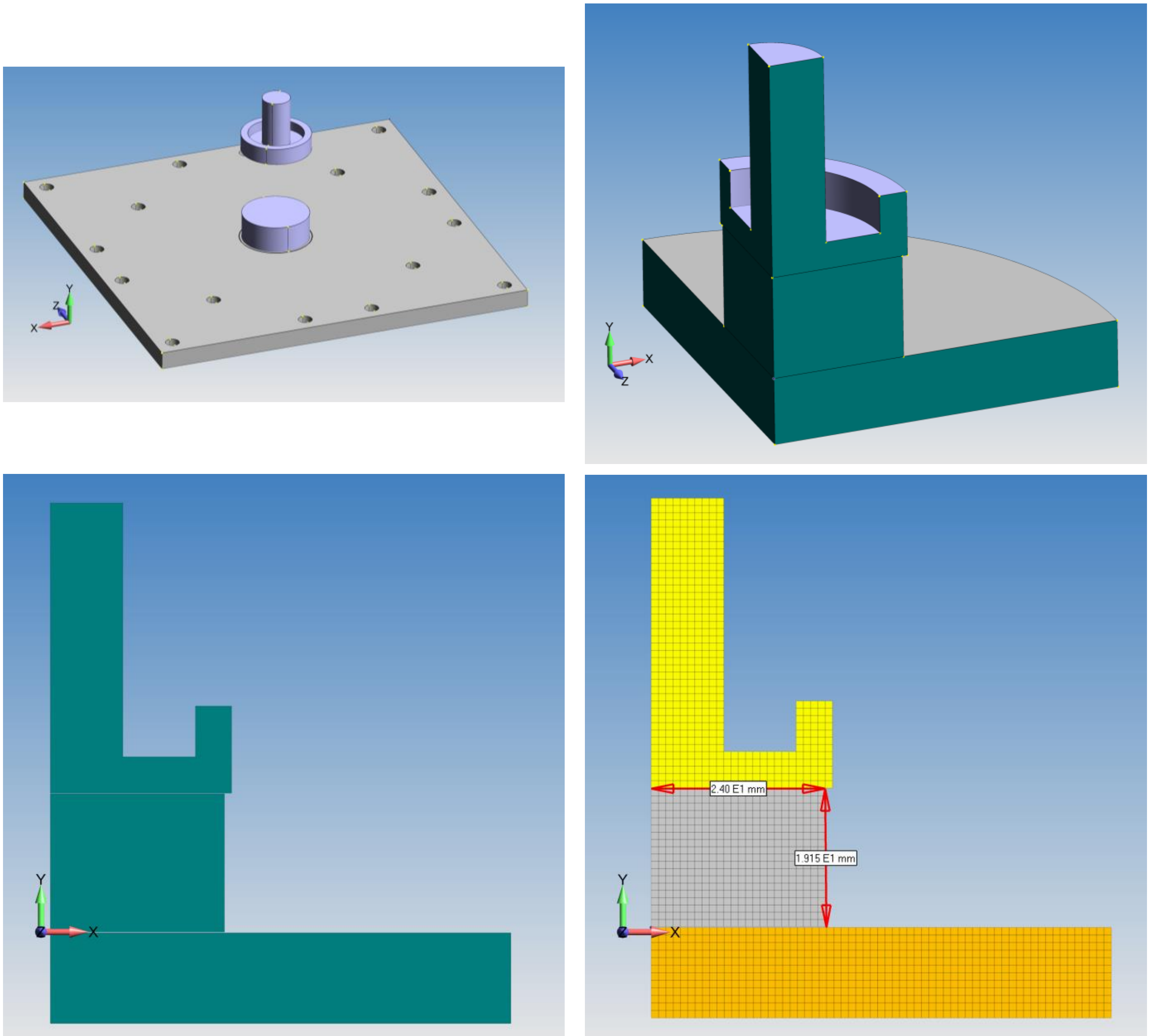

Figure 7: Impact geometry to axisymmetric FEA model

4.2 Unit System

The FEA model uses a SI system with N, mm, s and Tonne. Stresses are then calculated as MPa. As an example, the density of steel is $7.83\text{x}10^{-9}$ tonne/mm^3. The impact velocity is likewise converted from FPS to mm/s.

4.3 FEA Model Setup for Impact Testing

The impact hammer is given an initial velocity equivalent to the desired FPS. The hammer and base are modeled as rigid materials since steel as compared to elastomeric materials is equivalent to a rigid analogy. The mass of the hammer is set to impact weight of 0.0031 tonne (3.1 kg). The axisymmetric FEA model reports mass on a per radian basis. Figure 8 provides verification data on the impact hammer's mass.

Natick-1017-01 Analysis Worksheet

$$\text{Impact}_{\text{Velocity}} := 17.3 \cdot \frac{\text{ft}}{\text{s}} = 5.273 \times 10^{3} \cdot \frac{\text{mm}}{\text{s}}$$

Impact Hammer Mass $\qquad \text{Impact}_{\text{Hammer}} := 0.003104 \cdot \text{tonne}$

LS-DYNA is by radian: $\qquad \text{Impact}_{\text{Hammer\_DYNA}} := \frac{\text{Impact}_{\text{Hammer}}}{2 \cdot \pi} = 4.94 \times 10^{-4} \cdot \text{tonne}$

```
⊟ summary of mass
   part id  =   1  mass= 0.10972734E-04
   part id  =   2  mass= 0.49401424E-03 rigid body
   part id  =   3  mass= 0.17641058E-03 rigid body
⊟ total mass    = 0.68139755E-03
   mass center: 20.7657, 21.3302, 3.27344e-16
```

Figure 8: Verification of impact hammer mass on per radian basis

This covers the major features of the impact model: (i) initial impact velocity and (ii) correct application of impact hammer mass. Another detail to note is that contact is enforced using a 2D formulation.

5. PHASE I

5.1 WORK OUTLINE

Develop 2D axisymmetric "puck" Model – this model will duplicate the impact test being performed at NSRDEC to collect material properties of various "3D printed" elastomers. The model will consist of a flat rigid anvil with an elastomer "puck" resting above. A rigid striker will be dropped onto the "puck" where mechanical properties of the elastomer will be collected.

a) Three materials models will be developed based on dynamic impact data provided by NSRDEC (three relevant velocities for each material).
b) The model will first be used to replicate the dynamic impact test to ensure a close match with each of the three material models
c) Once the material models are validated an optimization model will be developed and implemented to identify an ideal lattice/open structure for the 2D axisymmetric case
d) Finally a report documenting Phase I will be written.

5.1.1 INTERDEPENDENCIES

- Raw dynamic mechanical test data from three different materials
- Mechanical test set up information and pictures

5.1.2 DELIVERABLES

- Three material models which reasonably match mechanical response from real world test
- Phase 1 report
    - Results from the 2D axisymmetric FEA model showing a close match to real world test results ("solid puck")

Table 4 provides a graphical summary of the material modeling work in two graphs. The graphs show the material model correlation to impact tests at 10, 14 and 17 ft/s. Due to difficulties in the material modeling process, only two materials were characterized.

Table 4: Summary of Phase I results showing material modeling and correlation to impact test

Material 1: Form2Flex / FLFLGRO2 – Photopolymer Resin	Material 2: Carbon EPU40
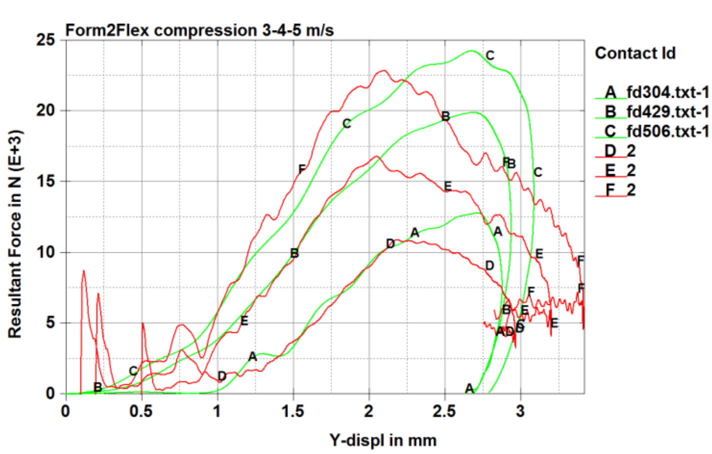	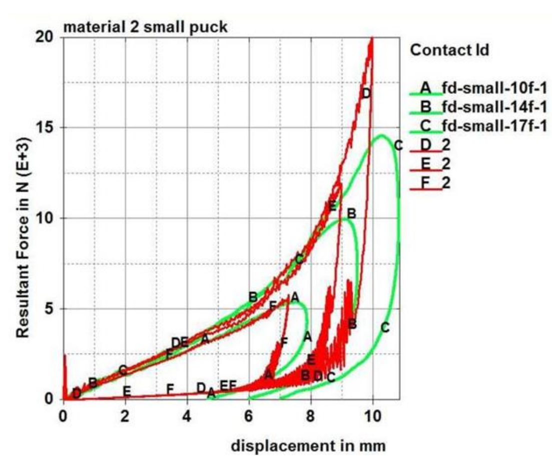

5.1.2.1 FEA Impact Material Models

Figure 9 shows the implementation of the material modeling results in the FEA model. The strain rate dependent curves are given from static (0) to 300 strain per second.

Material 1: Form2Flex / FLFLGRO2 – Photopolymer Resin

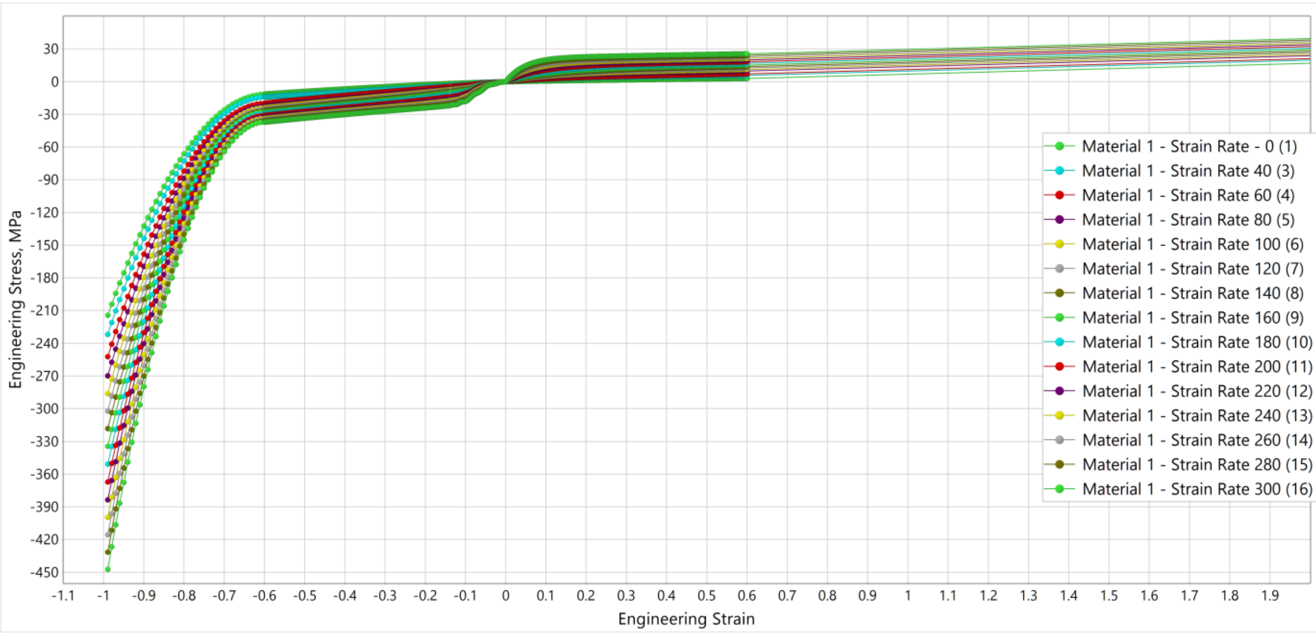

Material 2: Carbon EPU40

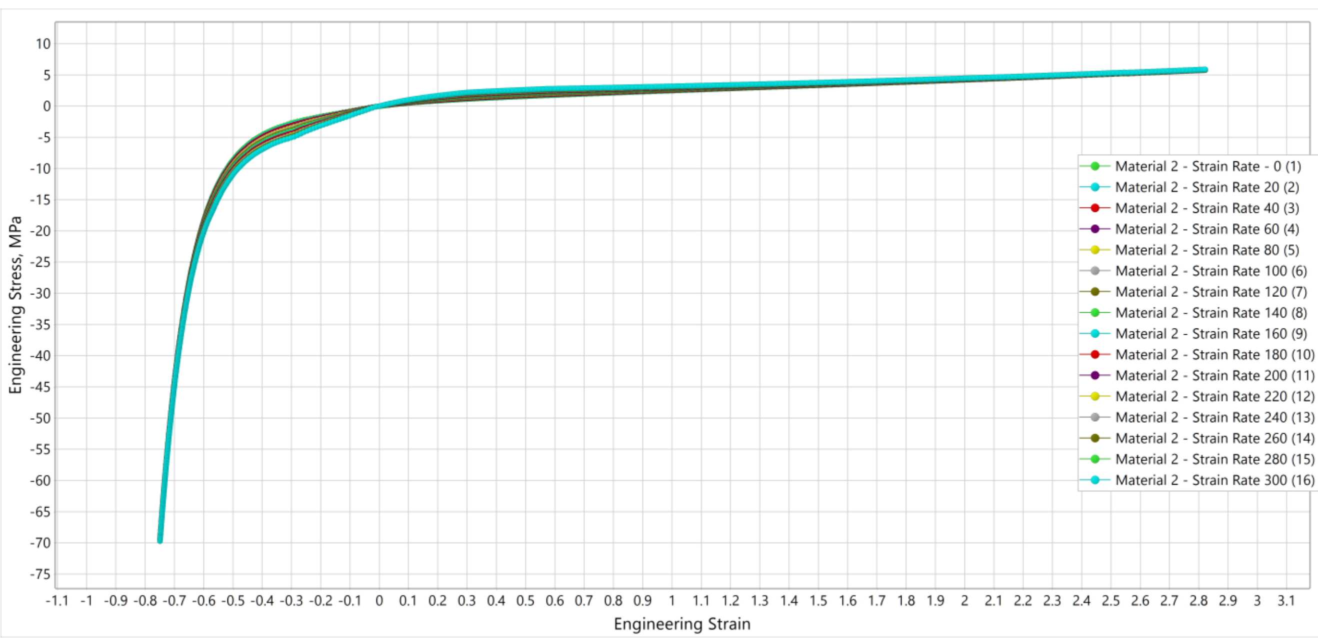

Figure 9: FEA material modeling results for Material 1 and Material 2

Figure 10 shows a close-up view of the same curves.

Material 1: Form2Flex / FLFLGRO2 – Photopolymer Resin

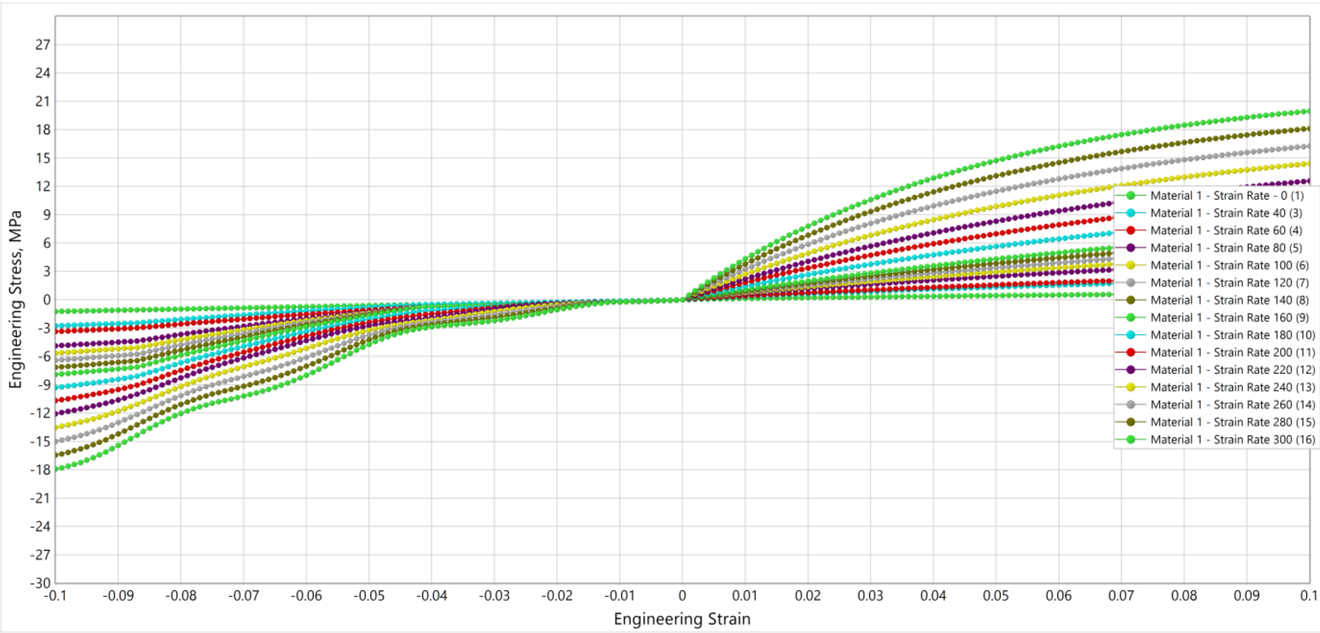

Material 2: Carbon EPU40

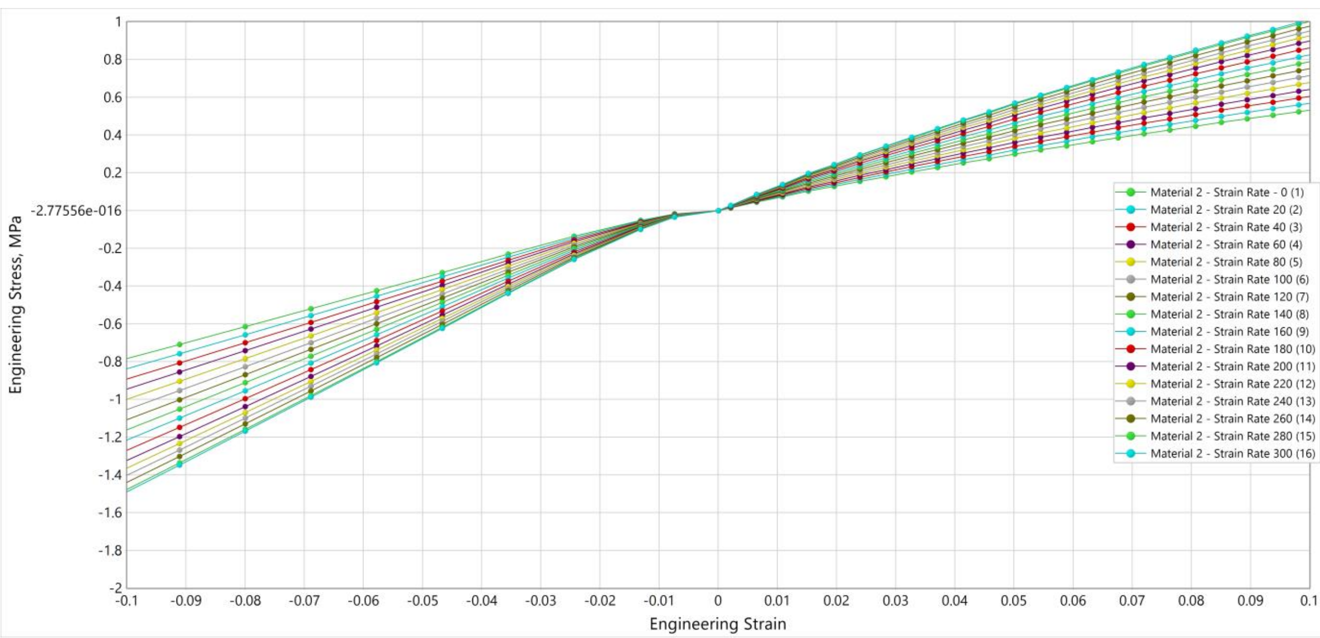

Figure 10: Close-up view of FEA material modeling results for Material 1 and Material 2

6. PHASE II

6.1 Work Outline

Develop 3D "puck" Model - this model will duplicate the impact test being performed at NSRDEC to collect material properties of various "3D printed" elastomers. The model will consist of a flat rigid anvil with an elastomer "puck" resting above. A rigid striker will be dropped onto the "puck" where mechanical properties of the elastomer will be collected. In the 3D version geometries can become more complicated, truss or lattice structures can now develop in all three dimensions.

a) The 3D model will first be used to replicate the dynamic impact test to ensure a close match with each of the three material models
b) Once the material models are validated an optimization model will be developed and implemented to identify an "ideal" lattice/open structure for the 3D case
c) Finally a report documenting Phase I will be written.

6.1.1 Interdependencies

- CAD geometries to assist in feeding the optimization models
    - Not all CAD geometries will be provided by NSRDEC, Predictive Engineering is encouraged to develop their own geometries, collaborate with NSRDEC to develop new geometries and create geometries based on outputs from optimization modeling; the provided geometries are intended to be a starting point

6.1.2 Deliverables

- Phase II report
    - Results from the 3D FEA model showing close match to real world test results
    - Results from 3D lattice/open structure optimization model

6.2 Lattice Structures

6.2.1 Geometry CVC E1

Figure 11 shows the lattice structure of the Cubic Vertex Centroid (CVC) E1 model. The impact energy absorption will be measured at three striker velocities: 10, 14.1 and 17.3 ft/s. The striker has a mass of 3.104 kg with a diameter of 50mm. The testing was performed at ambient temperature.

Figure 11: Lattice structure for CVC E1

6.2.2 Geometry CBS E1

Figure 12 shows the lattice structure of the Cubic Beam Sphere (CBS) E1 model. The impact energy absorption will be measured at three striker velocities: 10, 14.1 and 17.3 ft/s. The striker has a mass of 3.104 kg with a diameter of 50mm. The testing was performed at ambient temperature.

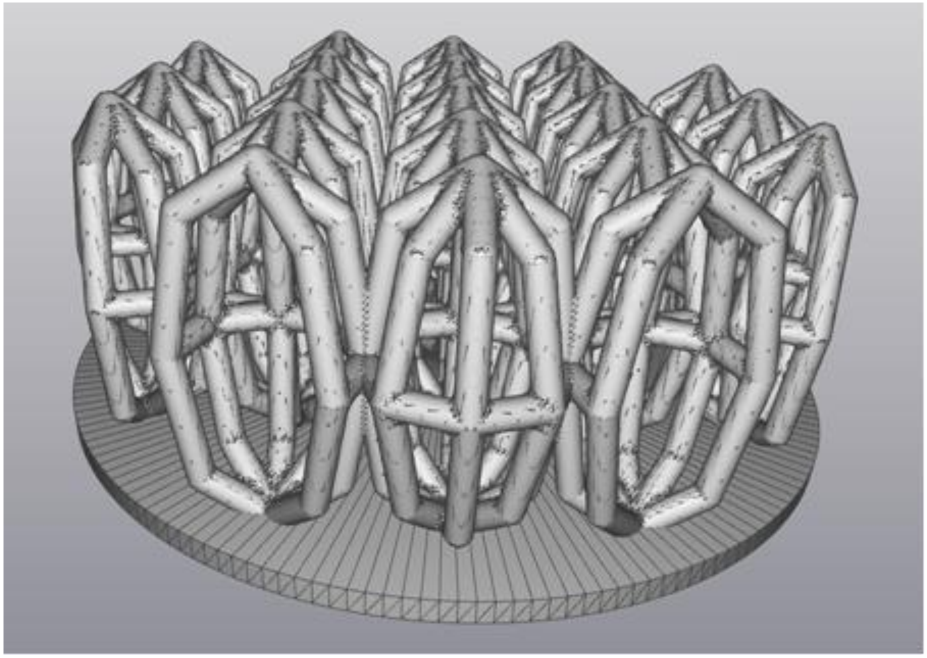

Figure 12: Lattice structure for CBS E1

6.2.3 Geometry CF A1

Figure 13 shows the lattice structure of the Cubic Fluorite (CF) A1 model. The impact energy absorption will be measured at three striker velocities: 10, 14.1 and 17.3 ft/s. The striker has a mass of 3.104 kg with a diameter of 50mm. The testing was performed at ambient temperature.

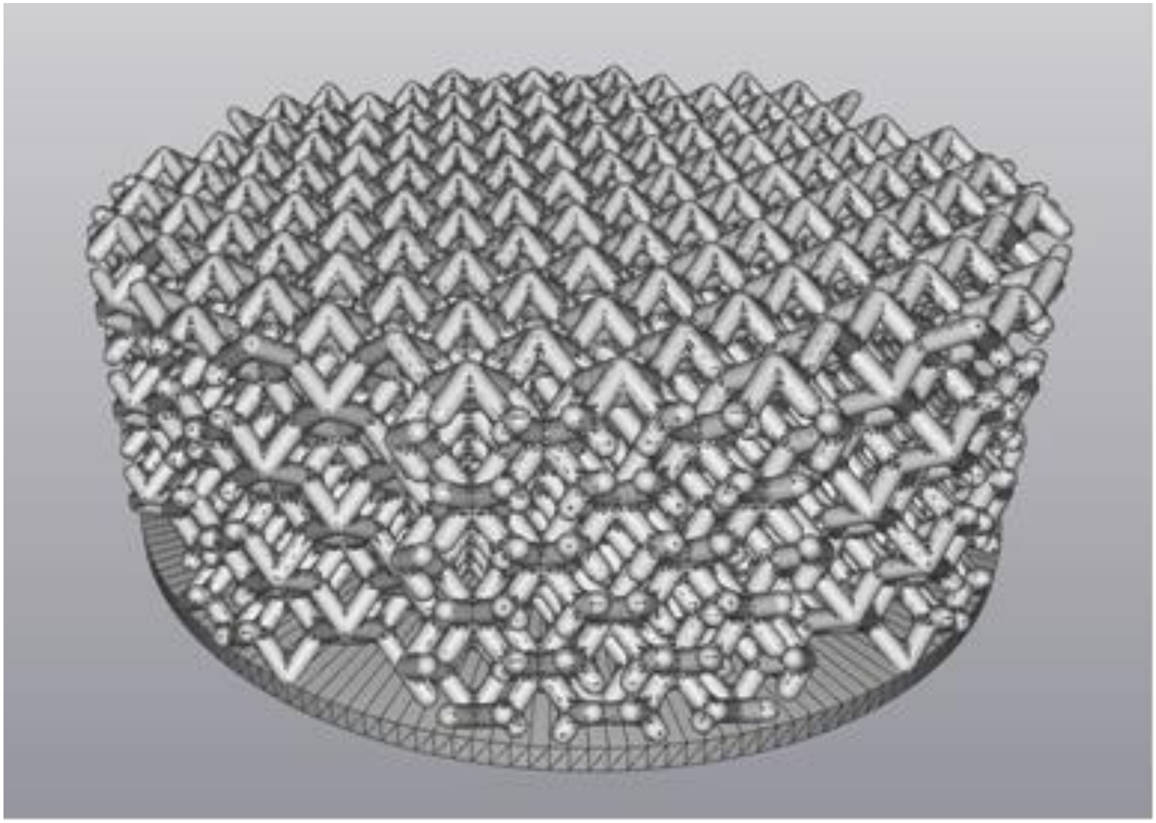

Figure 13: Lattice structure for CF A1

6.2.4 MESHING

An example of the meshing procedure is presented using the CBS E1 geometry. The lattice structure was first seeded with a global mesh size of 0.45 mm. After which, 4-noded solid tetrahedral elements were meshed onto the surface of the solid geometry. The element quality was checked by contouring the mesh with the Jacobian, as seen in top left image in Figure 14. An isoparametric element has the best quality (i.e. no distortion) with a Jacobian of 0.0 (note: normally this value is 1.0, but FEMAP uses a normalized Jacobian, so 0.0 is ideal). Elements with a high Jacobian were resized to reduced element distortion. This process can be seen in the top right and bottom left images of Figure 14. After the mesh was fully refined, 4-node tetra elements were generated with a 1:1 growth ratio through the volume of the solid to complete the mesh. As a final quality check, the explicit time step was contoured to verify that the elements were of uniform size. This is shown in the bottom right image of Figure 14. The tetra element formulation is ELFORM=13. The base of the lattice was meshed using 8-noded hex elements with ELFORM=-1. The bottom surface nodes of the lattice were tied to the base. A similar meshing procedure was performed for all geometries. The final meshes of the geometries, including the rigid element platens, are shown below in Figure 15 - Figure 17.

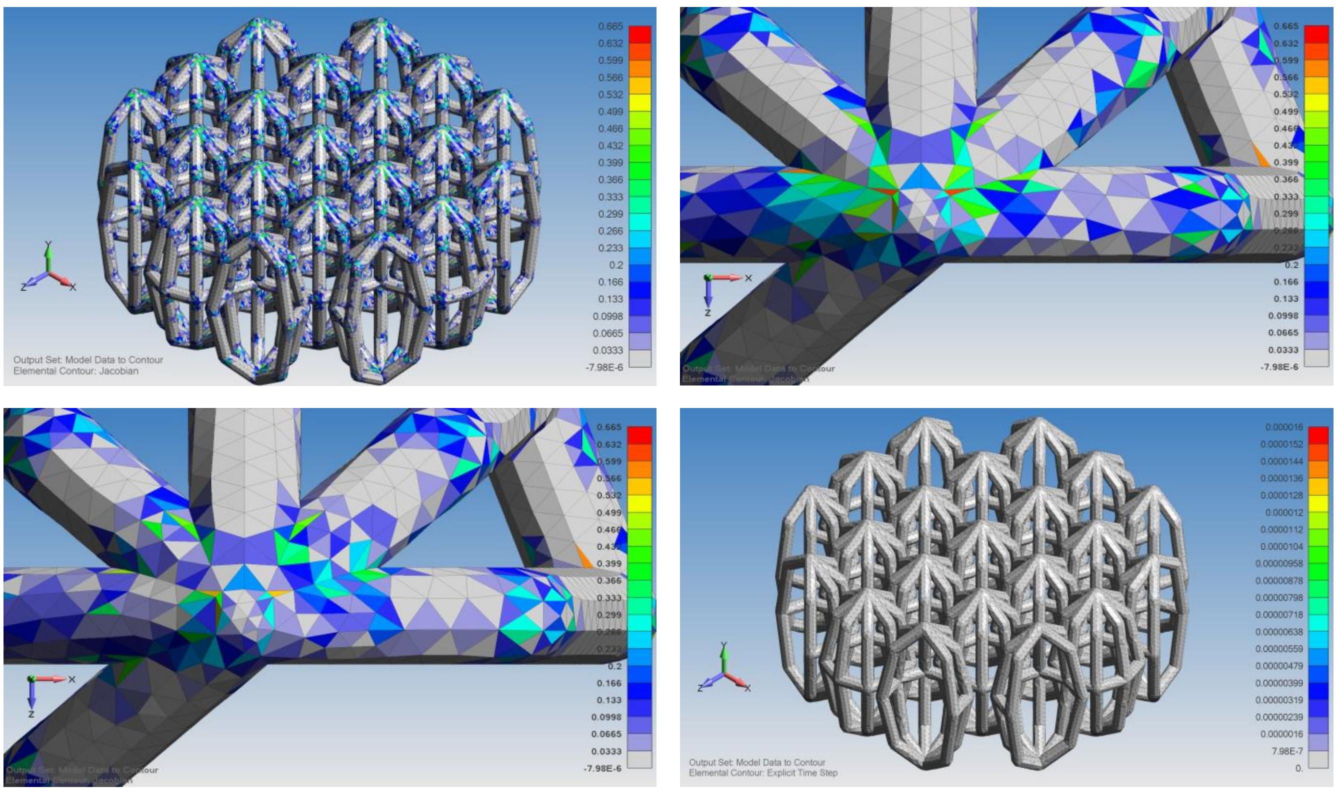

Figure 14: Element quality checks using Jacobian and explicit time step contours

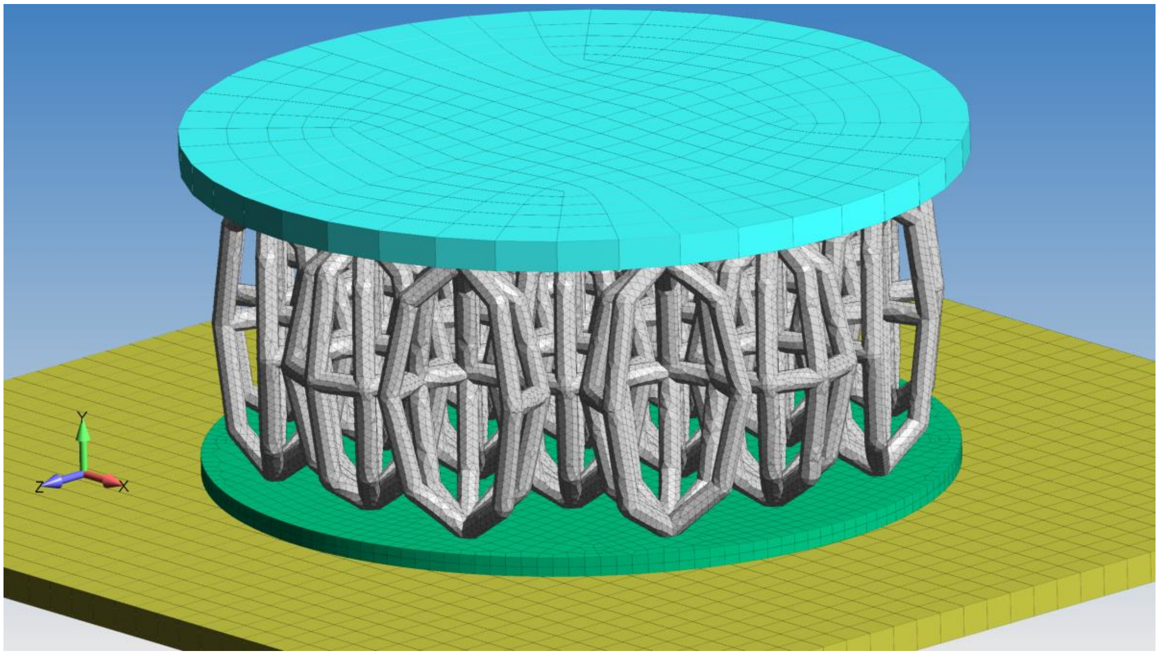

Figure 15: CBS E1 Mesh

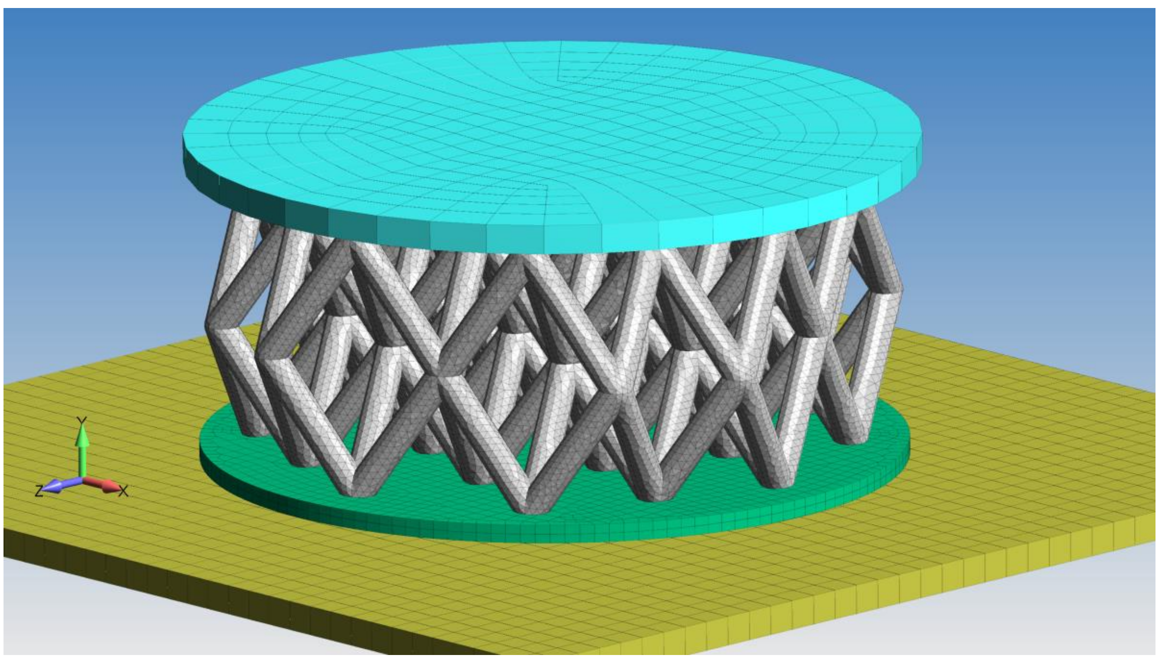

Figure 16: CVC E1 Mesh

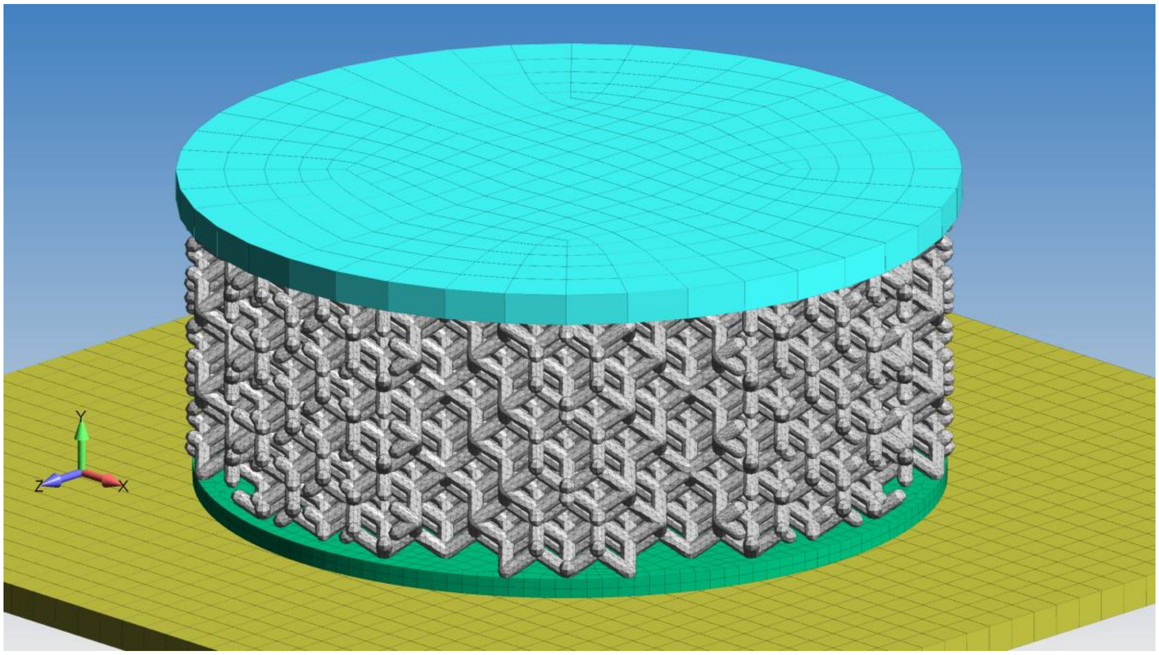

Figure 17: CF A1 Mesh

6.3 Numerical Impact Testing Results

Results are presented for Material 1 and Material 2 in a sequence of geometries CVC E1, CBS E1 and CF A1. The analyses were conducted using the same contact specifications and with a friction of 0.3 between all components. The mass of the striker was fixed at 3.104 kg for all numerical testing. The sliding interface energy (SLE) for the lattice was compared against the internal energy (IE) to provide verification of the analyses numerical behavior with respect to contact. The sliding interface energy is the energy required to prevent interpenetrations between contacting adjacent mesh surfaces. In the absence of friction, this value is artificial and should be positive. If the ratio between SLE/IE exceeds 10%, too much energy was artificially introduced into the system, thus indicating a need for refinement. Likewise, when friction is included, this value should be positive. A negative value for SLE is caused by undetected initial penetrations and is undesirable as it is not realistic. Negative SLE can be resolved by refining the mesh and/or decreasing the explicit time step. The objective for all simulations was that the SLE/IE ratio should be around 10%. For each run, the maximum impact force is given along with plots of strain rate.

6.3.1 Material 1

6.3.1.1 CVC E1

Impact test results for CVC E1 are shown in Figure 18 through the time sequence up to full impact. The first image is the force versus displacement curve for the impact followed by images of the lattice structure being compressed. The mesh is contoured with the strain rate. The legend is capped at 300 strain/sec and is the maximum strain rate that was captured in the material law formulation. The ratio of SLE/IE = 0.8k/13.0k and the maximum impact force is 10 kN.

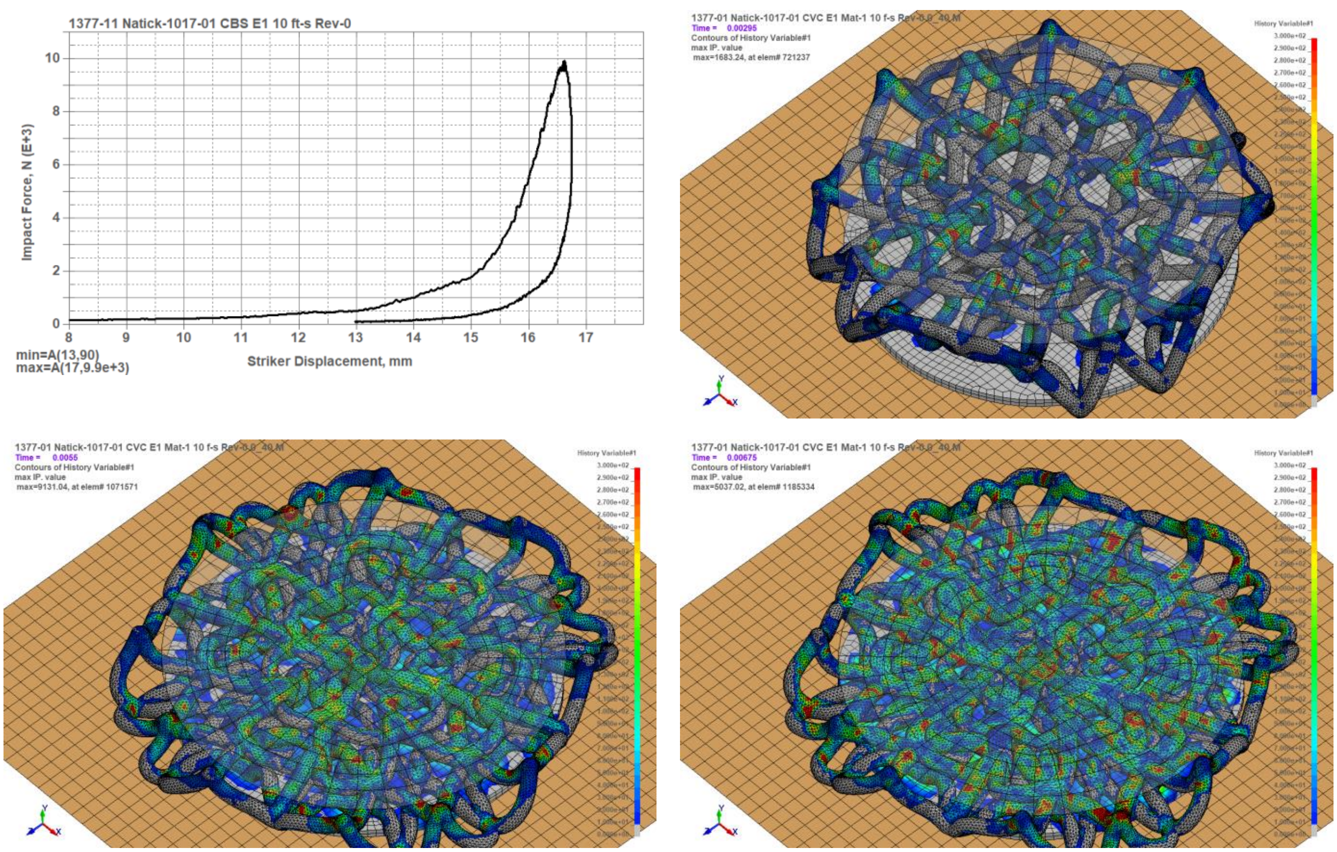

Figure 18: Impact analysis of CVC E1 Material 1 at 10 ft/s

6.3.1.2 CBS E1

Impact test results for CBS E1 are shown in Figure 19 through the time sequence up to full impact. The first image is the force versus displacement curve for the impact followed by images of the lattice structure being compressed. The mesh is contoured with the strain rate. The legend is capped at 300 strain/sec and is the maximum strain rate that was captured in the material law formulation. The ratio of SLE/IE = 1.5k/13k and the maximum impact force is 13 kN.

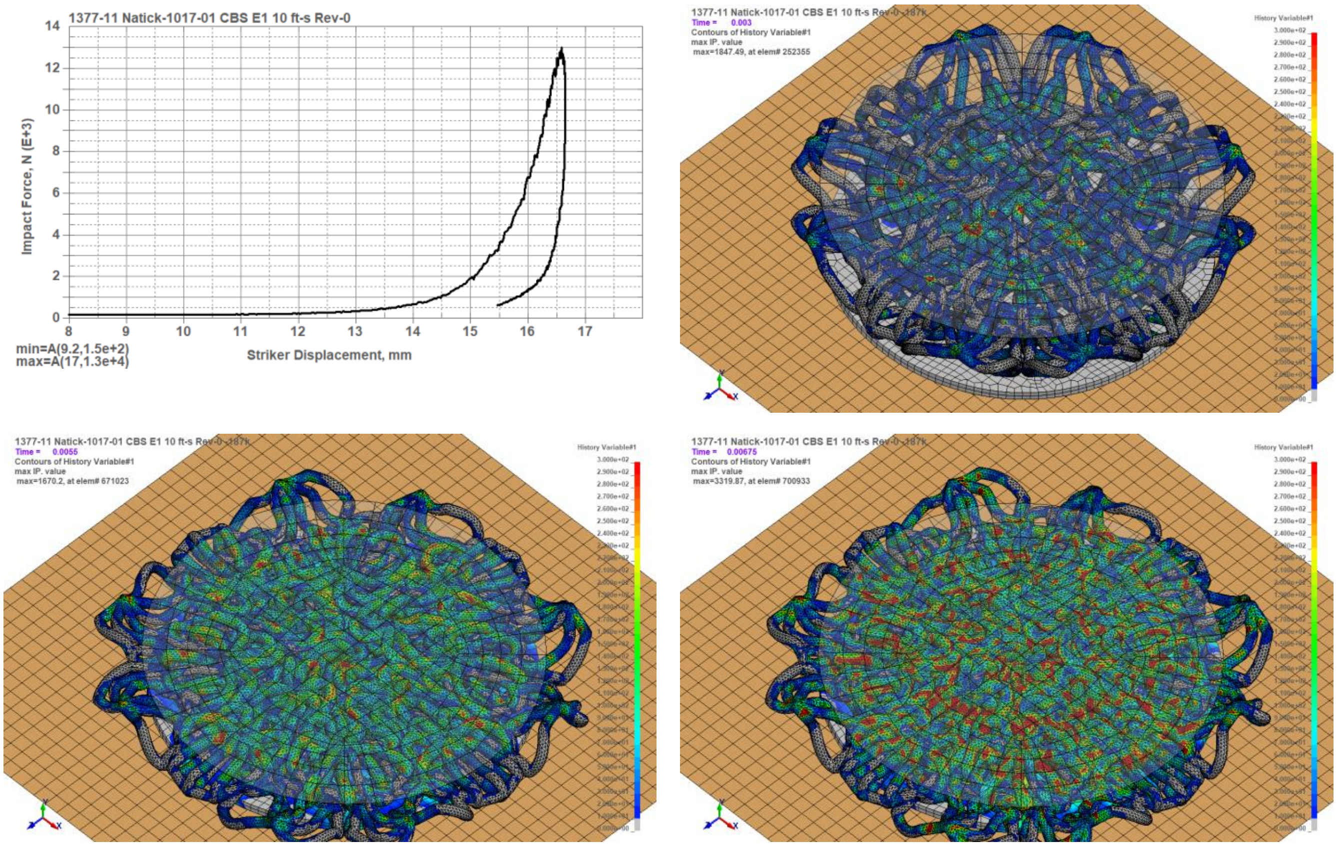

Figure 19: Impact analysis of CBS E1 Material 1 at 10 ft/s

6.3.1.3 CF A1

Impact test results for CF A1 are shown in Figure 20 through the time sequence up to full impact. The first image is the force versus displacement curve for the impact followed by images of the lattice structure being compressed. The mesh is contoured with the strain rate. The legend is capped at 300 strain/sec and is the maximum strain rate that was captured in the material law formulation. The ratio of SLE (Mat 1 only)/IE = 0.8k/13k and the maximum impact force is 8.4kN.

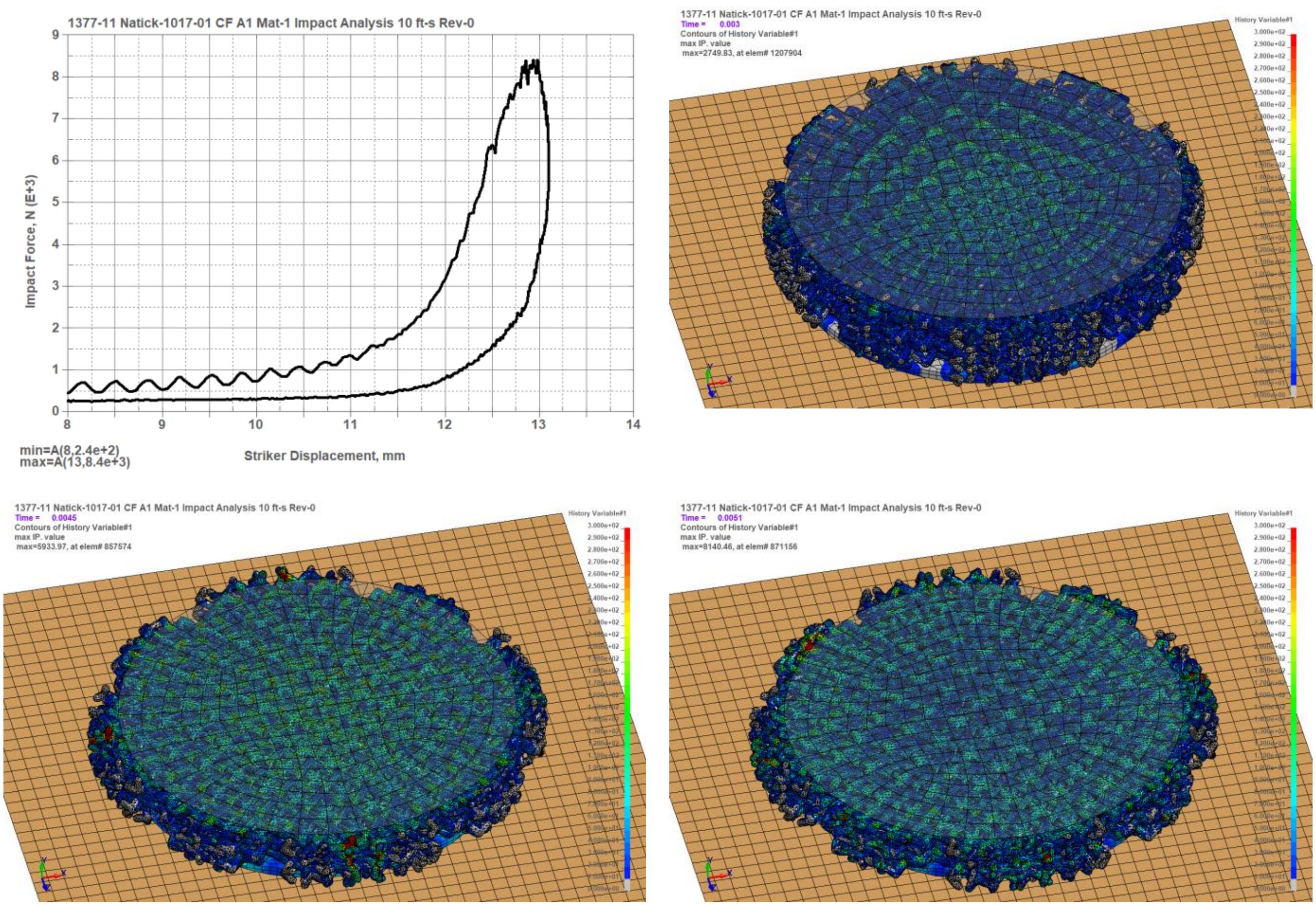

Figure 20: Impact analysis of CF A1 Material 1 at 10 ft/s

6.3.2 MATERIAL 2

6.3.2.1 CVC E1

Impact test results for CVC E1 are shown in Figure 21 through the time sequence up to full impact. The first image is the force versus displacement curve for the impact followed by images of the lattice structure being compressed. The mesh is contoured with the strain rate. The legend is capped at 300 strain/sec and is the maximum strain rate that was captured in the material law formulation. The ratio of SLE/IE = 1.4k/12k and the maximum impact force is 21 kN.

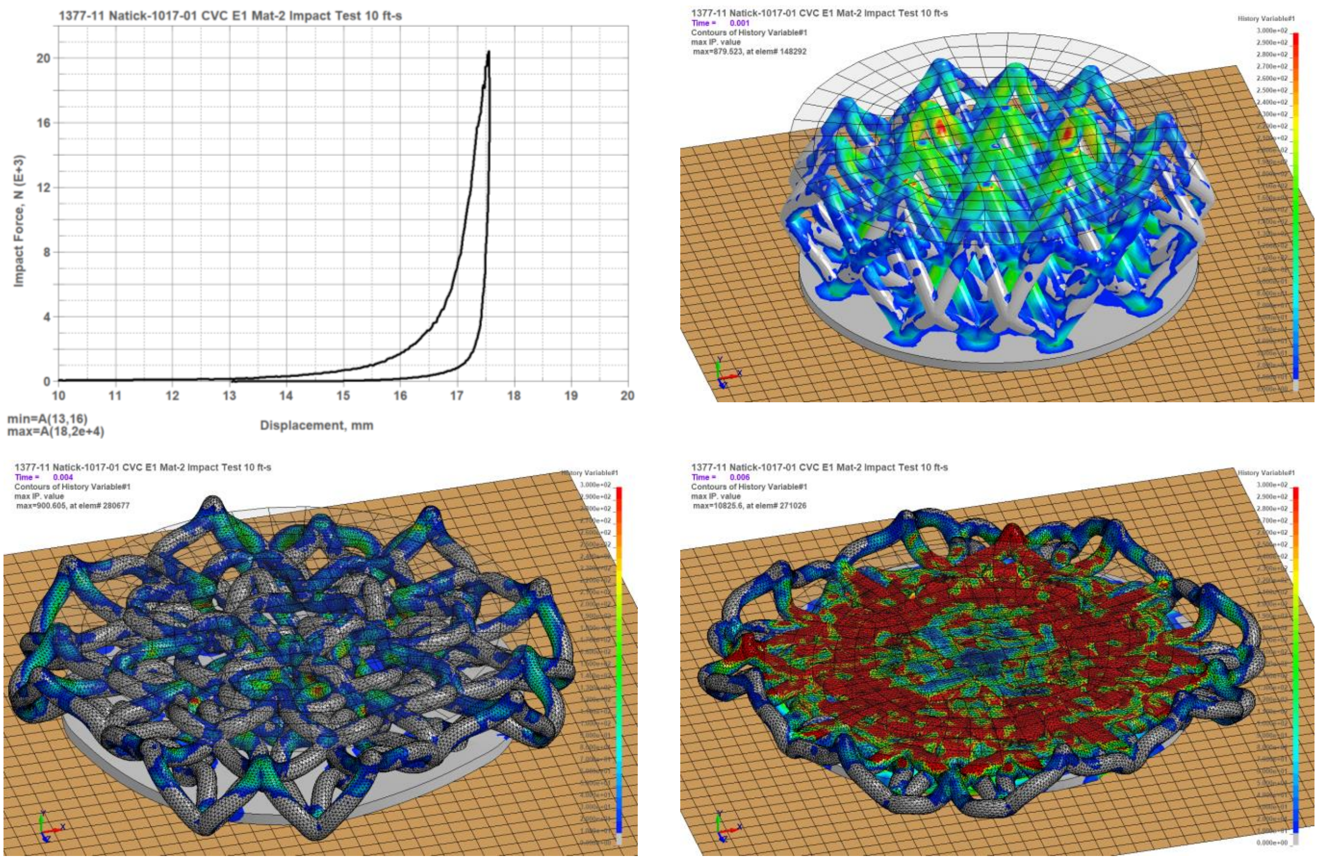

Figure 21: Impact analysis of CVC E1 Material 2 at 10 ft/s

6.3.2.2 CBS E1

Impact test results for CBS E1 are shown in Figure 22 through the time sequence up to full impact. The first image is the force versus displacement curve for the impact followed by images of the lattice structure being compressed. The mesh is contoured with the strain rate. The legend is capped at 300 strain/sec and is the maximum strain rate that was captured in the material law formulation. The ratio of SLE/IE = 2.3k/11.0k and the maximum impact force is 21 kN.

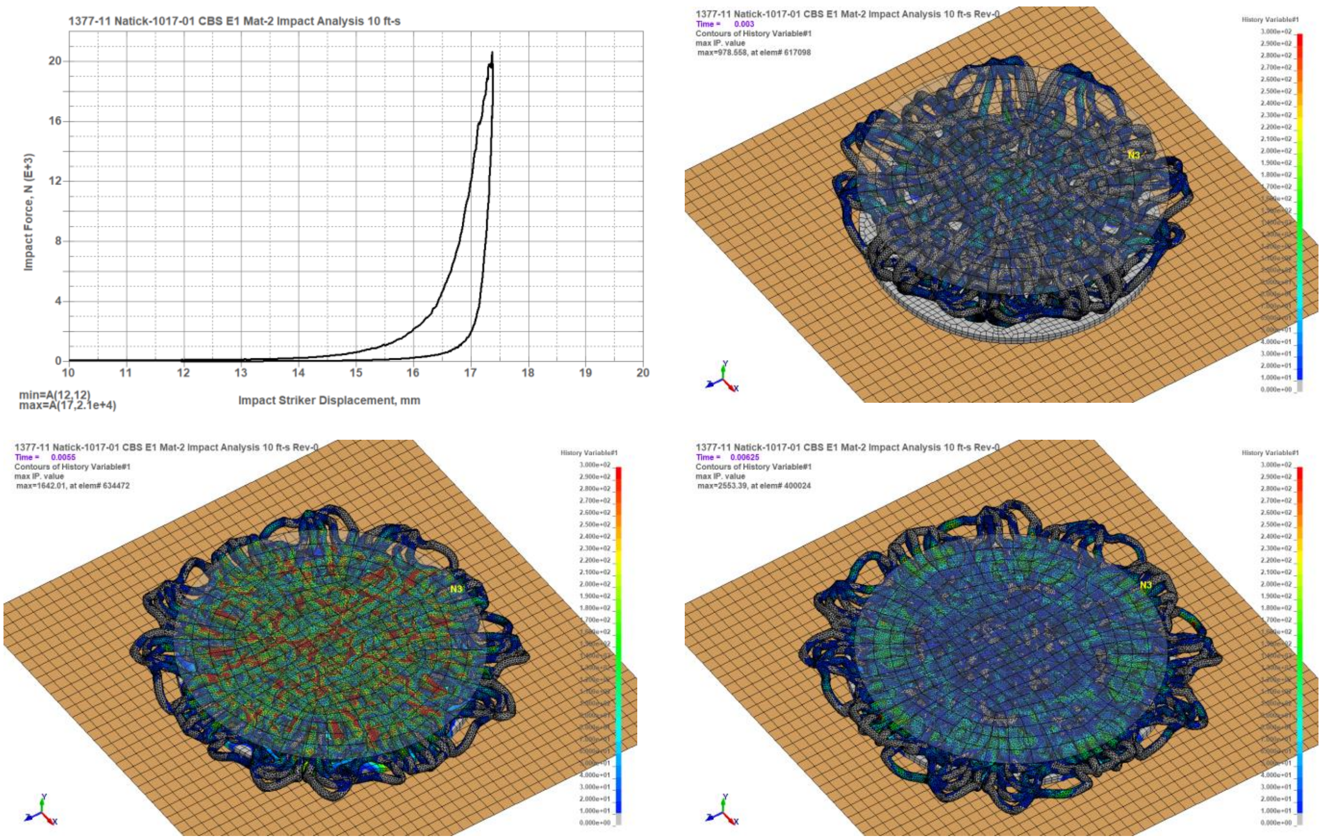

Figure 22: Impact analysis of CBS E1 Material 2 at 10 ft/s

6.3.2.3 CF A1

Impact test results for CF A1 are shown in Figure 23 through the time sequence up to full impact. The first image is the force versus displacement curve for the impact followed by images of the lattice structure being compressed. The mesh is contoured with the strain rate. The legend is capped at 300 strain/sec and is the maximum strain rate that was captured in the material law formulation. The ratio of SLE (Mat 1)/IE = 0.9k/13k and the maximum impact force is 13 kN.

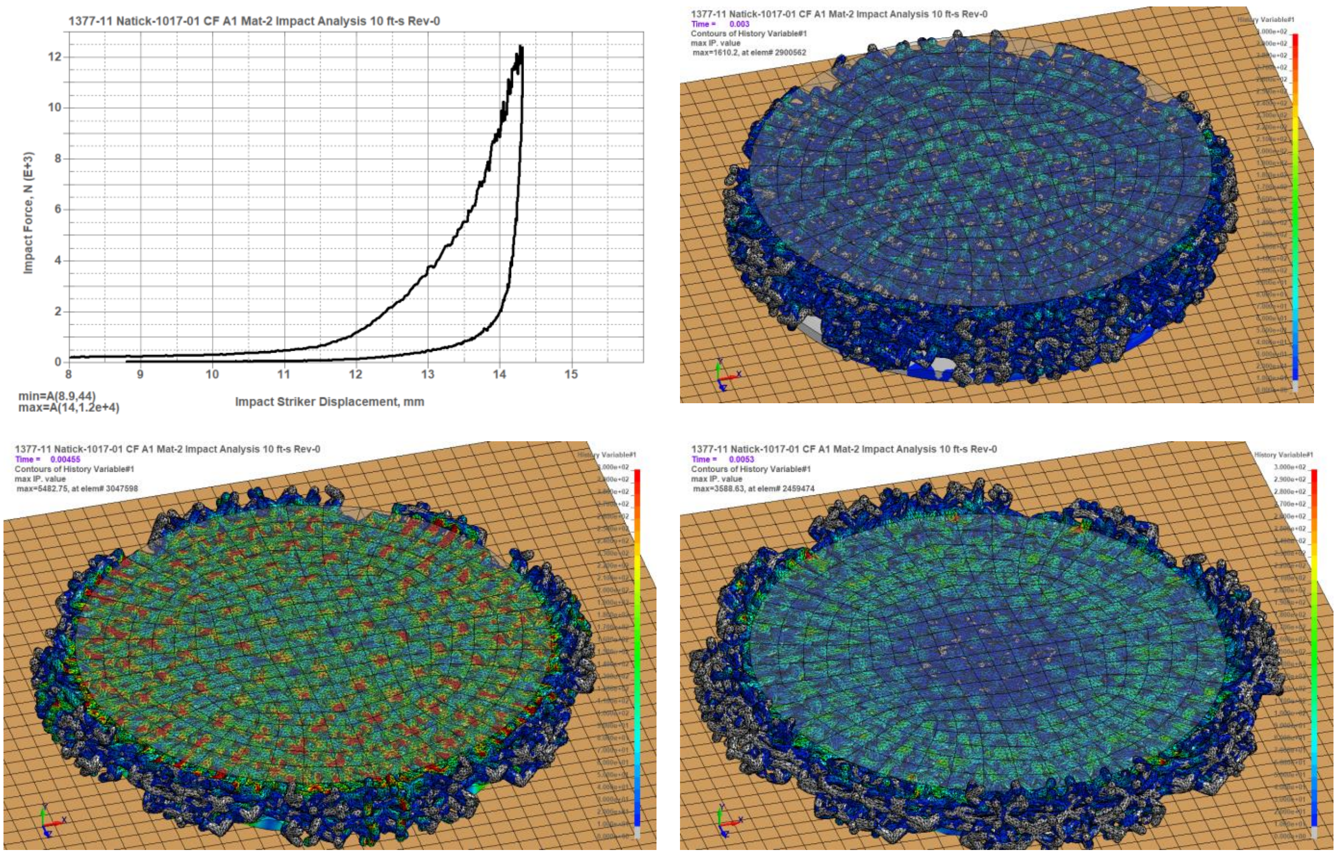

Figure 23: Impact analysis of CF A1 Material 2 at 10 ft/s

7. APPENDIX

7.1 Material Modeling

7.1.1 Material 1: FloFloGro2

7.1.1.1 Quasi-Static Response

The experimental test data for the tensile and compression tests are shown below in Figure 24.

Experimental Data: Tensile Tests	Experimental Data: Compression Tests
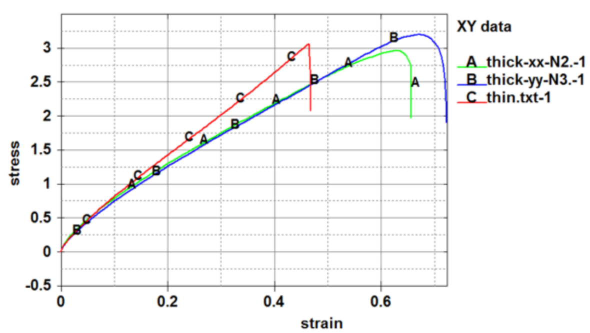	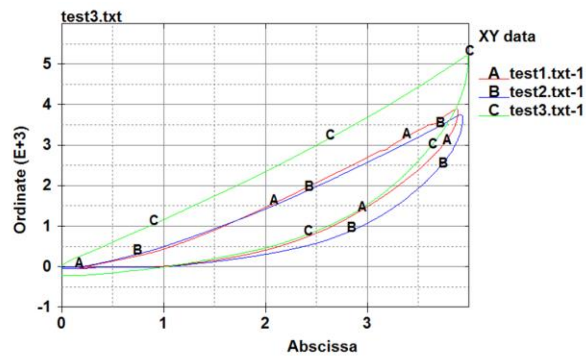

Figure 24: Tensile and compression experimental test data

Experimental Data Review: Tensile Tests

- Tests were quasi-static
- DIC shows reasonably uniform strain field
- Good repeatability in x and y directions on the large (3 hour cure) samples
- Different result on the small (1 hour cure) sample
- POSSIBLY the small sample was cured better in 1 hour then the larger samples in 3 hours but failure in the small sample seems somewhat premature, as we only have 1 test we do not know how repeatable this is
- We selected test N3 (y-direction, large sample) as a base for the numerical model
- There was no information on the unloading in tension as all experiments were done up to failure, consequently the tensile unloading characteristic had to be 'created' based on measurements made in compression

Experimental Data Review: Bulk Modulus

- The bulk modulus was measured in both force driven and displacement driven tests at velocities of 0.1 mm/s and 0.006 mm/s
- The value of the bulk modulus consistently was measured as 2.5 GPa
- If this value is 10-100 times larger than the tangent modulus to the stress-strain curves measured in unconfined tension and compression at any strain and at any strain rate, then the Ogden rubber model would be a valid choice for this material (Form2Flex)

Experimental Data Review: Compression Tests

- Good repeatability between test 1 and test 2 (1 and 3 hour cure)
- Test 3 gives a different result (1000 min cure) … maybe it takes a long time to properly cure a puck ?
- A consistent choice for the base of the numerical model would be test 2 (3 hours cure time), however we selected test 3 (1000 min cure) as a base for the numerical model
- Tests 1 and 2 were not chosen because of the initial zero stress plateau at small strains , this looks very unphysical, could it be the result of a/ irregular surface of the puck ? or b/ problems of identifying the time of contact in the test setup ?
- In any case such a zero-stress plateau is an open invitation to numerical problems in large scale applications

Figure 25 shows the loading and unloading curves from Test 3 transformed into engineering stress-strain.

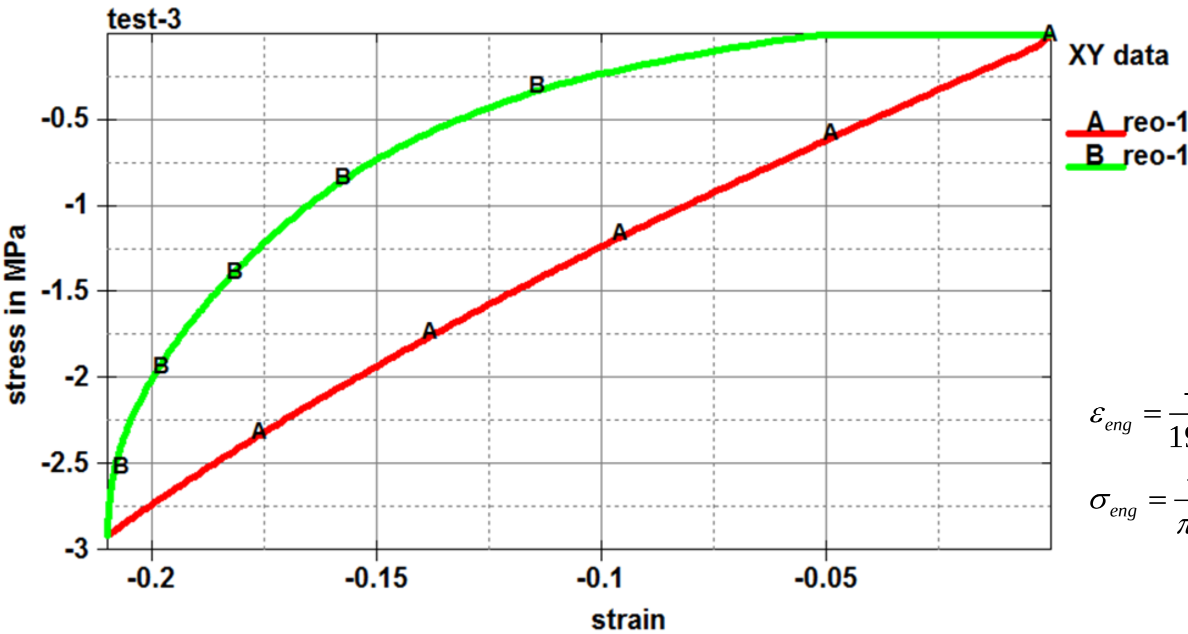

$$\varepsilon_{eng} = \frac{-d}{19.05}$$

$$\sigma_{eng} = \frac{-f}{\pi 24^2}$$

Figure 25: Loading and unloading curves transformed into engineering stress-strain

Figure 26 below shows the master unloading curve for Test 3.

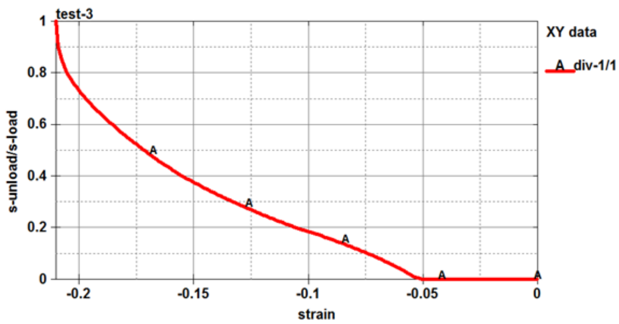

$$1-d=\frac{\sigma_{unl}}{\sigma_{load}}$$

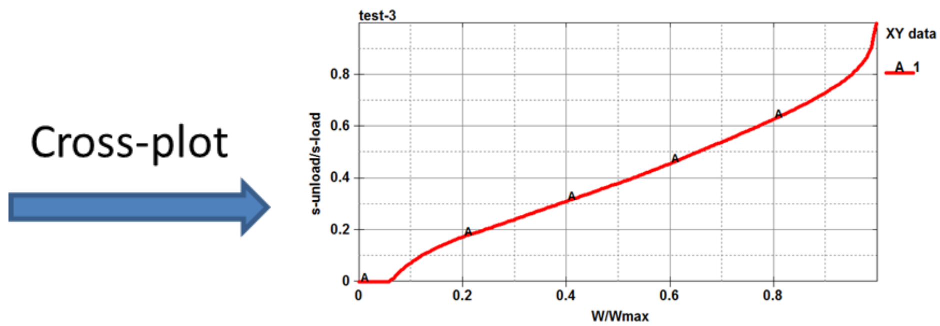

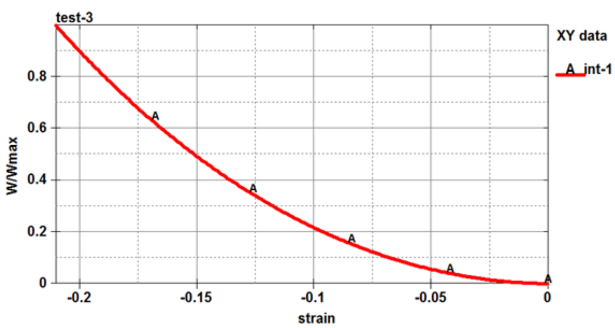

$$\frac{W}{W_{\max}}=\frac{\int_0^{\varepsilon}\sigma_{load}\,d\varepsilon}{\int_0^{\varepsilon_{\max}}\sigma_{load}\,d\varepsilon}$$

Figure 26: Master unloading curve

The tensile stress-strain curve was integrated and normalized with respect to the maximum energy value at 0.21 strain. The sign of the abscissa was then flipped for that the strains become compressive. The results are shown in Figure 27.

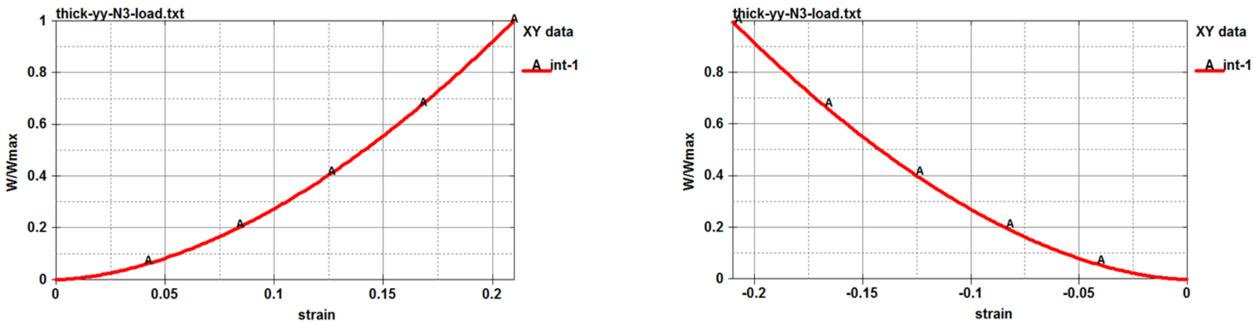

Figure 27: Tensile stress-strain curve integrated

Figure 28 below shows the master unloading curve in tension for Test 3.

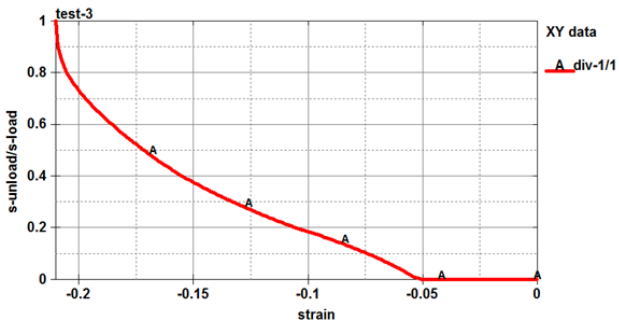

$$1-d=\frac{\sigma_{unl}}{\sigma_{load}}$$

Damage curve from compression test

Cross-plot

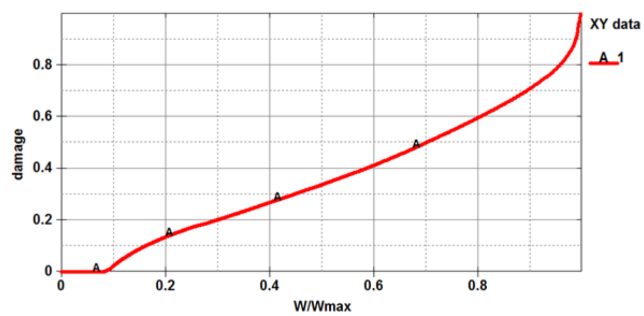

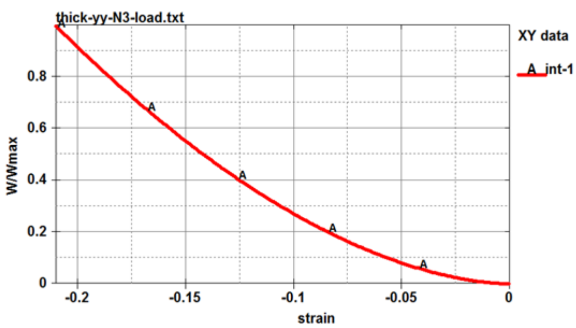

$$\frac{W}{W_{\max}}=\frac{\int_0^{\varepsilon}\sigma_{load}\,d\varepsilon}{\int_0^{\varepsilon_{\max}}\sigma_{load}\,d\varepsilon}$$

Energy curve from tensile test

Figure 28: Master unloading curve in tension

Figure 29 below shows the damage curve in tension for Test 3.

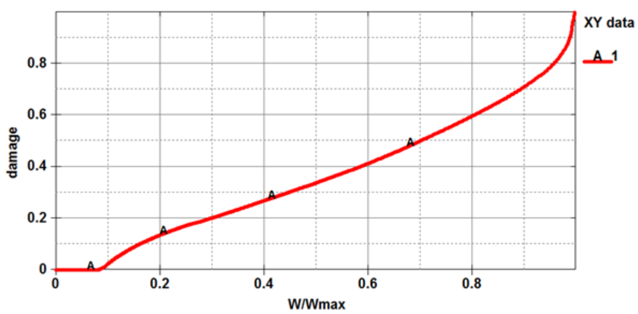

$$1 - d = \frac{\sigma_{unl}}{\sigma_{load}}$$

Master curve in tension

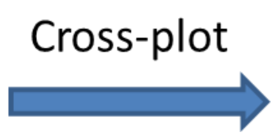

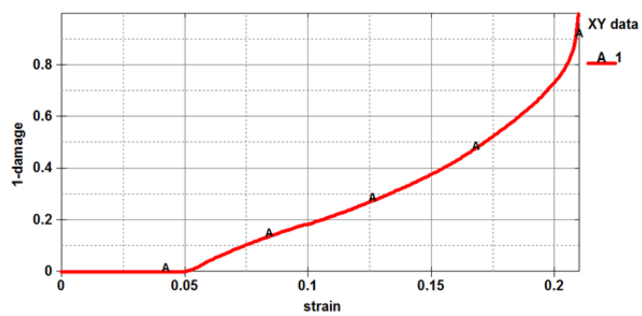

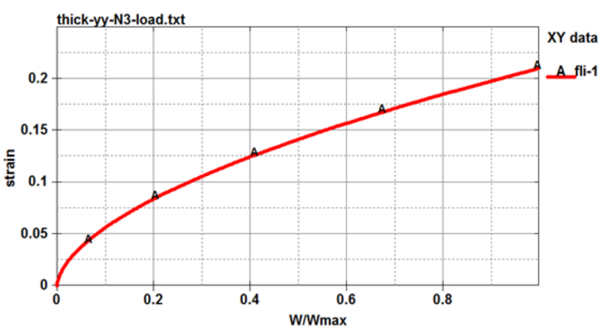

$$\frac{W}{W_{\max}} = \frac{\int_0^{\varepsilon} \sigma_{load}\, d\varepsilon}{\int_0^{\varepsilon_{\max}} \sigma_{load}\, d\varepsilon}$$

Flipped energy curve in tension

Figure 29: Damage curve in tension

Figure 30 below shows the unloading curve in tension for Test 3.

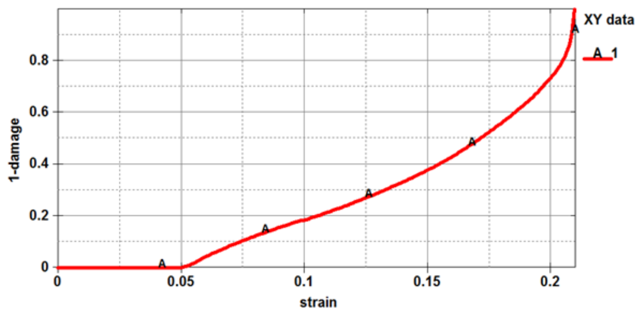

$$1-d=\frac{\sigma_{unl}}{\sigma_{load}}$$

Damage curve in tension

Multiply curves

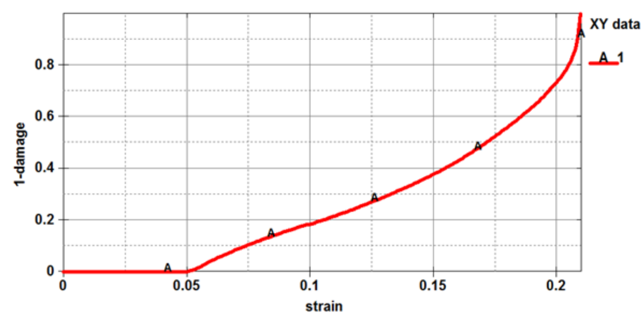

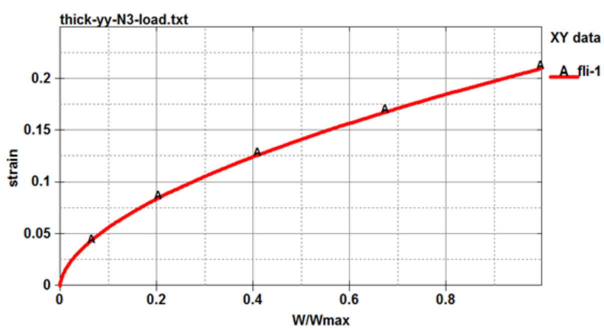

$$\sigma_{unload}=\sigma_{load}\left(1-d\right)$$

$$\sigma_{load}$$

Loading curve in tension

Figure 30: Unloading curve in tension

Figure 31 shows the combined tension/compression loading and unloading response. As seen at strains below 21%, the modulae do not exceed 40 MPa and the bulk modulus is 2500 MPa, so the Ogden model is justified for quasi-static. The complete stress-strain curve was added to the closed loop to define the loading and unloading response. The tensile portion is from the test, while the compressive portion is extrapolated beyond -0.21 strain with linearly growing modulus.

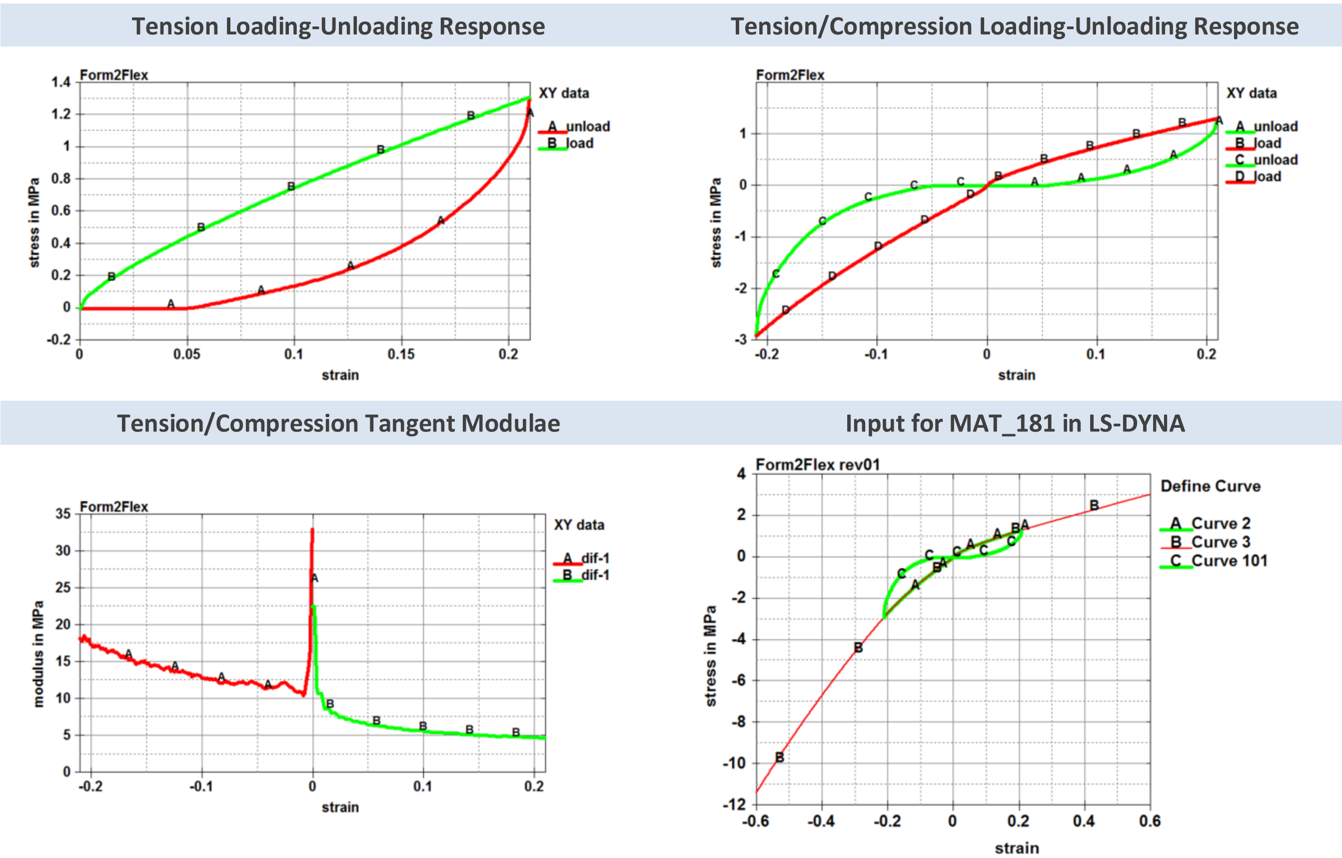

Figure 31: Completed quasi-static stress strain curve

7.1.1.2 Dynamic Response

Review of Test Data 1

- Drop tower tests on large pucks (48 mm diameter, 19.05 mm height)
- Drop tower tests on small pucks (30 mm diameter, 19.05 mm height)
- Drop mass was derived from data on initial velocity and total energy and turns out to be variable for large pucks (v in m/s, mass in kg) :

1	3.04999995	3.03595829
2	4.30000019	3.02509451
3	5.26999998	2.86689544
4	3.04999995	3.00005388
5	4.30000019	3.00216317
6	5.26999998	2.77759981
7	4.30000019	2.99091387

- Assumed a drop mass of 3 kg

Review of Test Data 2

- Drop tower tests on large pucks (48 mm diameter, 19.05 mm height)
- Drop tower tests on small pucks (30 mm diameter, 19.05 mm height)
- Drop mass was derived from data on initial velocity and total energy and turns out to be variable for small pucks (v in m/s, mass in kg) :

1	3.04999995	4.49492073
2	4.30000019	4.52904224
3	5.26999998	4.38708258
4	5.26999998	4.40926218

- Assumed a drop mass of 4.5 kg

The drop test data for the large and small pucks are shown below in Figure 32. The large and small pucks were used in the material formulation. It seems peculiar that the large and small pucks give the same force at the same displacement.

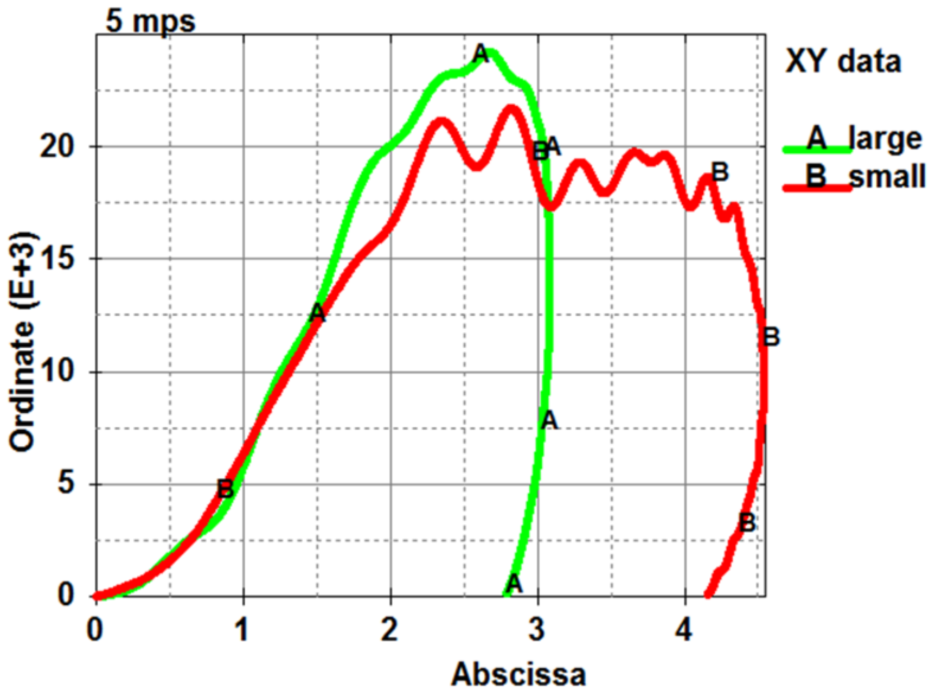

Figure 32: Drop test data for the large and small pucks

GENERATION OF DYNAMIC CURVES

- Experiments are not at constant engineering strain rate
- Experiments are not at constant true strain rate
- For many tests the initial slope (very small strains) was close to the static compression curve, therefore we did not neglect the initial ‘offset’ in the dynamic f-d curves
- Determination of dynamic stress-strain curves is a process of iterative reverse engineering
- 35 iterations done so far
- Density has some influence on the results, thus inertia seems important.

The load curves and the results of iteration #8 for 5 m/s are shown below in Figure 33. Iteration #8 uses TENSION=0, RYTPE-1, and AVGOPT=1. The results at 3 m/s and 4 m/s did not have good correlation at this point.

Load Curves for Iteration #8

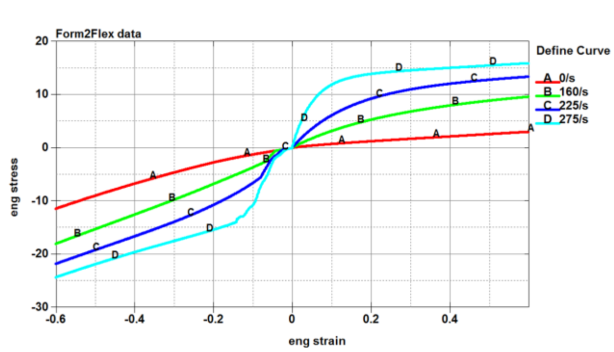

Drop Test Results for 5 m/s

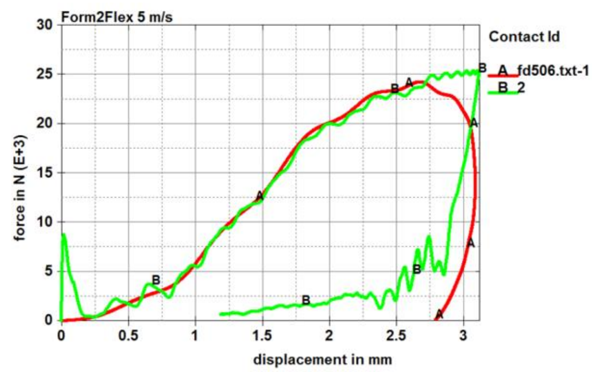

Figure 33: Load curves and drop test results of iteration #8 for 5 m/s

Simulations on 2D Drop Tower Model

- Unloading parameters were kept at HU=0.2 and SHAPE=8. (they are usually calibrated wrt. Quasi-static data)
- Damping parameter was kept at 0.4
- RTYPE parameter was kept at 1 (engineering strain rate)
- TENSION parameter was kept at 0 (compression only)
- Very high dependency of the results upon parameter AVGOPT, this parameter became part of the reverse engineering process
- A smoothing interval of 0.1 ms seems to work well (= about 300 timesteps, vs . default = 12)
- General remark : transition into unloading is always less smooth in the simulation then in the test as the model is rate dependent elastic and the material is viscoelastic

The table of load curves for iterations #35 with TENSION=0, RTYPE=1, AVGOPT=-0.0001 is shown below in Figure 34.

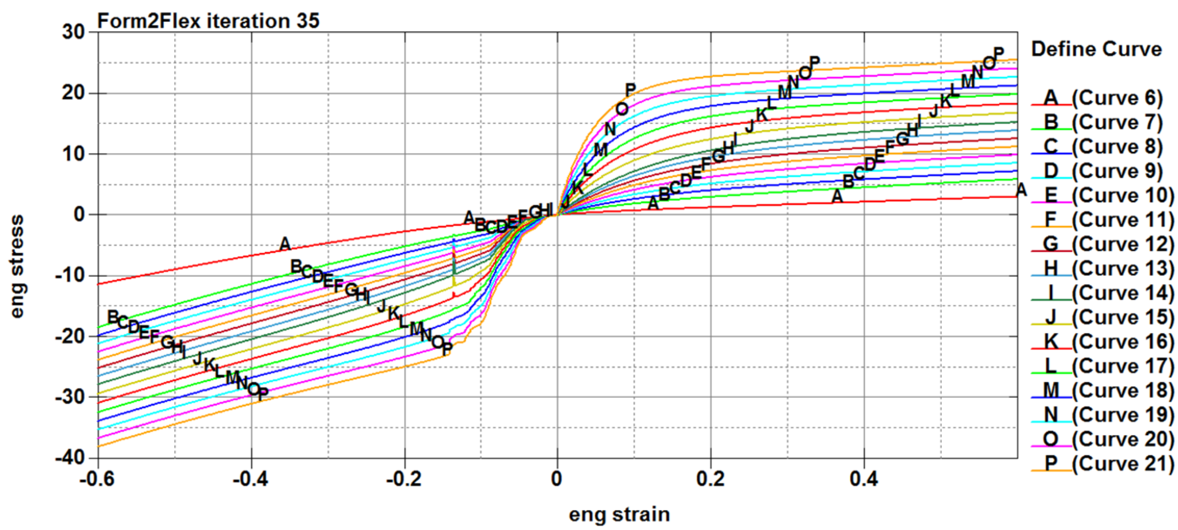

Figure 34: Load curves for iteration #35

The results of iteration #35 plotted with the experimental results are shown below in Figure 35.

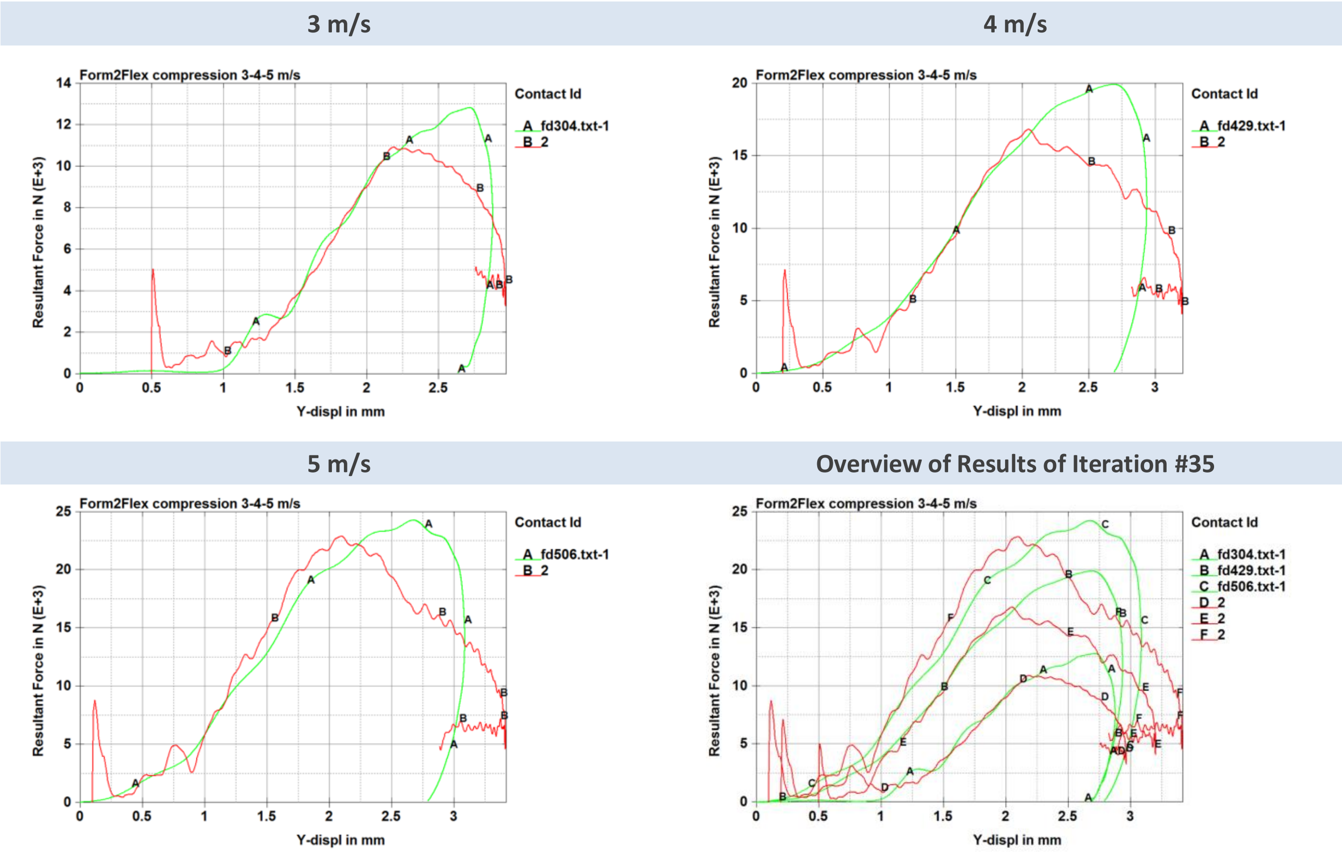

Figure 35: FEA (iteration #35) and Experimental drop test results

The results of the small puck for iteration #35 plotted with the experimental results are shown below in Figure 49.

3 m/s

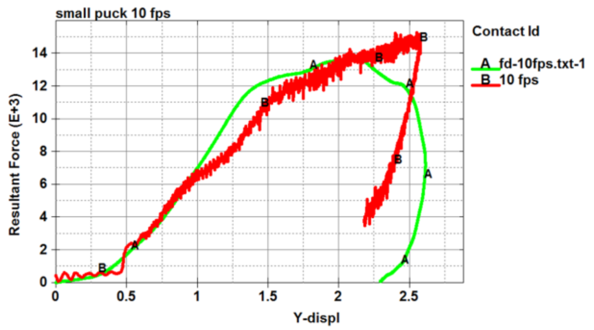

4 m/s

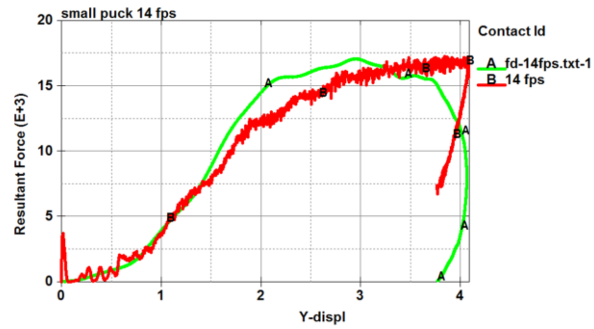

5 m/s

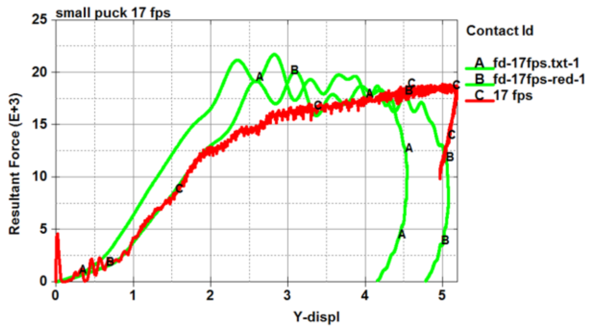

Overview of Results of Iteration #35

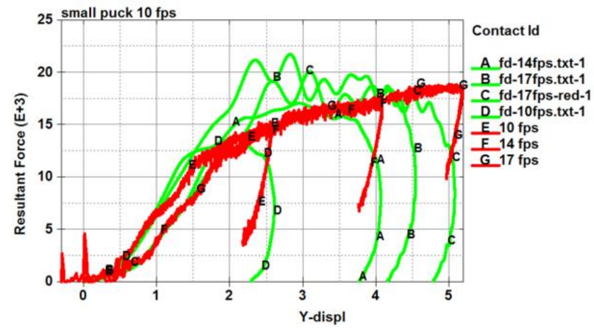

Figure 36: Small puck FEA (iteration #35) and Experimental drop test results

VERIFICATION OF MAT_181 (DYNAMIC)

For verification, a single element test on 20/20/20 cube using density/10 to avoid inertia effects and prescribed velocity of 3m/s, 4m/s and 5m/s was tested. The velocity-time history for the test case is shown in Figure 37.

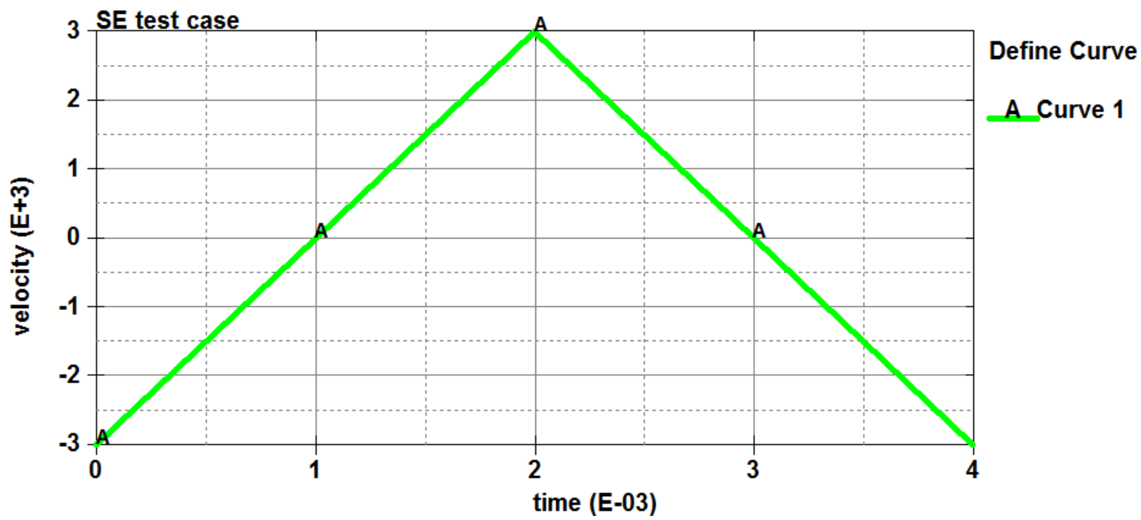

Figure 37: Velocity-Time profile for the MAT_181 test case

The comparison of different TENSION values is shown in Figure 38.

TENSION=0 to TENSION=1	TENSION=0 to TENSION=-1
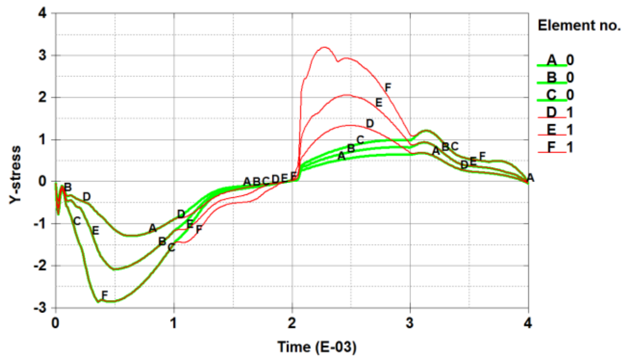	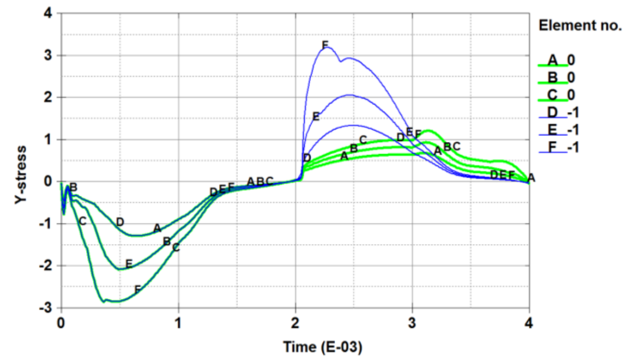

TENSION=1 to TENSION=1

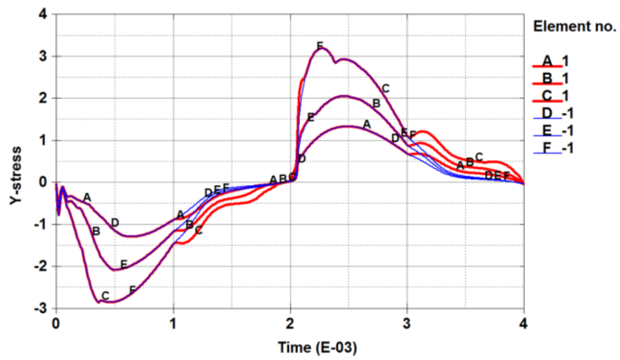

Figure 38: Comparison of different TENSION values

The conclusions about the rate effects in MAT_181 are listed below in Table 5.

Table 5: Rate effects in MAT_181

TENSION	Compression loading	Compression unloading	Tension loading	Tension unloading
0	yes	no	no	yes
1	yes	yes	yes	yes
-1	yes	no	yes	no

	$\varepsilon < 0$	$\varepsilon < 0$	$\varepsilon > 0$	$\varepsilon > 0$
	$\dot{\varepsilon} < 0$	$\dot{\varepsilon} > 0$	$\dot{\varepsilon} > 0$	$\dot{\varepsilon} < 0$

7.1.2 Material 2: Carbon EPU40

The procedure for characterizing Material 2 is the same as shown previously for Material 1. A summary for the characterization of Material 2 is presented below.

7.1.2.1 Quasi-Static Response

The experimental results for the Carbon EPU40 tensile tests are presented in Figure 39.

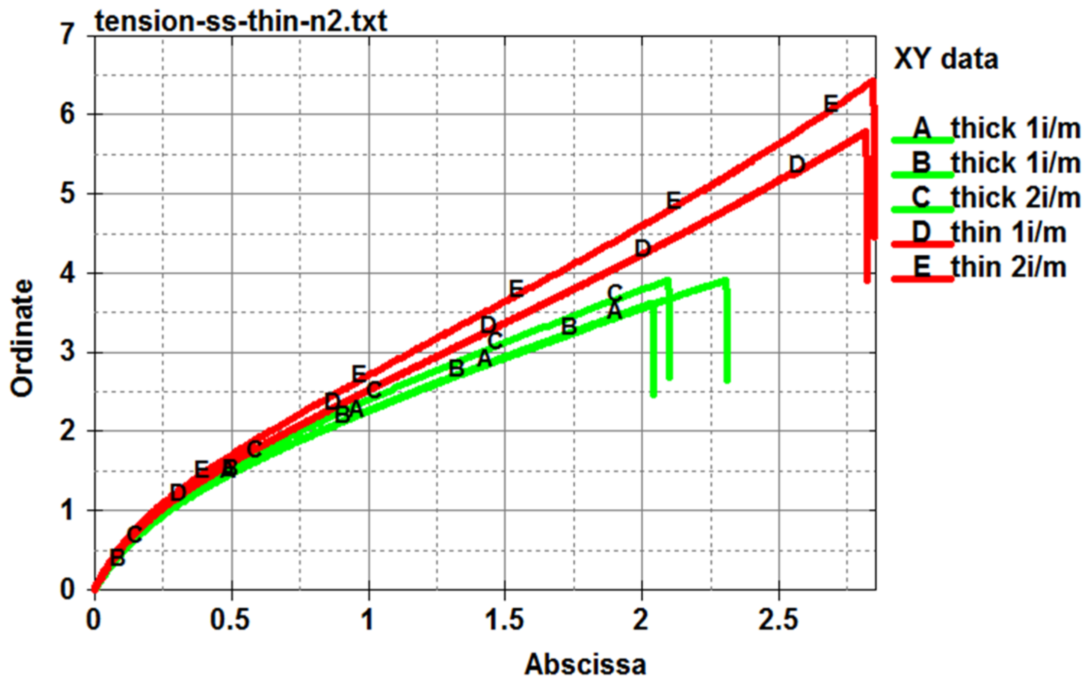

Figure 39: Carbon EPU40 tensile tests

Experimental Data Review: Tensile Tests

- Tests were quasi-static
- 2i/m consistently stiffer then 1i/m
- Different results between thin and thick samples
- We selected test N1 (thin, 1i/m) as a base for the numerical model
- Same unloading parameters (HU=0.2 and SHAPE=8) were used as for material 1

Experimental Data Review: Bulk Modulus

- The value of the bulk modulus consistently was measured as 2350 MPa
- If this value is 10-100 times larger than the tangent modulus to the stress-strain curves measured in unconfined tension and compression at any strain and at any strain rate, then the Ogden rubber model would be a valid choice for this material (Carbon EPU40)

The experimental results for the Carbon EPU40 compression tests are presented in Figure 40.

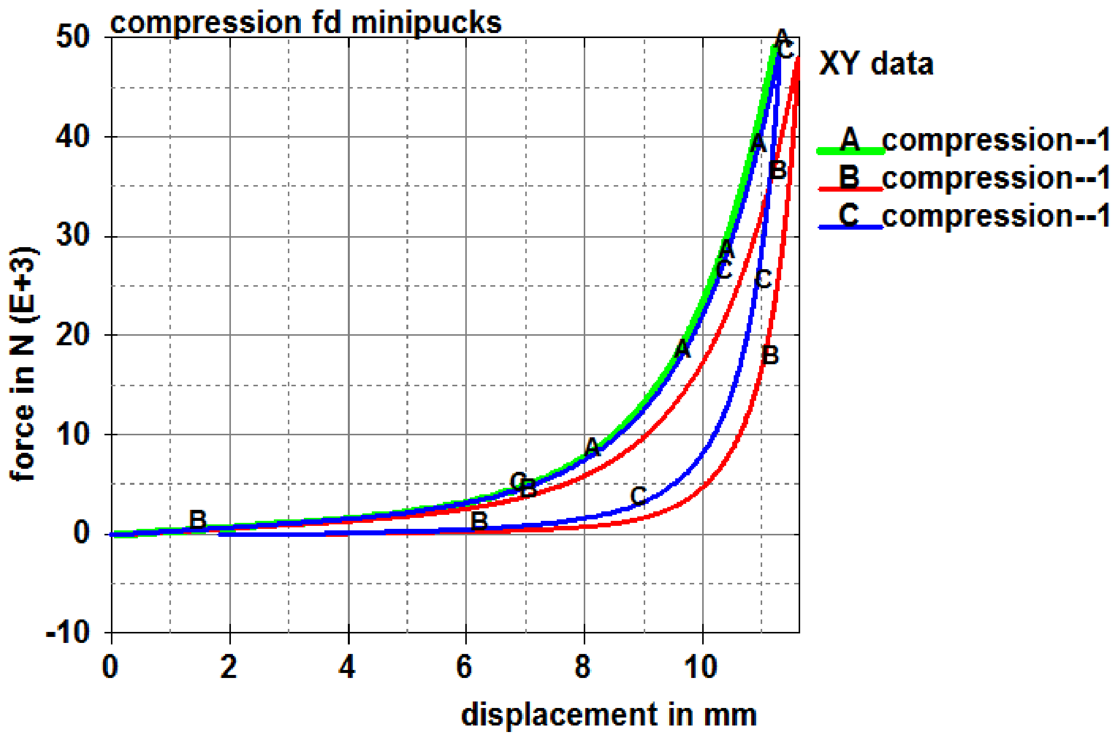

Figure 40: Quasi-static compression tests

Experimental Data Review: Quasi-Static Compression Tests

- Reviewed compression tests on minipucks
- Good repeatability between test 1 and test 3
- Test 2 slightly different
- Test 1 selected as base for the numerical model

The MAT_181 input curves are shown below in Figure 41.

Stress-Strain Curve	Tension/Compression Loading Repsonse

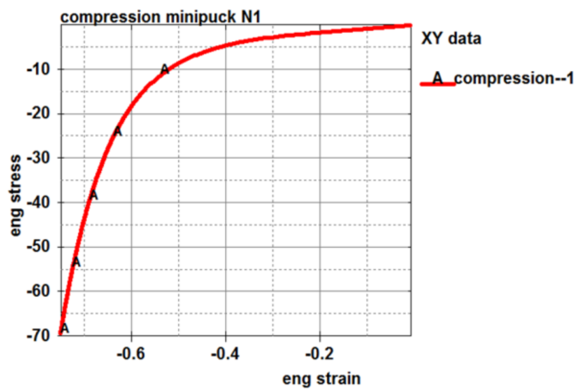

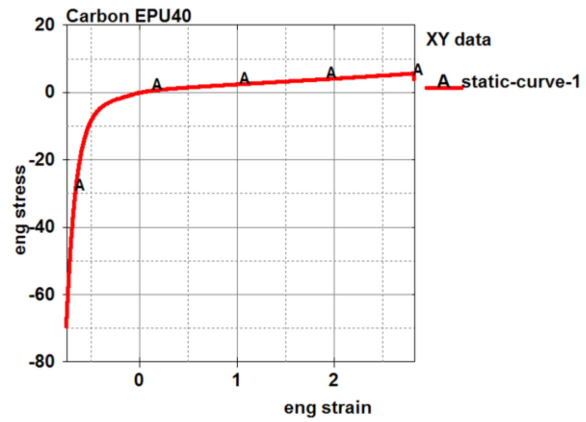

Tension/Compression Tangent Modulae	Input for MAT_181 in LS-DYNA

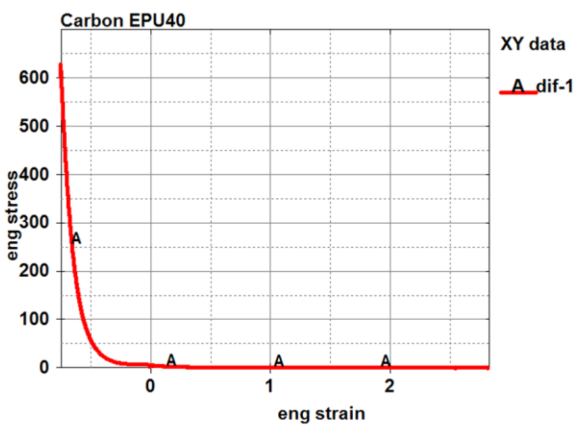

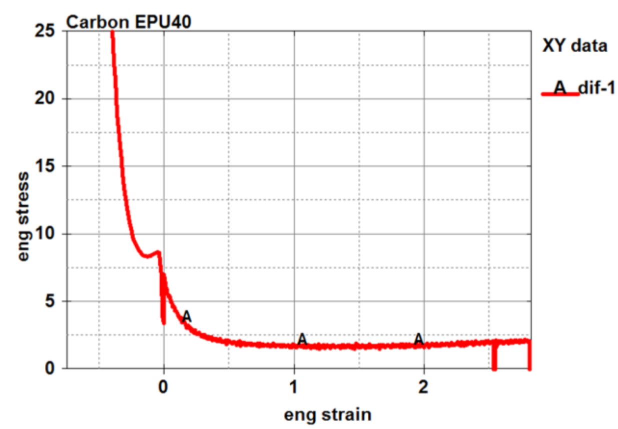

Figure 41: Engineering stress-strain input curves for MAT_181 in LS-DYNA

7.1.2.2 DYNAMIC RESPONSE

REVIEW OF TEST DATA

- Droptower tests on small pucks (15 mm diameter, 16.61 mm height)
- Assumed a dropmass of 3 kg
- Impact velocities of 3.05m /s,   4.3 m/s and 5.27 m/s

GENERATION OF DYNAMIC CURVES

- Determination of dynamic stress-strain curves is a process of iterative reverse engineering
- 11 iterations were performed

Figure 42 presents the dynamic input curves. The dynamic curves approach the static curve for strain >60%.

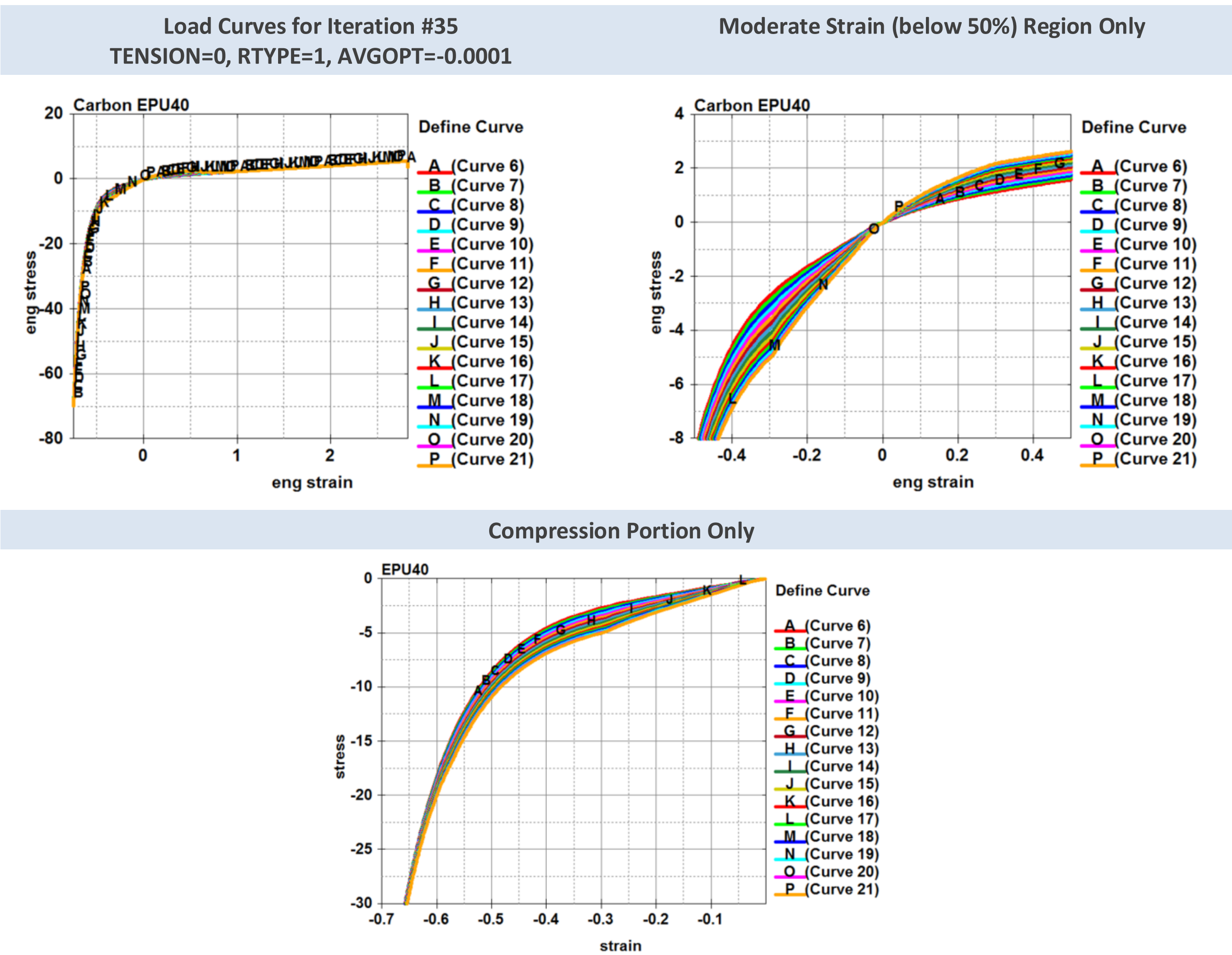

Figure 42: Dynamic curves

The simulation results for the small puck made from Material 2 compared to the drop test experimental results are shown below in Figure 43.

Small Puck 17 fps	Small Puck Results Overview
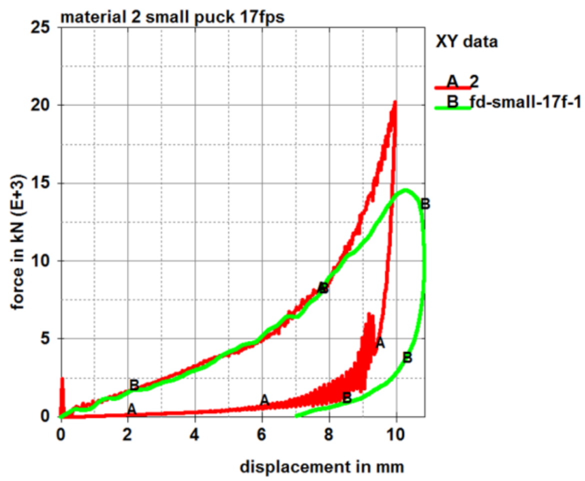	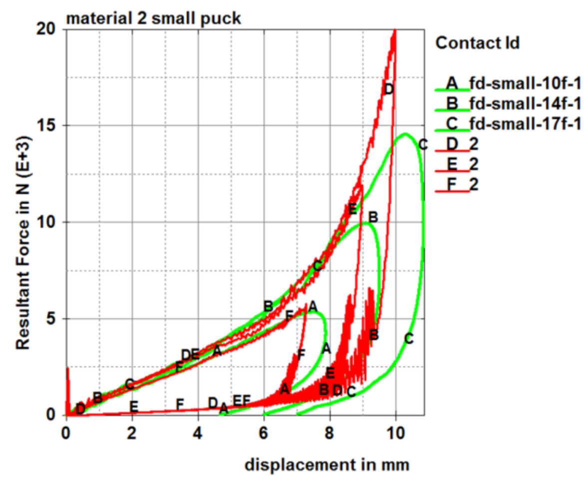

Figure 43: Simulation vs. experimental results

CONCLUSIONS

- Some viscous effects seem hard to model with the rate dependent elastic model in MAT_181 (not surprising)
- However linear visco-elastic models would not be able to capture the non-linearity in the rate dependent response
- These effects seem small compared to the influence of the geometry (puck vs thin spaghetti like structures)

7.2 Bulk Modulus Testing

Figure 44 shows the geometry and mesh setup for the bulk modulus simulation. The maximum plunger load is 40 kN given that the test machine's maximum load capacity is 50 kN. The test plug is 20 mm diameter by 25 mm tall.

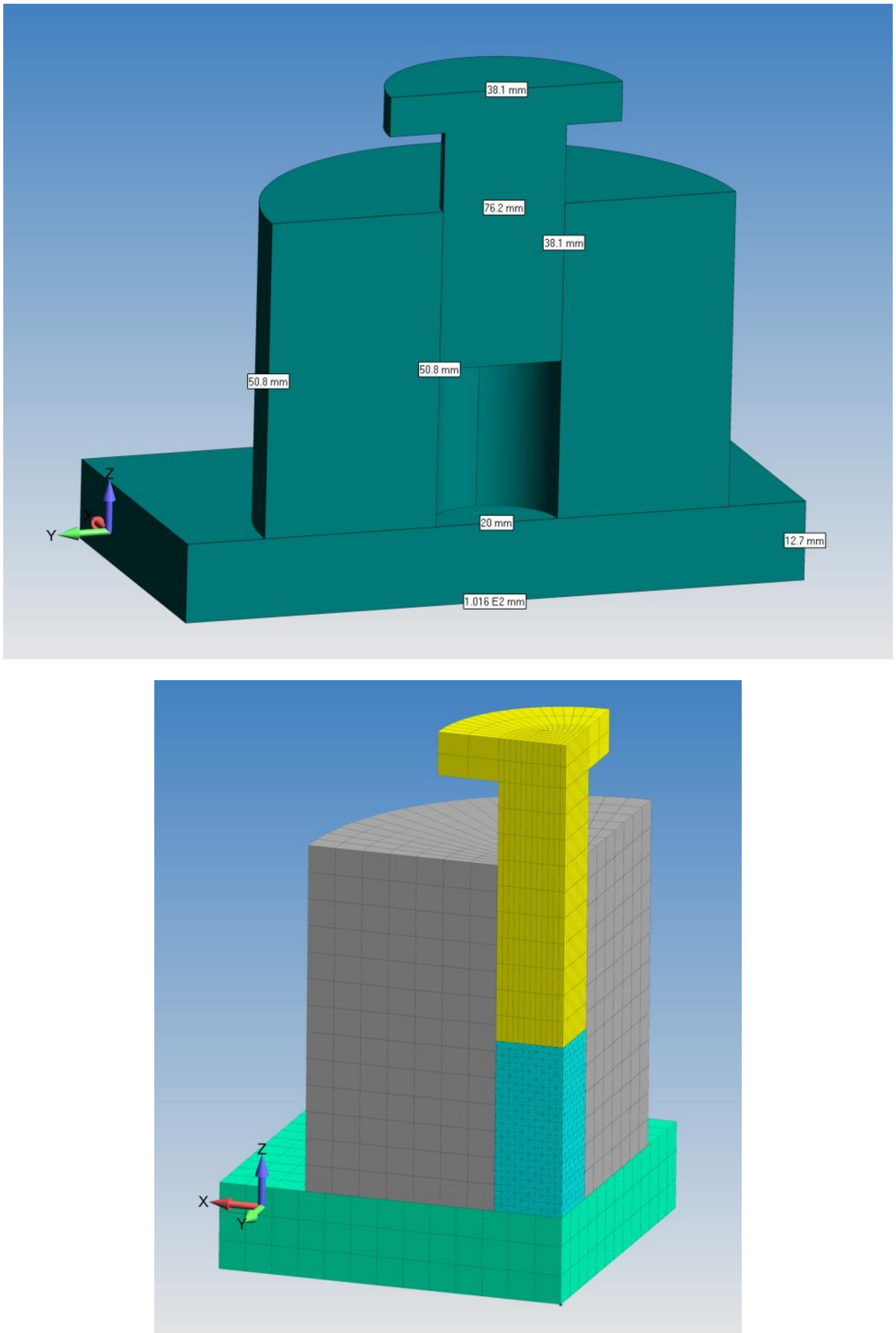

Figure 44: Bulk modulus testing simulation using material plug of 20 mm diameter by 25 mm tall

Using a placeholder material law, Figure 45 shows a representative force-displacement response from the bulk modulus testing simulation.

Stress-Strain Material Law (Placeholder)	Force-Displacement Response

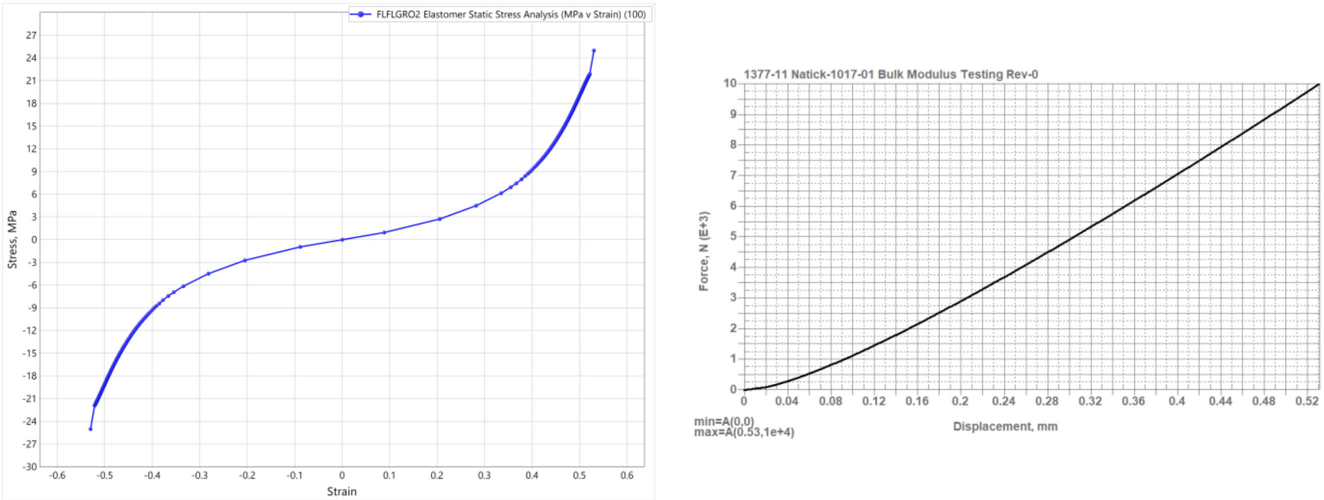

Figure 45: Representative bulk modulus testing result

As a design note to the fixture, we'll need to lock the cylinder to the base place via a countersunk screw or some other mechanism, of we might see the following occur as shown in Figure 46.

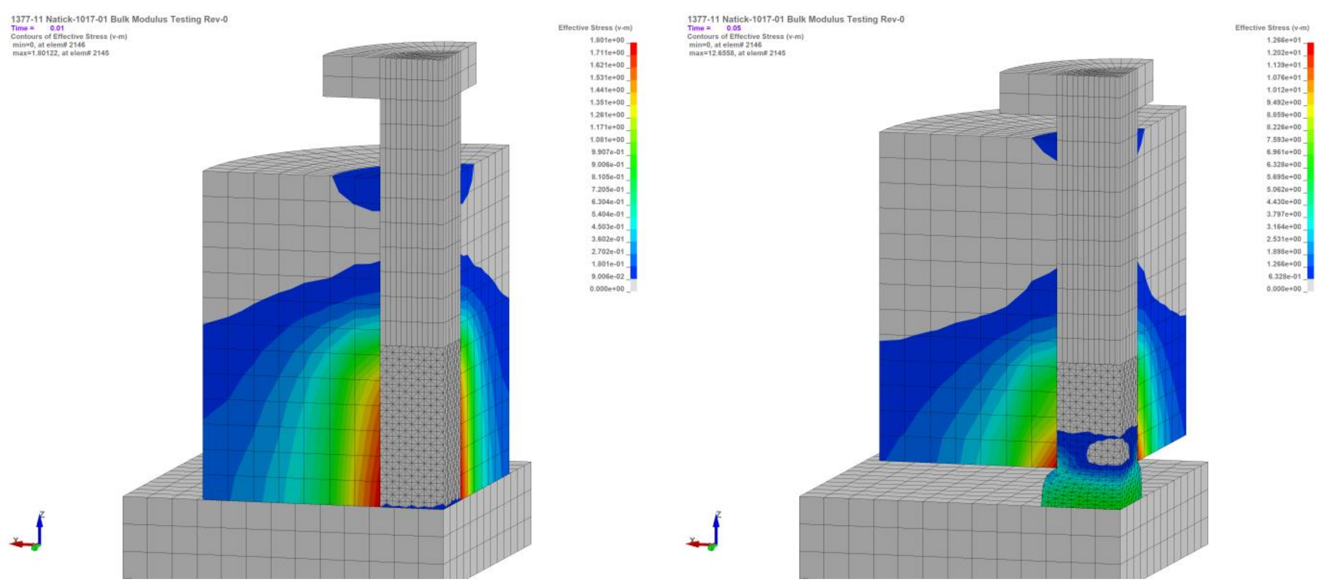

Figure 46: Base cylinder slipping upward as sample squeezes out at the bottom

Test results from the bulk modulus are shown in Figure 47. As the load is ramped up from 0 to 40 kN, the stress in the material correspondently increases. Given the cross-section area of the sample (20 mm diameter = 314.2 mm^2) and the maximum load of 40 kN, the maximum pressure that can be obtained is 127.3 MPa. If we obtain true hydrostatic conditions in the sample, the effective stress (von Mises) should be near 0.0 MPa.

Stress in Steel Cylindrical Retainer – 180 MPa

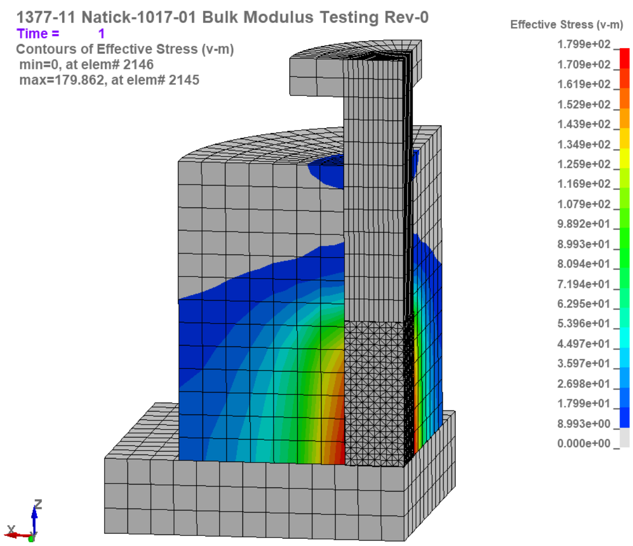

Slightly Non-Uniform Effective Stress

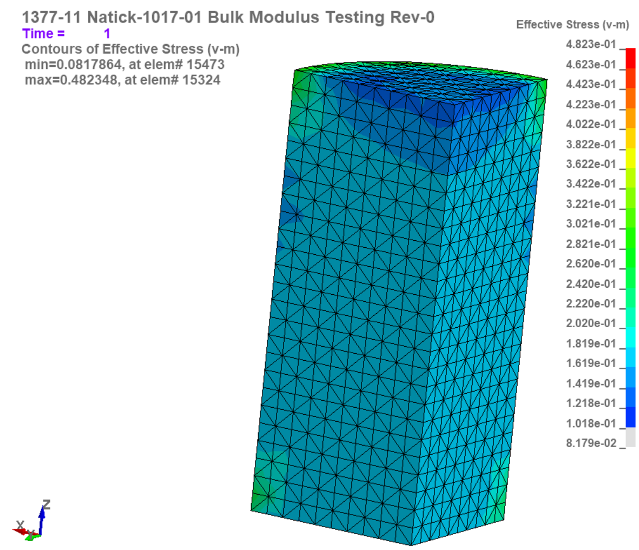

Pressure values in test sample – should be uniform 127.3 MPa

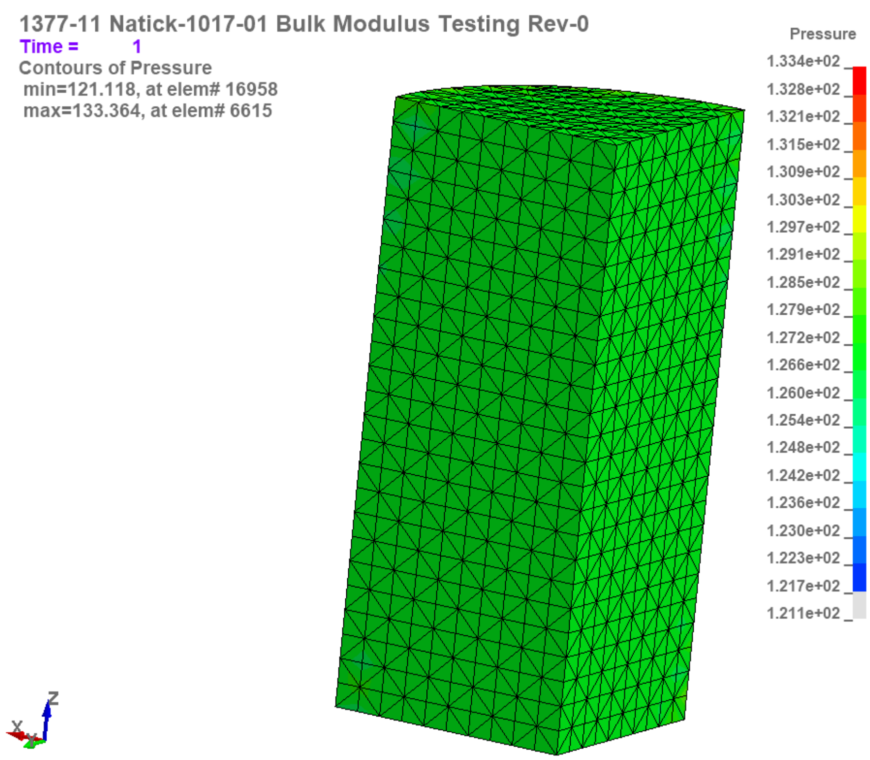

Figure 47: Stress results from bulk modulus testing

7.3 Exploratory Analysis of 3D Structures

Figure 48 shows the lattice structure used in this investigation. It has external dimensions of 19 x 45 mm. The individual lattice members are 1.48 mm in diameter. The trial mesh uses 4-node tetrahedrals based on LS-DYNA's element formulation (ELFORM) 13.

Static loading was used to compress the structure. The maximum displacement achieved prior to convergence failure was 16.4 mm. At this level of compression, the 3D structure had compacted. It should be noted that this work is preliminary and that most likely with an improved material law, the simulation would have achieved higher levels of compaction.

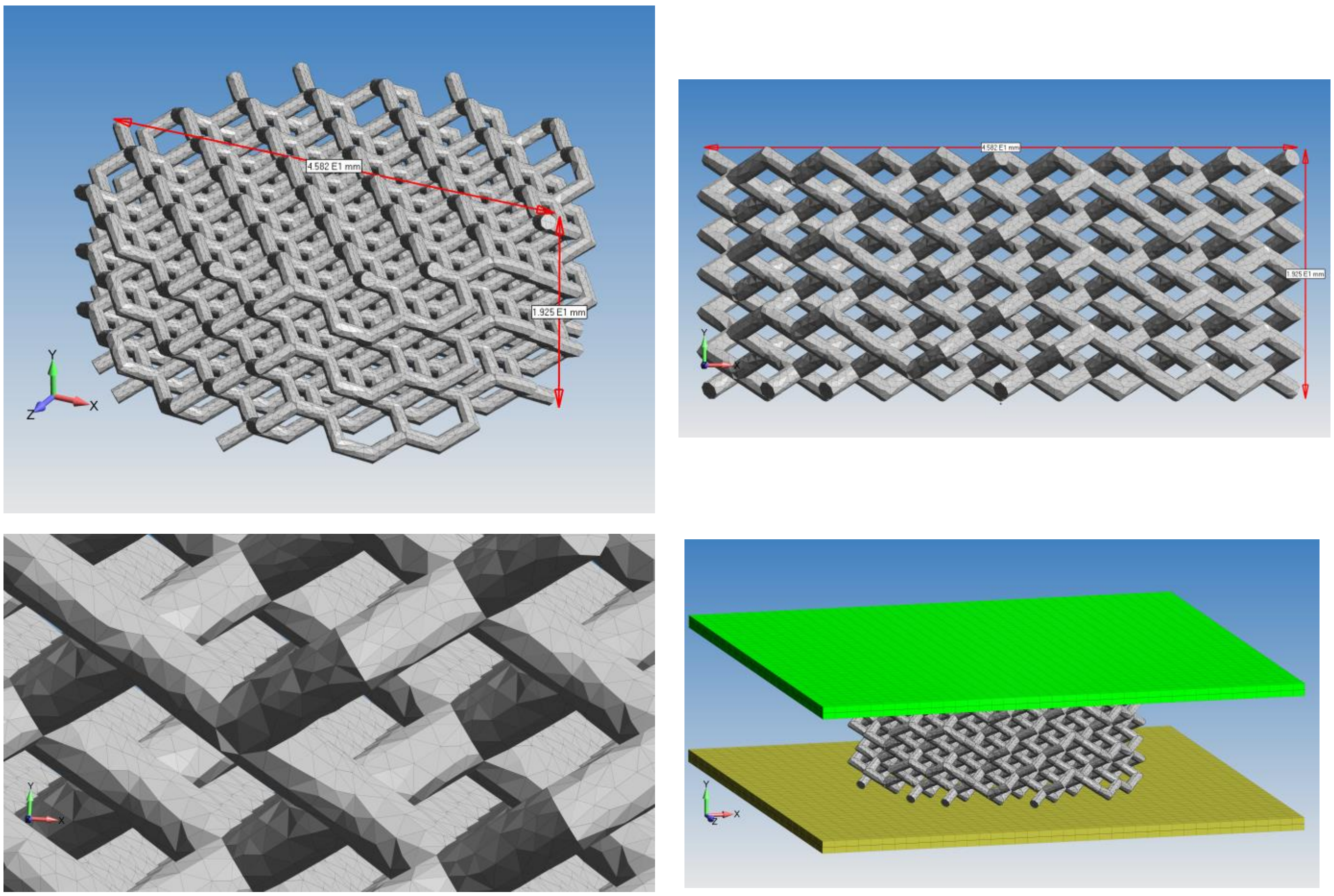

Figure 48: 3D lattice structure for compression test using placeholder material model

Figure 49 shows the material law curve (placeholder) and the response of the 3D lattice structure to compression loading. The material law is representative of how material 1 should respond but is not accurate, i.e., it is not tied to any mechanical test.

Stress-Strain Material Law (Placeholder)	Force-Displacement Response

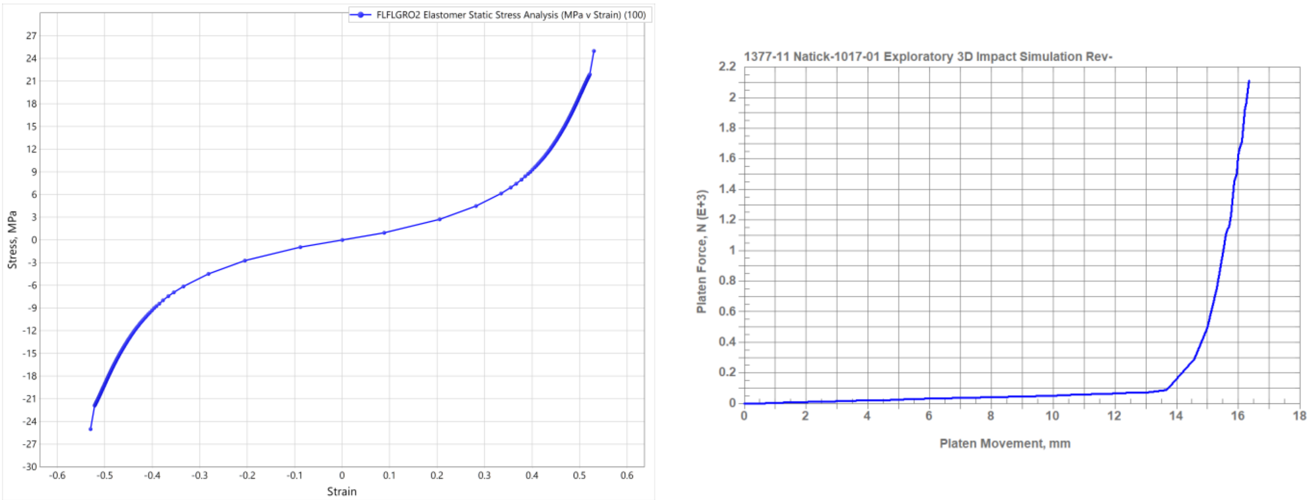

Figure 49: Material curve and response of structure to compression

Figure 50 shows the 3D structure under compression loading. The maximum displacement was 16.4 mm. The height of the un-deformed 3D structure is 19 mm.

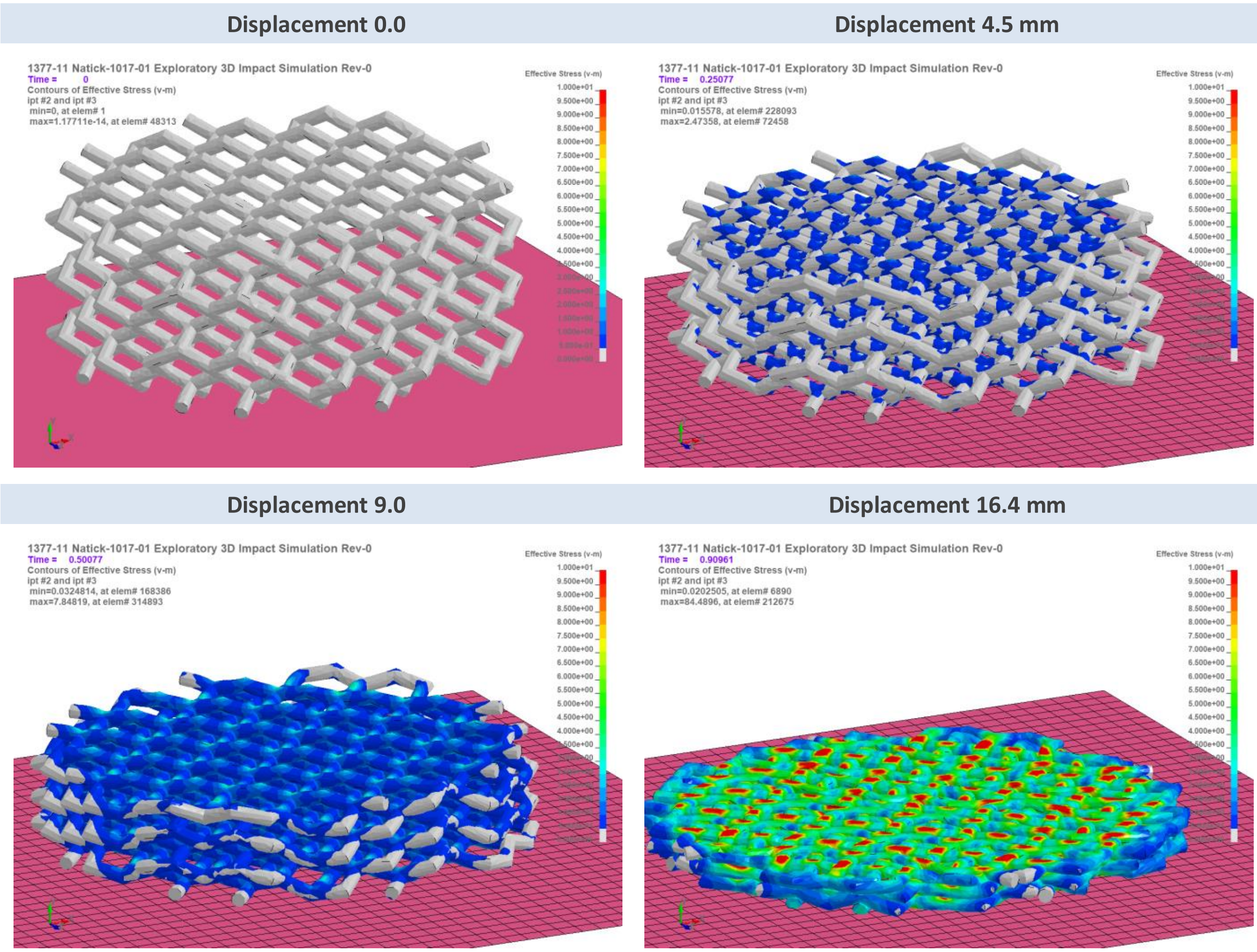

Figure 50: Step-by-step stress plots during compression loading

Section cut views are shown in Figure 51.

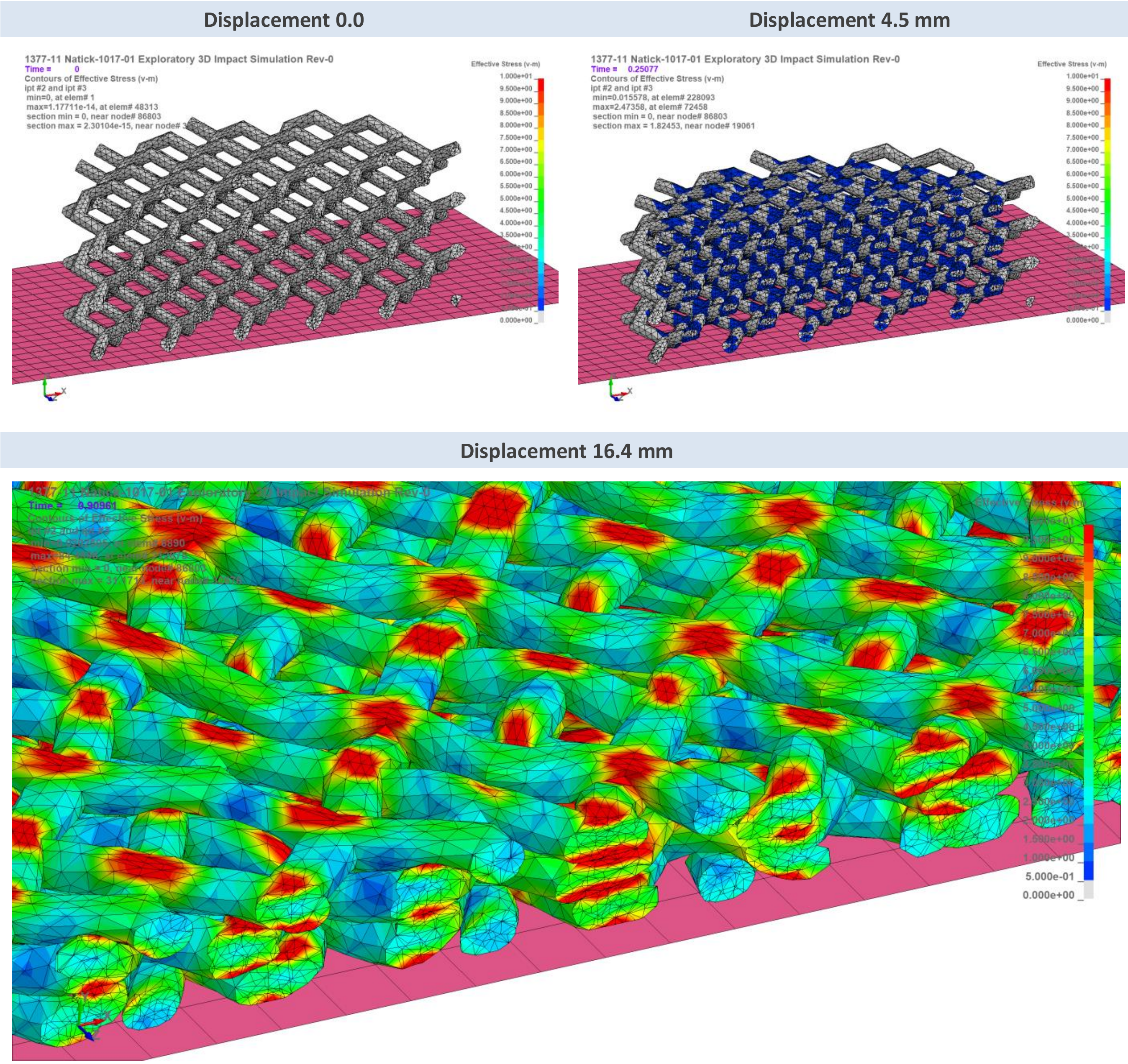

Figure 51: Section cut views of the 3D lattice structure under compression loading

7.3.1 Verification of Impact Analysis LS-DYNA Parameters with CVC E1 and CBS E1

Given the material and fine lattice structure, results could vary widely (>50%) depending upon mesh size and contact parameters. The purpose of this effort was to determine acceptable parameters that would confidently provide limited variability (<10%) between analyses. Table 6 give results from this study where the mesh density and time step was varied. In Table 4, the friction coefficient was also varied from 0.3 to 1.0. In this case, the maximum force decreased from 10 to 8.3 kN. Another outstanding result was seen when the time step was increased, the maximum force likewise decreased from 10 to 8.5 kN. Both of these results not valid since a friction coefficient of 1.0 and a large time step invalidate the results. In general, the maximum force value of 10 kN for CVC E1 is stable.

Table 6: Parameter assessment with CVC E1 at 10 ft/s

Trial	No. Nodes	Contact Type	_TIMESTEP	SLE/IE (k)	Max Force (kN)
1	87k	SOFT=2	5e-8	0.84/13.4	10.6
2	109k	SOFT=2	5e-8	0.82/13.4	10.0
3	146k	SOFT=2	5e-8	0.85/13.0	10.4
4	146k	SOFT=2	2.5e-8	0.72/13.0	10.0
5[1]	145k	SOFT=2	5e-8	0.54/14	8.3
6	145k	SOFT=2	1.5e-7	0.29/11	8.5

[1]Friction value increased from 0.3 (used in all models) to 1.0 as an upper bound of reality.

Table 7 presents results for CVC E1 at an impact velocity of 14 ft/s. The maximum force value of 24 to 26 kN is shown to be stable and not dependent upon the timestep.

Table 7: Parameter assessment with CVC E1 at 14 ft/s

Trial	No. Nodes	Contact Type	_TIMESTEP	SLE/IE (k)	Max Force (kN)
1	146k	SOFT=2	5e-8	2.6/25	24
2	146k	SOFT=2	1e-8	2.2/26	26

A more limited study was done on CBS E1 through mesh refinement and limited timestep variation. Table 8 presents these results and indicates stability of maximum force calculation at 13 kN.

Table 8: Parametric mesh assessment with CBS E1 at 10 ft/s

Trial	No. Nodes	Contact Type	_TIMESTEP	SLE/IE (k)	Max Force (kN)
1	112k	SOFT=2	5e8	1.7/13	13
2	187k	SOFT=2	4e-8	1.5/13	13
3	212k	SOFT=2	4e-8	1.5/13	13

7.4 Element Formulation and Mesh Sensitivity Study

7.4.1 Simple Impact Test on Small Sample

Figure 52 shows the quarter-symmetry impact simulated used to explore how element formulation and mesh quality would affect the force versus displacement response of the simulation. The impact simulation follows that used for the small sample impact test (sample size 15x30mm). Element formulations explored were hex, 4-node tetrahedral and then 10-node tetrahedral. The tetrahedral mesh was then skewed to form elements of distorted shapes (e.g., Jacobian's higher than 0.60).

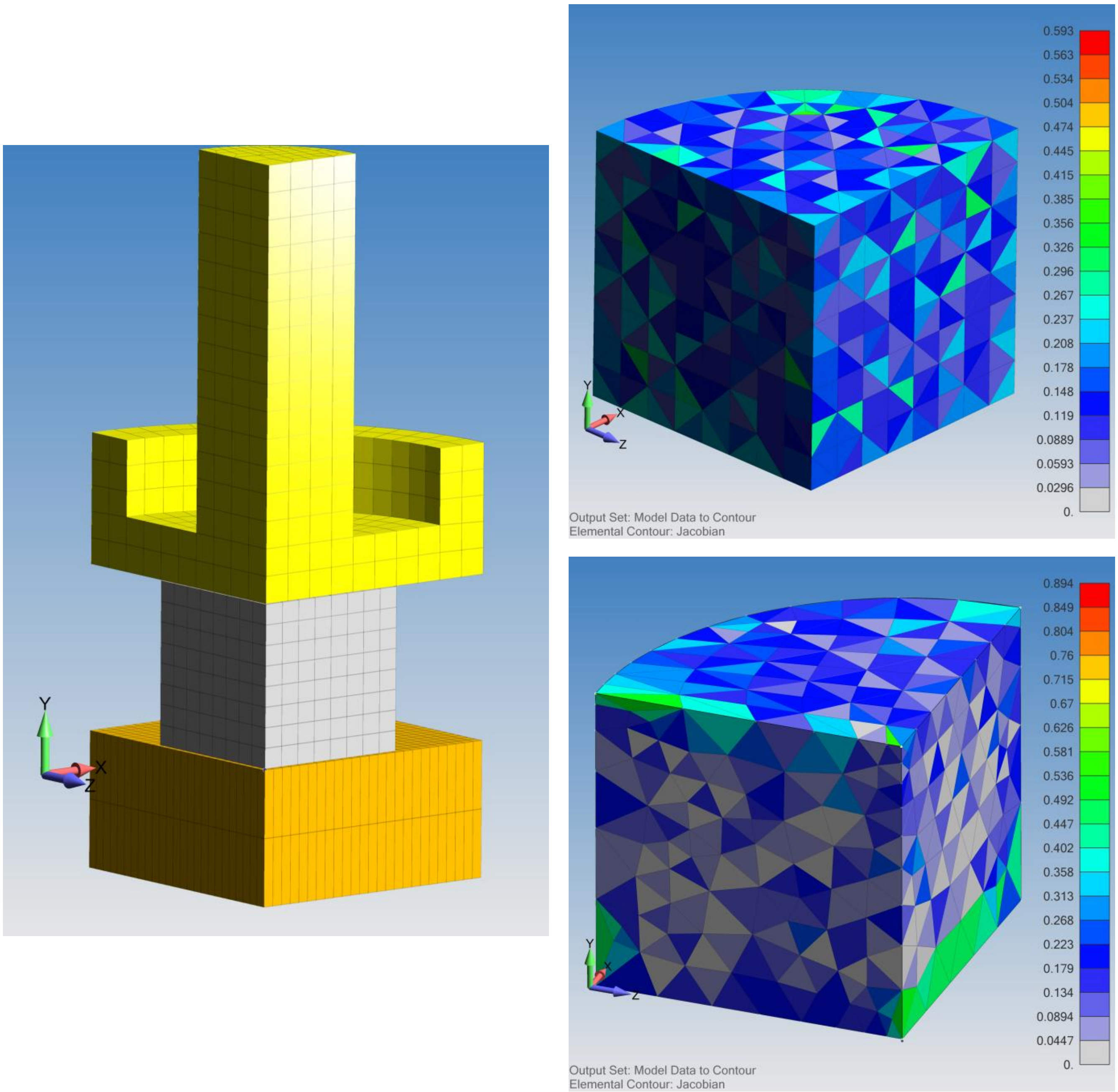

Figure 52: An impact simulation (quarter-symmetry) was used to explore element formulation and mesh quality effects

Figure 53 provides some information on the virtual impact test. The hammer was given a weight of 1.15 kg (quarter-symmetry – full weight 4.6 kg) and an impact velocity of 3,050 mm/s. The provided an impact energy of 5.3 J or 21.2 J for the complete model. This aligns with the Natick test parameters using small samples having an impact energy of 21.4 J.

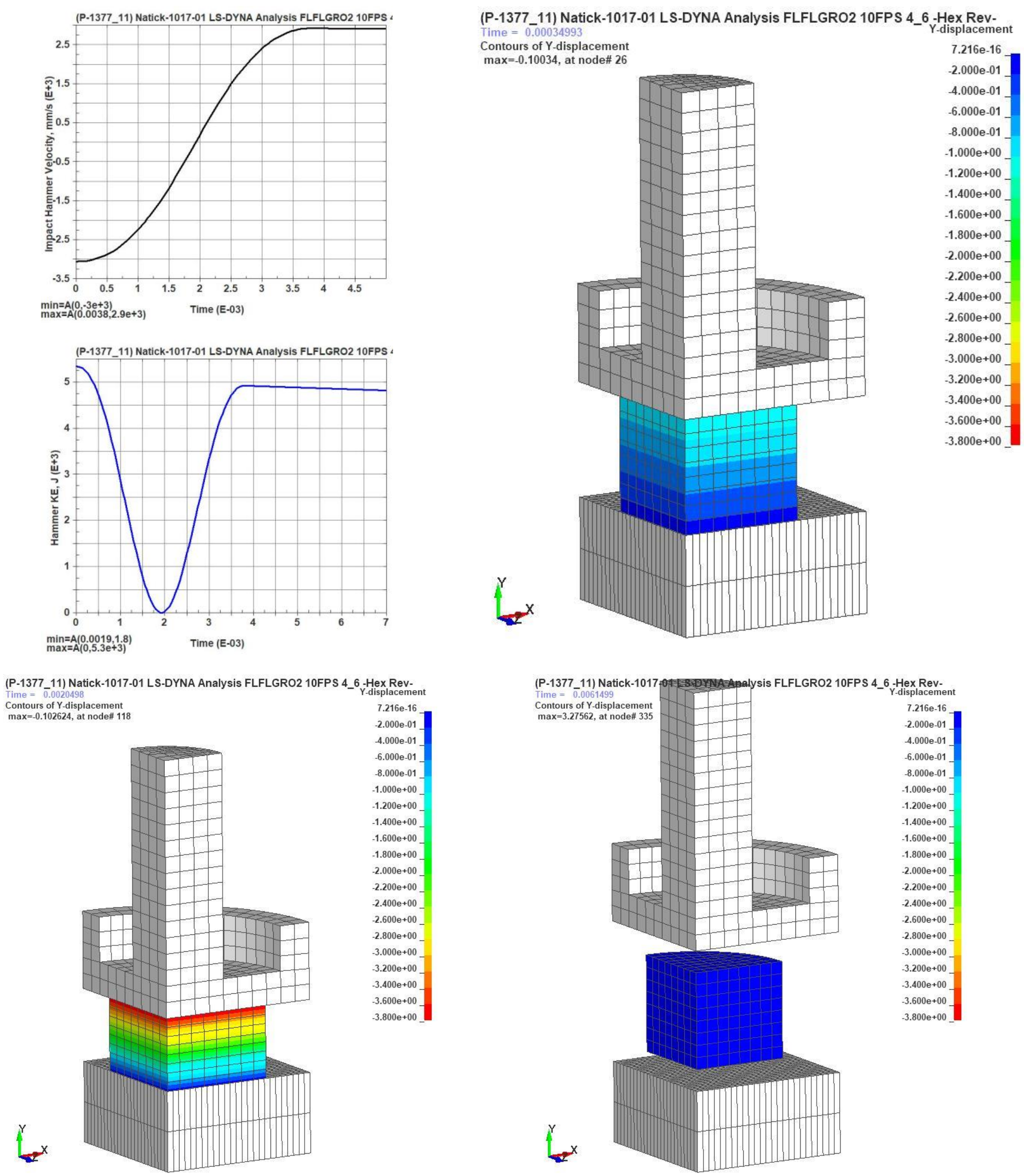

Figure 53: Impact test results for hex mesh

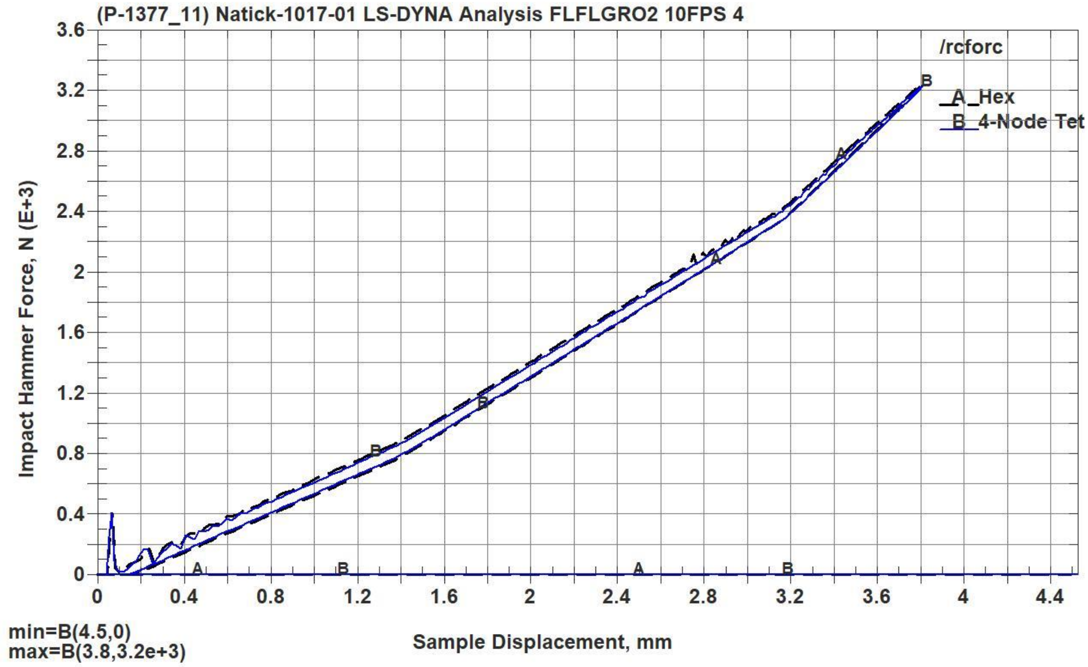

Figure 54 shows the results for the impact test on three element formulations with the tet meshes skewed. Everything aligns well with a small outlier for the 10-note tet model. Interesting enough, this outlier behavior disappears once the mesh is skewed. The last figure shows the force versus displacement behavior for the hex and the 4-Node tet model and the results are identical.

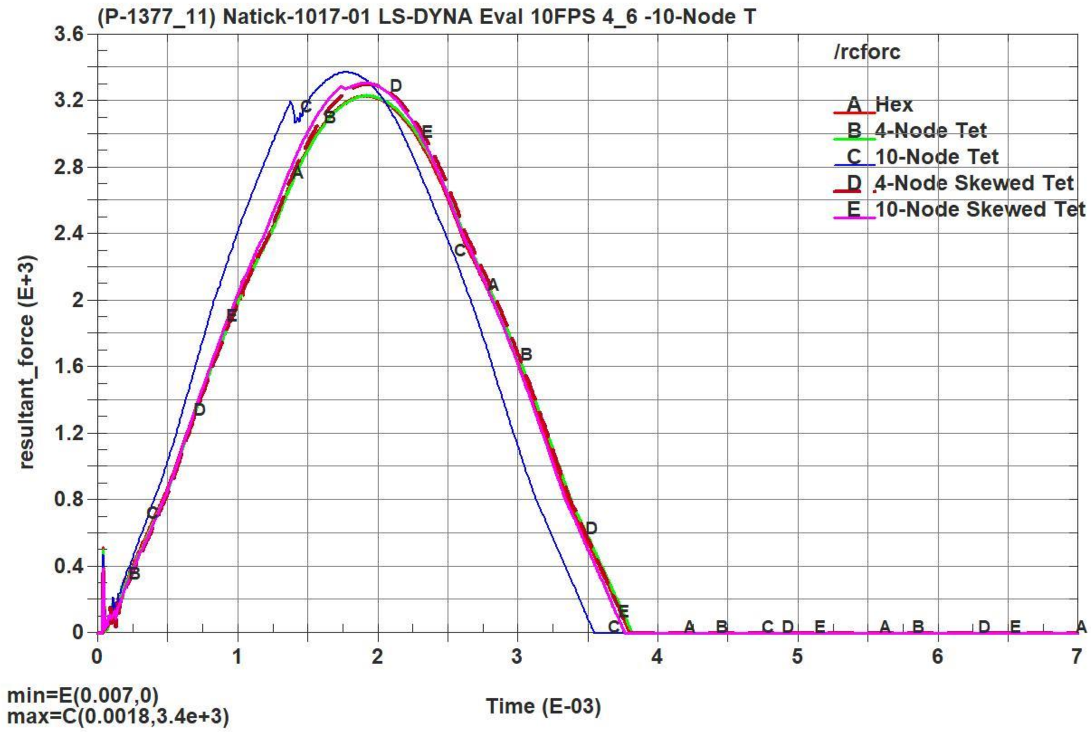

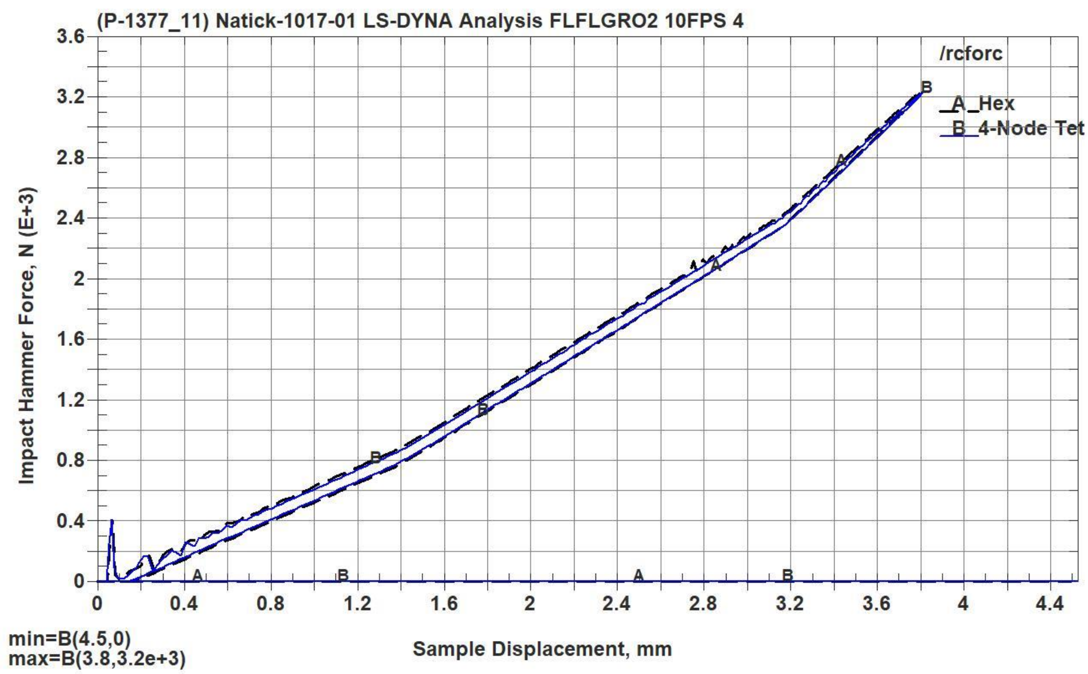

Figure 54: Impact test results (force v time) for element formulation and quality

7.4.2 Impact Test on 3D Lattice Structure

This work investigates how element formulation would affect the response of the proposed 3D lattice structure under investigation. Figure 55 shows the setup. The prior lattice model was cut down to quarter-symmetry and then mesh with 4-Node and 10-Node tetrahedrals. The 4-Node mesh was refined to a higher density to assess its effect on the force vs. displacement response.

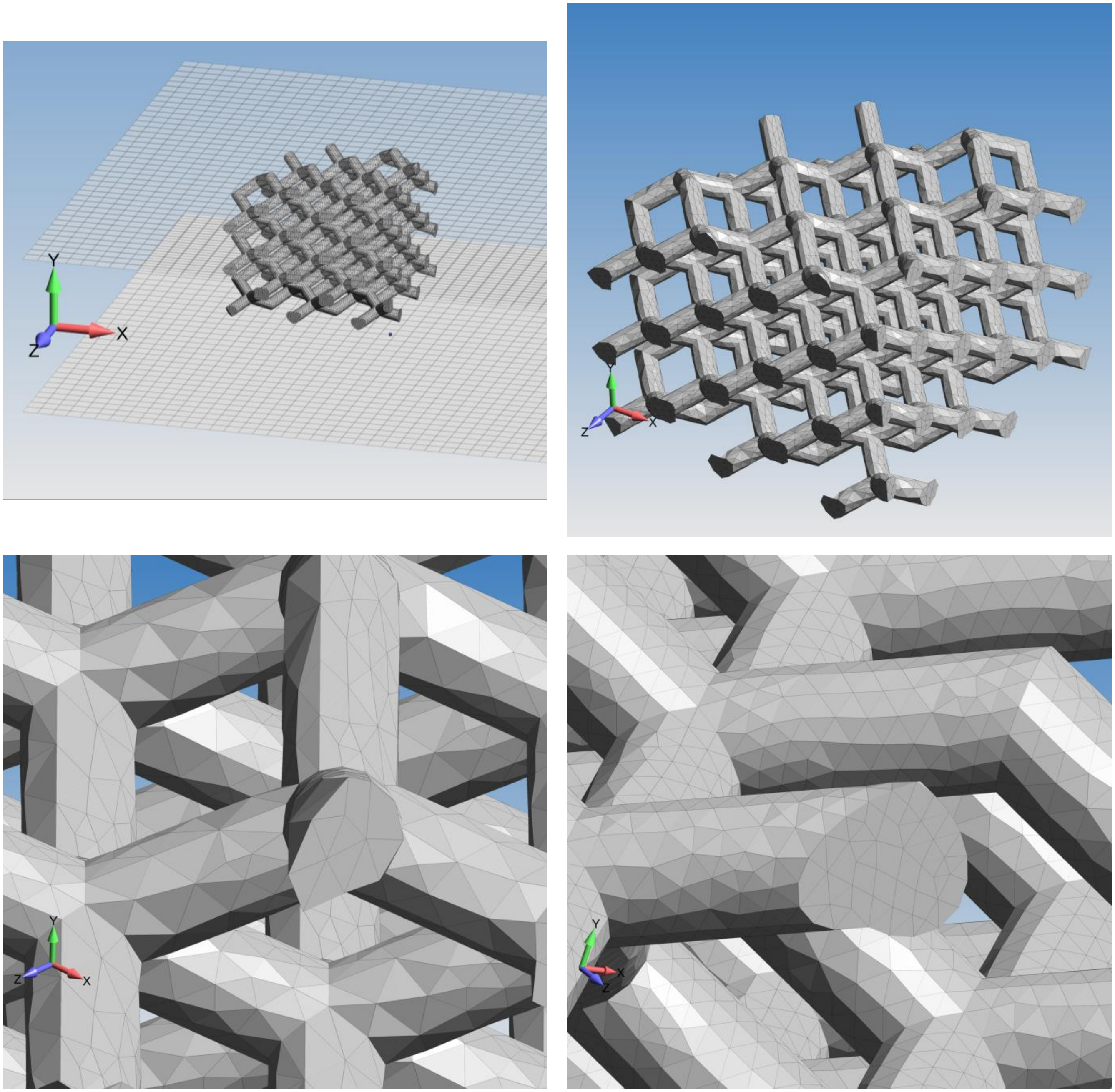

Figure 55: Impact testing of 3D lattice structures with 4-Node and 10-Node tetrahedral meshes

The same impact setup (hammer mass 4.6 kg with an impact velocity of 3.05 m/s) was employed for this virtual simulation work. Figure 22 shows example results of the quarter symmetric structure getting compressed.

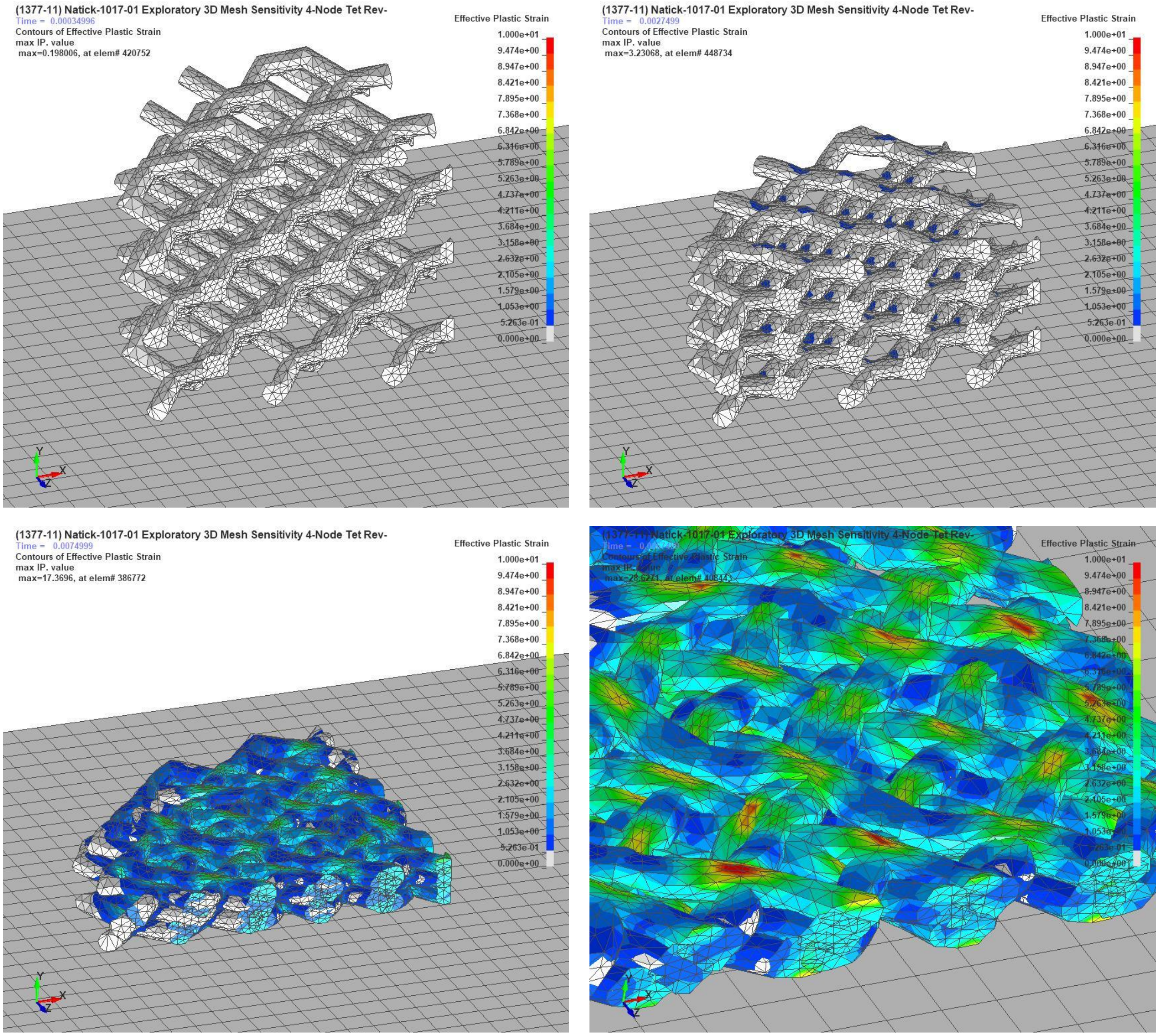

Figure 56: Impact testing of 4-Node 3D lattice structure

Figure 57 shows the impact force versus time for the simulations where the element formulation (4-Node and 10-Node) was investigated along with 4-Node tetrahedral mesh density. The 10-Node tet analysis could not finish due to element distortion. As the 4-Node tet mesh density increased, so did the impact force. These results are not good since the impact force is not converging. Something is wrong.

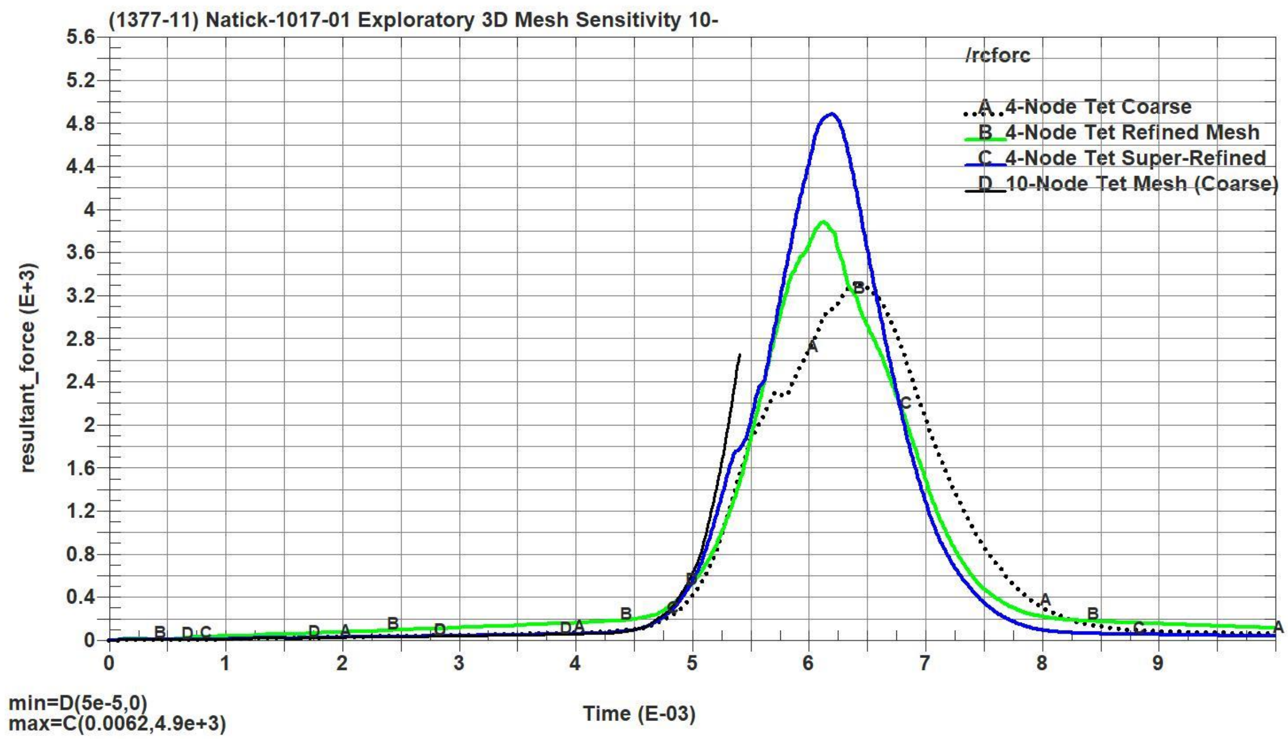

Figure 57: Comparison of impact forces with different element formulations and mesh densities

With additional discussion, it was determined that the default LS-DYNA contact stiffness was allowing the soft elastomeric material to interpenetrate. An additional study was conducted to increase the contact stiffness and assess the results. When the contact stiffness was increased, the positive sliding interface energy was noticed to significantly decrease. This is shown in Figure 58 where the same mesh density (double-mesh) is used but the contact stiffness is scaled from its default value of 1.0 to 25x. As the contact stiffness is increased, the sliding interface energy drops. For frictionless contact (as simulated for elastomeric contact), the sliding interface energy should be 0.0; however, some positive value is tolerable if small (<10% of the internal energy). Figure 58 indicates that even with the stiffness scaled by 25x, some sliding interface energy is present but it is tolerable.

Default Contact Stiffness	Contact Stiffness Scaled by 25x

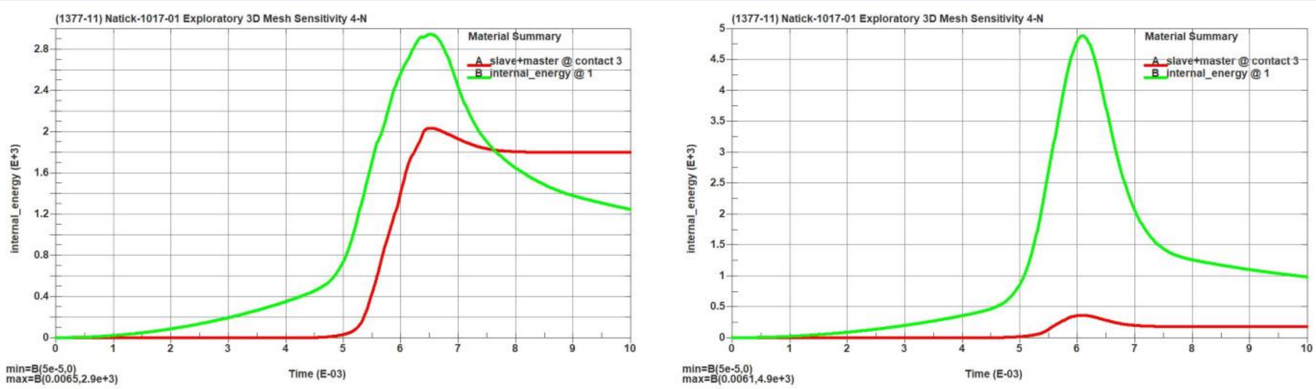

Figure 58: Comparison of internal energy and sliding interface energy as the contact stiffness is scaled

Finally, the impact force results shown in Figure 59 indicate that the impact force does not change as a function of mesh density. This is the desired result. For comparison, the impact force result for the initial 4-Node Tet Double-Mesh with the initial default contact stiffness is shown. With a scaled contact stiffness of 25x, the double- and triple-mesh densities provide the same impact force.

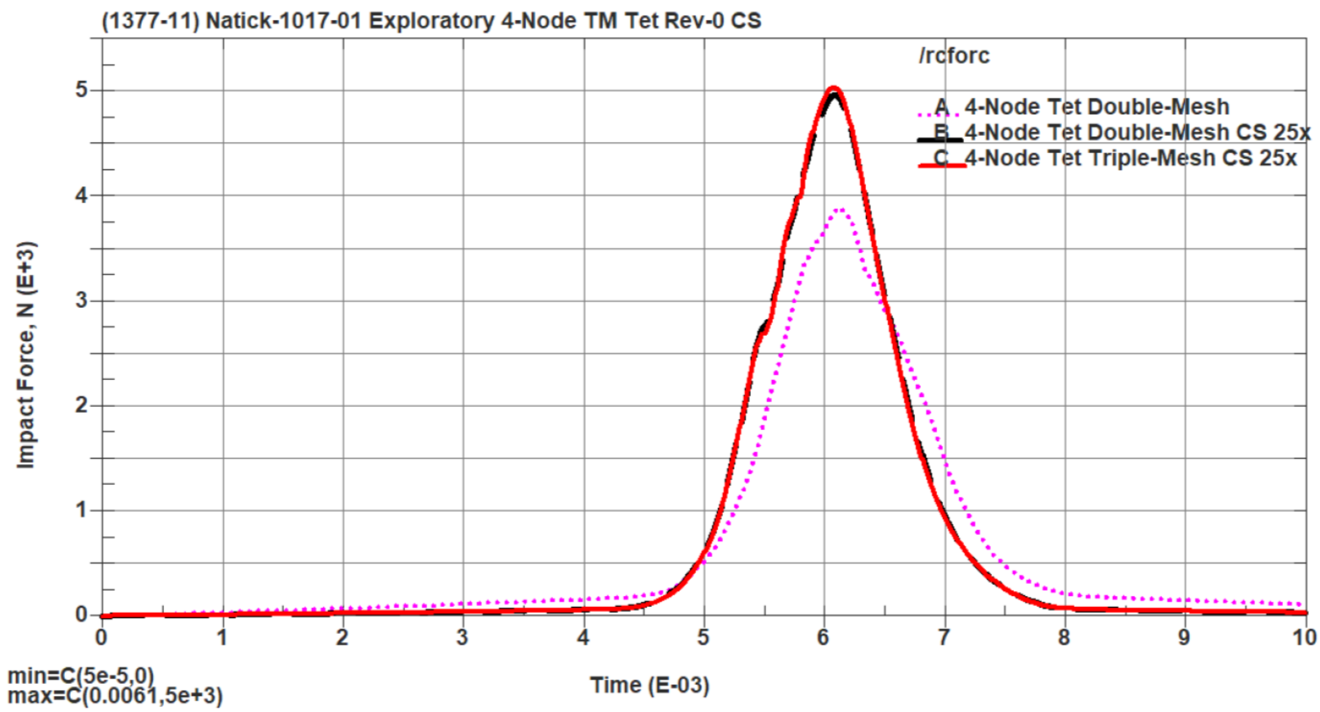

Figure 59: Revised impact force results using scaled contact stiffness

7.5 Material Data Sheets

7.5.1 FloFloGro2

The sample was post cured for 60 minutes prior to testing.

Formlabs Flexible resin has elastomeric properties allowing you to print parts on the Form 1+ and Form 2 3D printers that are bendable and compressible. Parts are pliable when thin and resilient when thick. Flexible has compression characteristics that make it great for creating parts like custom grips, stamps, keypads, gaskets and wearable prototypes. It does not shatter upon failure making it ideal for high impact applications.

	METRIC[1]		IMPERIAL[1]		METHOD
	Green	Postcured[2]	Green	Postcured[2]	
Mechanical Properties					
Ultimate Tensile Strength[3]	3.3 – 3.4 MPa	7.7 – 8.5 MPa	483 – 494 psi	1110 – 1230 psi	ASTM D412-06 (A)
Elongation at Failure[3]	60%	75 – 85%	60%	75 – 85%	ASTM D412-06 (A)
Compression Set[4]	0.40%	0.40%	0.40%	0.40%	ASTM D395-03 (B)
Tear Strength[5]	9.5 – 9.6 kN/m	13.3 – 14.1 kN/m	54 – 55 lbf/in	76 – 80 lbf/in	ASTM D624-00
Shore Hardness	70 – 75 A	80 – 85 A	70 – 75 A	80 – 85 A	ASTM 2240
Thermal Properties					
Vicat Softening Point[6]	231 °C	230 °C	448 °F	446 °F	ASTM D1525-09

NOTES:

[1]Material properties can vary with part geometry, print orientation, print settings and temperature.
[2]Data was obtained from parts printed using Form 2, 100 µm, Flexible settings and post-cured with 80.5 mW/cm^2 of 365 nm fluorescent light for 60 minutes.
[3]Tensile testing was performed after 3+ hours at 23 °C, using a Die C dumbbell and 20 in/min cross head speed.
[4]Compression testing was performed at 23 °C after aging at 23 °C for 22 hours.
[5]Tear testing was performed after 3+ hours at 23 °C, using a Die C tear specimen and a 20 in/min cross head speed.
[6]Thermal testing was performed after 40+ hours with a 10 N loading at 50 °C/hour. Cracks formed in samples during testing.

FORMLABS MATERIAL PROPERTIES – FLEXIBLE: Photopolymer Resin for Form 2 and Form 1+ 3D Printers 2

7.5.2 CARBON EPU 40

CarbonResin EPU 40

DOC #103208 REV C
TECHNICAL DATA SHEET, LAST UPDATED 08/14/2017

Tensile Properties ASTM D412, Die-C, 500 mm/min	Metric	U.S.
Ultimate Tensile Strength	10.2 ± 1.6 MPa	1.48 ± 0.23 ksi
Elongation at Break	310 ± 25 %	
Tensile Set, 100 % Elongation	2.1 %	
Stress at 50 % Elongation	1.9 MPa	0.28 ksi
Stress at 100 % Elongation	3.0 MPa	0.44 ksi
Stress at 200 % Elongation	5.5 MPa	0.80 ksi

Mechanical Properties	Metric	U.S.
Tear Strength, ASTM D624-C	23 ± 3 kN/m	130 ± 17 lb_f /in
Compression Set, 23 °C, 72 hrs, ASTM D395-B	23 %	
Bayshore Rebound Resilience, ASTM D2632	29 %	

Thermal Properties	Metric	U.S.
Coefficient of Thermal Expansion, ASTM D696	190 ppm/°C	106 ppm/°F
T_g (DMA, E')	-50 °C	-58 °F
T_g (DMA, tan(d))	-6 °C	21 °F

Dielectric Properties ASTM D150, 1 MHz	Metric
Dissipation Factor	0.031
Dielectric Constant	3.9

General Properties	Metric
Hardness, ASTM D2240	68, Shore A
Density, ASTM D792	1.025 g/cm^3
Density (liquid resin)	1.00 g/cm^3

NOTES—Results in this data sheet are representative of specific sample generation and testing processes and may vary if the established protocols are not followed. Contact Carbon for the specific process used to generate the test samples to determine each of these values. Tensile are average ± 1 standard deviation from 8 specimens. The U.S. values are converted from Metric measurements and are for reference only.